# Optic Disc Pallor and Brain Health

*Samuel Gibbon*


*Doctor of Philosophy*

The University of Edinburgh

2025

My kid's favourite sayings at the point of handing in this thesis

*Toasht?*

*Not in a minute, NOW!*

# Abstract


**Background**

There is a growing need for accurate and cost-effective biomarkers for neurological disorders. Brain imaging is not suited to mass screening, owing to its cost and complexity of operation. The retina offers a promising and accessible alternative as it is directly connected to the brain via the optic nerve and shares its blood supply, embryological origins, and structural features. Changes in the brain are often reflected in the retina. One such change observed in multiple neurological disorders is thinning of the retinal nerve fibre layer (RNFL), which is measured using Optical Coherence Tomography (OCT), reflecting loss of nerve tissue in the brain. However, OCT is not universally accessible and may be challenging to use with certain populations, such as frail individuals or those with movement disorders. An alternative approach still utilising the retina involves assessing the paleness of the optic disc in colour fundus photographs, based on the premise that a pale disc indicates RNFL degeneration or loss. Fundus photographs are the most widely available retinal imaging modality and routinely captured during high-street eye examinations and other standard clinical settings.

**Objective**

In this thesis I aim to develop a method for quantifying optic disc pallor in fundus images, and to investigate optic disc pallor and in conditions affecting the health of the brain.

**Methods**

I developed software to measure optic disc pallor using a combination of image processing techniques and deep learning segmentation networks. Validation was performed by comparing pallor measurements to peripapillary RNFL thickness from the same eyes and by assessing how pallor values aligned with clinically diagnosed pallor in an external dataset. I applied the software to three clinical datasets using linear, logistic, and linear mixed-effects models to investigate associations between pallor measurements and clinical features, including MRI-detected lesions, cerebral small vessel disease (cSVD) ratings, stroke type, and Parkinson's disease (PD) status and duration. I also manually reviewed 1,485 images from an aggregated dataset and used these labels to create two methods for automated quality control.

**Results**

The resulting software can process an image in under one second. In clinical research, I found that disc pallor was associated with MRI-visible enlarged perivascular spaces (indicative of underlying cSVD), lacunar stroke, cSVD ratings, and PD status and disease duration.

**Conclusion**

Optic disc pallor, measured in colour fundus photographs, reveals insights into neurological dysfunction. Future investigation is warranted to see if pallor could be an imaged-derived biomarker of disease or whether it holds predictive value in addition to conventional risk factors used clinically.

# Lay summary

Neurological disorders, such as stroke and Parkinson's disease, require reliable and accessible biomarkers to aid in diagnosis and monitoring. While brain imaging techniques provide valuable insights, they are expensive and not a practice for large-scale screening. The retina offers a promising alternative, as it is directly connected to the brain and reflects neurological changes. One established retinal biomarker is the thinning of the retinal nerve fibre layer (RNFL), typically measured using Optical Coherence Tomography (OCT). However, OCT is not always accessible and may be difficult to use in certain populations, such as individuals with movement disorders.

This research explores an alternative method – quantifying optic disc pallor from standard colour fundus photographs. A pale optic disc can indicate RNFL degeneration, potentially serving as a marker of neurological health. Fundus photography is widely used in routine eye exams, making it a practical tool for large-scale studies.

To assess this approach, I developed software that automatically measures optic disc pallor using image processing and deep learning techniques. The method was validated against RNFL thickness measurements and clinical assessments of pallor. I then applied the software to three clinical datasets to investigate the relationship between optic disc pallor and various neurological conditions, including cerebral small vessel disease (cSVD), stroke, and Parkinson's disease. My findings showed that disc pallor was associated with MRI-detected brain changes linked to cSVD, lacunar stroke, and Parkinson's disease status and progression.

These results suggest that optic disc pallor could provide valuable insights into brain health. Further research is needed to determine whether it could serve as a useful biomarker for neurological disease detection or risk prediction in clinical practice.

# Acknowledgements

I would like to thank my supervisor, Dr Tom MacGillivray, for his overall guidance throughout my PhD, and for giving me the freedom to pursue my own ideas. I am also deeply grateful to my additional supervisors and advisors – Prof. Manuel Trucco, Prof. Graciela Muniz-Terrera, Prof. Baljean Dhillon, and Dr Roly Megaw for their generous support, advice, and encouragement over the years.

I'm thankful to all my collaborators and co-authors, whose expertise and insight were vital across many of the studies that make up this thesis: David Breen, Fergus Doubal, Francesca Chappell, Joanna Wardlaw, Charlene Hamid, Adam Threlfall, Craig Ritchie, Ylenia Giarratano, Darwon Rashid, Emanuele Trucco, Audrey Low, Megan Reid-Schachter, Fabian Yii, Simon Cox, Ian MacCormick, Andrew Tatham, John O'Brien – and the UK Biobank Eye & Vision Consortium.

Thanks also to the EASTBIO doctoral training programme for funding this work and to Alzheimer's Research UK for providing a small grant. Thanks to the staff at the IRR, especially the ever-cheerful reception team and the building's unsung heroes: the cleaning crew. I've benefited greatly from the stimulating research environment at the Centre for Clinical Brain Sciences, the IRR, and beyond, including helpful feedback from Joanna Wardlaw's group, Miguel Bernabeu's group, and many others.

Finally, thank you to everyone who shared ideas, coffee, or kindness – your support made the journey most enjoyable.

# Declaration

I declare that this thesis was composed by myself, that the work contained herein - including the publications - is my own except where explicitly stated otherwise in the text, and that this work has not been submitted for any other degree or professional qualification except as specified.

**Funding**

My PhD was funded by EASTBIO, a consortium of Scottish Universities. I also received a small grant from Alzheimer's Research UK.

Samuel Gibbon

18th Feb 2025

# Abbreviations

AUC – area under the curve

CAA – cerebral amyloid angiopathy

CADASIL – cerebral autosomal dominant arteriopathy with subcortical infarcts and leukoencephalopathy

CNS – central nervous system

CSF – cerebral spinal fluid

cSVD – cerebral small vessel disease

DTI-ALPS – diffusion tensor imaging along the perivascular space

ePVS – enlarged perivascular spaces

FLAIR – fluid-attenuated inversion recovery

GCIPL – ganglion cell-inner plexiform layer

MSS – Mild Stroke Study

NPV – negative predictive value

OCT – optical coherence tomography

PD – Parkinson's disease

pRNFL – peripapillary retinal nerve fibre layer

RGC – retinal ganglion cell

RGB – red green blue

RNFL – retinal nerve fibre layer

SAA – seed amplification assay

SCONe – Scottish Collaborative Optometry-Ophthalmology Network e-research

WMH – white matter hyperintensities

All abbreviations are defined when first mentioned in the text.

# Contents

# Chapter 1

# Introduction

## 1.1 Introduction

My PhD was funded by EASTBIO, a consortium of Scottish universities, whose vision is to "*…inspire and empower a diverse cohort of scientists to spearhead bioscience research, equipping them with the tools to address pivotal issues in our society and strengthen the broader UK economy.*" One such pivotal issue facing the UK, and indeed the world, is the increasing prevalence age related neurological and cerebrovascular disorders.[1] Cerebral small vessel disease (cSVD) and Parkinson's disease (PD) are two such disorders, both of which have long preclinical and prodromal periods, which offer a critical window for intervention as therapies to slow or stop disease progression are being developed.[2–4] Accordingly, there is a growing clinical need for reliable, sensitive, and cost-effective tools to identify such diseases at their earliest stages, when therapies would be most effective.[4,5] Helping to address this clinical need was a major motivation for my research.

While MRI may be the most obvious tool for investigating neurological disorders, scanning the brain is expensive, and impractical as a mass screening tool. Increasingly, researchers are turning to the retina as a promising window into brain health.[6–9] In comparison with MRI, retinal imaging is faster, less-expensive, and more widely available – colour fundus photographs are taken routinely in high-street eye examinations. Fundus imaging, therefore,

has huge potential as a readily available and cost-effective biomarker. Recognising this, the overall aim of my PhD was "***to learn about brain health through images of the retina***".

Through my exploration of the literature in this field I noted frequent references to optic disc pallor – a clinical sign of irreversible damage to the anterior visual pathway, often linked to thinning of the retinal nerve fibre layer (RNFL).[10–12] Despite the importance of RNFL thinning in several ocular and neurological disorders,[6–9] I was surprised to find that methods for quantifying optic disc pallor were scarce. Existing approaches were either unavailable, reliant on red-free fundus photography (unavailable in most available datasets), or proprietary.

Recognising this gap, I focused on developing a method to quantify optic disc pallor in conventional fundus images and explore disc pallor in neurological diseases. Accordingly, I developed three specific objectives:

**Objective 1:** To develop a method of quantifying optic disc pallor in fundus images.

**Objective 2:** To investigate optic disc pallor in a cerebrovascular disease.

**Objective 3:** To investigate optic disc pallor in a neurodegenerative disease.

## 1.2 What's in this thesis

This thesis is centred around four publications related to the three core objectives: one publication on methodology and three publications applying the method to two different diseases across three datasets. In each "publication chapter", I provide a brief introduction to the work, acknowledge co-author contributions, detail my own contributions, and provide a conclusion. This structure complies with the University of Edinburgh's regulations for incorporating publications in postgraduate research theses, as approved by the Senate Academic Policy Regulations Committee on 23rd April 2015, with the next review scheduled

for 2026/27. All four publications are under Open Access agreements, so no additional permissions from the journals are required for reproduction here. Separately, all co-authors have granted permission for their inclusion in this thesis.

In Chapter 2, I provide the essential background information needed to contextualise the subsequent chapters. This begins with an overview of the basic anatomy of the retina and its connection to the brain, highlighting the retina's role as a window into brain health. I then explore why the eye is a uniquely suitable organ for investigating brain health, offering insights into its accessibility and shared pathophysiology with the brain. I also discuss two methods of imaging the retina, providing a foundation for understanding the techniques used in this research. Following this, I examine the impact of cSVD and PD on the eye, emphasising their relevance to optic disc changes. Finally, I focus on optic disc pallor, including its potential as a biomarker for brain health, and explain why a pale optic disc may signal underlying neurological or cerebrovascular compromise.

In Chapter 3, I present novel software for automatically quantifying optic disc pallor in fundus images. This work has been published in *Translational Vision Science & Technology* as:

> **Gibbon, S**., Muniz-Terrera, G., Yii, F.S., Hamid, C., Cox, S., Maccormick, I.J., Tatham, A.J., Ritchie, C., Trucco, E., Dhillon, B. and MacGillivray, T.J., 2024. PallorMetrics: Software for Automatically Quantifying Optic Disc Pallor in Fundus Photographs, and Associations With Peripapillary RNFL Thickness. *Translational Vision Science & Technology*, *13*(5), pp.20-20.

In Chapter 4, I discuss my work developing two automatic methods of performing quality control for the *PallorMetrics* software that analyses optic disc pallor. This step is crucial if the software is to be applied to large datasets, where manual quality control could be impractical. A shortened version of this chapter has been published in the journal *Ophthalmology Science* as a technical appendix for a paper titled "*Sectoral changes in*

*neuroretinal rim pallor across refractive error*", with Fabian Yii as the lead author.[13] In this work, *PallorMetrics* was applied to fundus images in the UK Biobank to investigate refractive error, and quality control was conducted with the method described here.

In Chapter 5, I apply *PallorMetrics* to a dataset called PREVENT Dementia to investigate cSVD. Specifically, I tested for associations between four MRI features of cSVD and both peripapillary RNFL (pRNFL) thickness and optic disc pallor measurements. This work has been published in *Alzheimer's & Dementia: Diagnosis, Assessment and Disease Monitoring* as:

> **Gibbon, S**., Low, A., Hamid, C., Reid-Schachter, M., Muniz-Terrera, G., Ritchie, C.W., Trucco, E., Dhillon, B., O'Brien, J.T. and MacGillivray, T.J., 2024. Association of optic disc pallor and RNFL thickness with cerebral small vessel disease in the PREVENT-Dementia study. *Alzheimer's & Dementia: Diagnosis, Assessment & Disease Monitoring*, *16*(3), p.e12633.

In Chapter 6, I apply *PallorMetrics* to a dataset called the Mild Stroke Study to investigate cSVD. Specifically, I tested for differences in optic disc pallor between two groups of hospital patients who had suffered a mild ischemic stroke (cortical or lacunar) and examined whether pallor correlated with a composite score of cSVD burden. This work has been published in *BMJ Neurology Open* as:

> **Gibbon, S**., Doubal, F., Chappell, F., Wardlaw, J.M., Dhillon, B. and MacGillivray, T., 2024. Association between optic disc pallor and lacunar stroke. *BMJ Neurology Open*, *6*(2), p.e000789.

In Chapter 7, I apply *PallorMetrics* to the UK Biobank to investigate PD. Specifically, I tested for differences in optic disc pallor between individuals with prevalent PD and an age- and sex-matched control group, as well as between individuals who would later develop PD (incident PD) and the same control group. Additionally, I examined whether pallor increased with disease duration. This work has been published in *Movement Disorders* as:

**Gibbon, S**., Breen, D.P., MacGillivray, T.J. and UK Biobank Eye & Vision Consortium, 2025. Optic Disc Pallor in Parkinson's Disease: A UK Biobank Study. *Movement Disorders*.

In Chapter 8, I summarise the main findings with respect to each objective and suggest areas for future research. Finally, I reflect on the broader significance of this research, highlighting its potential contributions to the fields of ophthalmology, neurology, and public health.

## 1.3 Summary

In this chapter, I have described the overall aim of my thesis – *to learn about brain health through images of the retina* – and specified three objectives: 1) to develop a tool to quantify optic disc pallor, 2) to explore disc pallor in a cerebrovascular disease, 3) to explore disc pallor in a neurological disease. In the next chapter, I will present the relevant background information.

# Chapter 2

# Background

## 2.1 Introduction

In this chapter, I will outline the background information necessary to understand the chapters that follow. This encompasses a discussion on the eye-brain connection, two methods of imaging the retina (fundus imaging, optical coherence tomography), two brain disorders (cSVD, PD), including how each disorder affects the eye, and optic disc pallor.

### 2.1.1 The eye-brain connection

From around 23 days of gestation, the retina and optic nerve emerge as direct extensions of the diencephalon, a part of the developing forebrain.[14] This embryological origin establishes a fundamental link between the eye and the brain and sets the stage for their intricate functional and structural relationships.

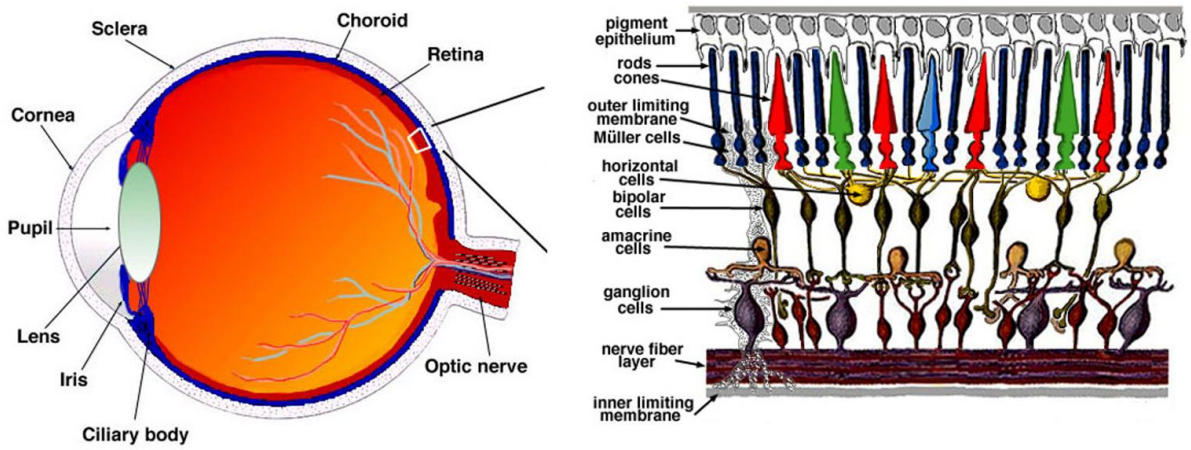


**Figure 1.** A diagram of the eye, retina, and retinal layers.[15]

The retina is composed of several layers of cells (Figure 1). When light enters the eye via the pupil, it is first refracted by the cornea and focused by the lens onto the retinal surface. When this focused light strikes the surface of the retina, it travels down through the various cell layers to activate the rods and cones, which send their signal up to the retinal ganglion cells (RGCs). RGCs have very long axons, which run unmyelinated (to maintain transparency) across the surface of the retina, and exit through the lamina cribrosa, a mesh-like structure in the centre of the optic disc (also called the optic cup), after which they become myelinated and bundle together to form the optic nerve. The optic nerves from both eyes meet at the optic chiasm, where approximately 50% of the fibres cross over (*decussate*) to the opposite side.[16] This partial decussation allows for binocular vision and depth perception. The optic tracts, formed after this crossing, continue to the lateral geniculate nucleus of the thalamus. The lateral geniculate nucleus serves as a relay station, processing and sorting visual information before sending it to the primary visual cortex in the occipital lobe. This pathway (Figure 2) completes the direct connection between the eye and the brain, forming the basis of our visual perception.[17]

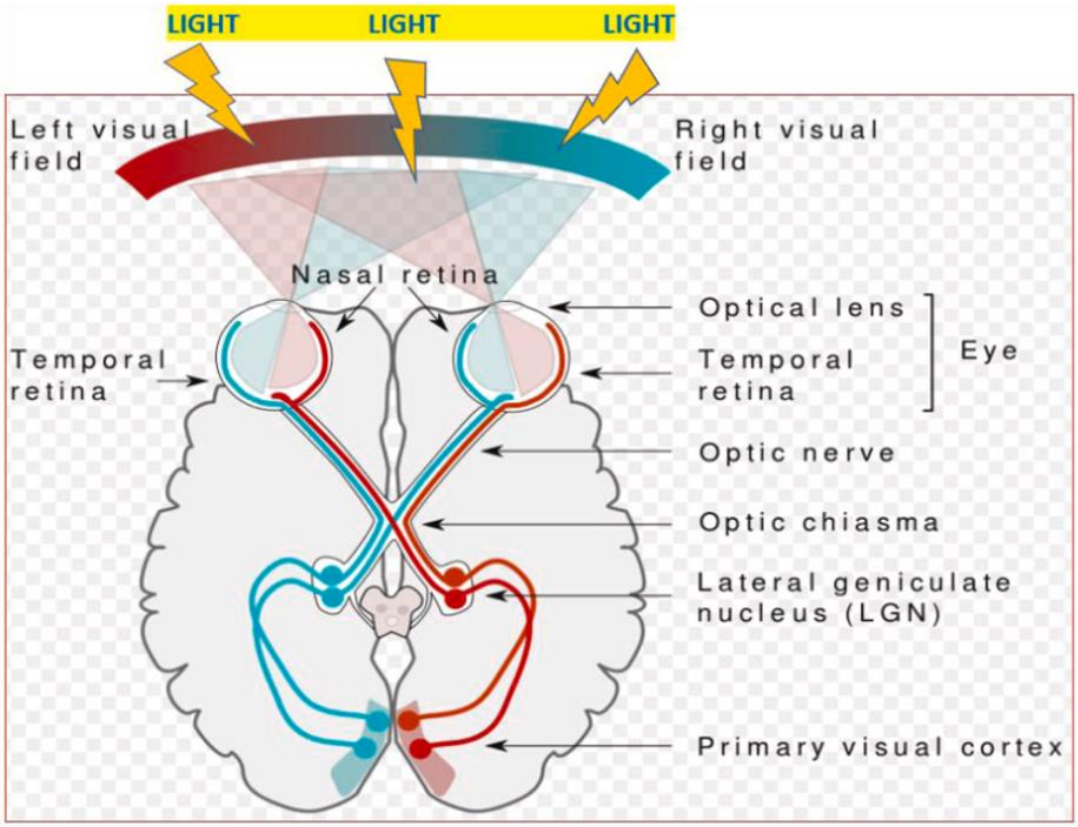


**Figure 2.** Diagram of the visual pathway.[18]

### 2.1.2 The eye as a window on brain health

The eye and brain share similarities in neuronal composition, vascular structure, and immune response. Like central nervous system (CNS) neurons, RGCs have cell bodies, dendrites, and axons. Both organs primarily use glutamate for communication.[19] The retinal microvasculature closely resembles the cerebral microvasculature, sharing both anatomical and physiological features including small vessel structure (small diameter arterioles, venules, and capillaries), autoregulation, and low-flow, high-oxygen extraction.[17,20] Both the retina and the brain have blood barrier systems, which help protect them from harmful substances in the general circulation and help maintain their respective internal environments – both barriers are similarly composed of non-fenestrated endothelial cells.[21,22] While the brain (and spinal cord) is surrounded by cerebrospinal fluid (CSF), the anterior chamber of the eye is filled with aqueous humor – CSF and aqueous humor are fluids similarly rich in anti-inflammatory and

immunoregulatory mediators.[23] Finally, like other CNS tracts, the optic nerve is vulnerable to retrograde and anterograde degeneration, scar formation, and myelin loss after injury, and because it is mostly myelinated by reactive astrocytes and oligodendrocytes, which express several inhibitory factors, the optic nerve has a similarly limited capacity for axonal regeneration.[6,24]

This close connection between the eye and brain suggests that neurodegenerative and cerebrovascular processes may present similarly in both organs.[6,20,25,26] This relationship positions the eye as a valuable model for brain research, with findings potentially applicable to both systems.

In this PhD, I explore what the retina can tell us about two conditions affecting the brain: cSVD and PD. First it is necessary to review different methods of imaging the retina.

## 2.2 Methods of imaging the retina

There are various ways to capture images of the retina. These include, but are not limited to, colour fundus photography, optical coherence tomography (OCT), optical coherence tomography angiography, and ultra-widefield scanning laser ophthalmoscopy. I will focus on the first two, as these are the ones featured and analysed in this thesis.

### 2.2.1 Colour fundus photography

Colour fundus photography, hereafter referred to as "fundus imaging", captures a two-dimensional image of the retina through the pupil. It is the most common and widely used form of retinal imaging.[27] Traditionally recorded on film from as early as 1886,[27] it is now performed using a fundus camera system, which combines a low-power microscope, a digital camera, and a flash of white light for illumination.[28] The result is a three-channel (red, green, blue – RGB),

digital colour photograph of the retina which provides detailed visualisation of key structures including the optic disc, macula, and retinal blood vessels (Figure 3). The most common field-of-view is 45° (as in Figure 3), but this can range from 30 to 50°. Fundus imaging is widely used in both community (e.g., high street optometry practices) and clinical settings (e.g., diabetic retinopathy screening programmes and hospital eye services).

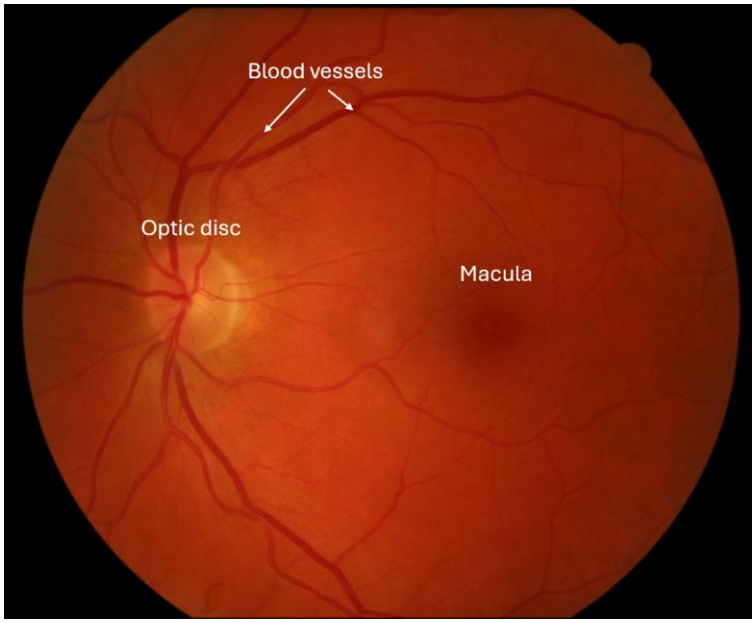


**Figure 3.** Fundus photograph of the human retina from the PREVENT Dementia dataset,[29] with key landmarks annotated.

### 2.2.2 Optical Coherence Tomography

Optical Coherence Tomography (OCT) is a non-invasive imaging technique that provides high-resolution cross-sectional images of the retina by using low-coherence light beams to capture depth information. Initially described in 1991, OCT has become a fundamental tool in ophthalmology and optometry for diagnosing and monitoring various retinal and optic nerve conditions such as age-related macular degeneration, diabetic retinopathy, glaucoma, retinal vein occlusion, diabetic macular oedema, and optic neuropathies.[25] In this imaging modality, multiple 2D cross-sectional scans are combined to generate a 3D reconstruction of the retina and choroid, offering detailed insight into its structure.

Typically, OCT scans are focused on key areas such as the macula, where fine visual acuity is processed, or the optic disc, which represents the point where the optic nerve exits the eye. The choice of the scan location depends on the clinical need, with macular scans often used to assess diseases like macular degeneration, and optic disc scans aiding in the evaluation of optic neuropathies such as glaucoma.

A major technical challenge in OCT image processing is the accurate segmentation of the retinal layers, a critical step for quantitative analysis.[28] For example, the retinal nerve fibre layer (RNFL), which is essential for assessing conditions like glaucoma, is the layer between the internal limiting membrane and the ganglion cell layer (see Figure 4 – B). Accurate delineation of this and other layers is crucial for identifying pathological changes related to eye disease and to neurodegenerative conditions that manifest in the eye.

Modern OCT devices now come equipped with advanced software that supports semi- or fully automated segmentation of these layers. This automation has improved the consistency and reliability of layer measurements. For instance, in the Heidelberg Engineering SPECTRALIS OCT devices, semi-automated segmentation performed by experienced raters has shown high reliability, particularly when applied to key retinal layers such as the RNFL.[30] Despite these advancements, manual adjustments by skilled operators is still necessary in cases where image quality is poor or the retinal anatomy is abnormal.

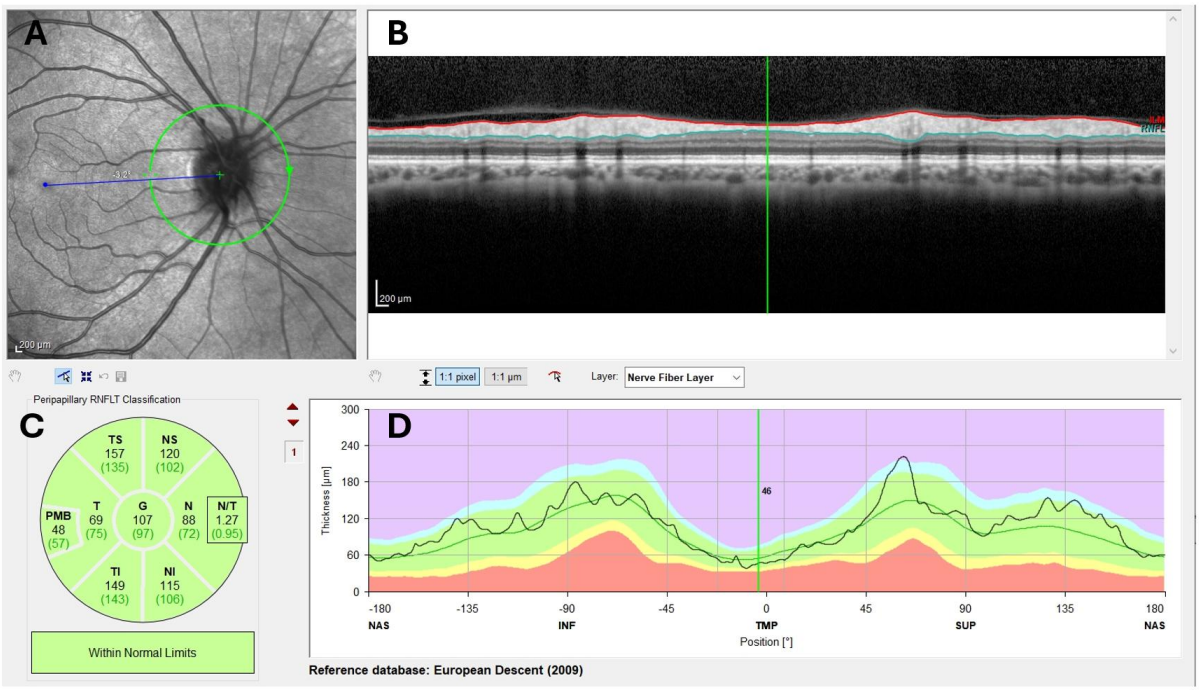


**Figure 4.** Screenshot of a SPECTRALIS (Heidelberg Engineering, Germany) peripapillary scan from a healthy eye. A) En face scanning laser ophthalmoscopy image indicating scan line around the optic disc, aligned with the macula, B) 2D visualisation of layers, C) Zone map with mean RNFL thickness values, D) Comparison of the imaged eye (red area) with normative values (red area). Image courtesy of Charlene Hamid.

## 2.3 Cerebral small vessel disease

cSVD is an age-related condition affecting the small blood vessels of the central nervous system, contributing to stroke, dementia, and cognitive decline.[31–33] It is characterised by a range of structural abnormalities in the small end arterioles, venules, and capillaries of the brain. These changes lead to impaired blood flow and disruption of the blood-brain barrier, contributing to various neurological symptoms.[31–33] cSVD is responsible for most haemorrhagic strokes, approximately a quarter of all ischaemic strokes, and frequently co-occurs with Alzheimer's disease – all in all, contributing to around 50% of all dementias.[32,34,35] Nearly 100% of people over the age of 90 will have radiological features consistent with cSVD.[5]

Over 90% of diagnosed cSVD cases are sporadic (not genetic). There are two main subtypes of sporadic cSVD: cerebral amyloid angiopathy (CAA), which is amyloidal, and hypertension related angiopathy, also called hypertensive arteriopathy, which is non-amyloidal.[31] In CAA, β-amyloid gradually accumulates in the walls of small arteries located in the cortex and leptomeninges, resulting in vessel dysfunction and damage to the brain's parenchyma.[32,36] Hypertensive arteriopathy, by contrast, largely results from chronic hypertension, which leads to structural changes to small blood vessels, and subsequent ischaemic damage.[36] The most common genetic form is cerebral autosomal dominant arteriopathy with subcortical infarcts and leukoencephalopathy (CADASIL), which effects a gene that expresses vascular smooth cells and pericytes,[37] leading to vessel pathology similar to that seen in CAA.

### 2.3.1 Lacunar stroke

An important consequence of cSVD is lacunar stroke, which occurs when a deep perforating arteriole is occluded in a non-cortical area, causing hypoxia and resulting tissue death.[38,39] Over time, these lesions can become filled with cerebrospinal fluid – hence the term "lacunar", which is from the French word for "lake", owing to their propensity to form lacunes (see section 2.3.5). Importantly, not all lacunes are caused by lacunar strokes. Lacunar strokes account for between 20 – 30% of all ischaemic strokes.[39,40] Distinguishing lacunar stroke from other types of stroke is important because prognosis, therapy, and prevention strategies differ.[40–43]

### 2.3.2 Risk factors

Beyond age, the most significant risk factor for cSVD is arterial hypertension, defined as a sustained blood pressure above 140/90 mm Hg.[44] Hypertension contributes to vessel wall thickening, endothelial dysfunction, and increased arterial stiffness, all of which are implicated

in the pathogenesis of cSVD.[32] Other important risk factors include diabetes mellitus, which exacerbates vascular damage through hyperglycaemia and inflammation;[45] chronic kidney disease, where impaired renal function is associated with microvascular damage;[46] smoking, which promotes oxidative stress and endothelial injury;[45] and obstructive sleep apnea, which leads to intermittent hypoxia and vascular dysregulation.[47] Some of these risk factors, such as hypertension, smoking, and diabetes, are modifiable, and targeted interventions can reduce overall disease burden.

Among these interventions, antihypertensive therapies have been shown to significantly reduce the risk of cSVD progression.[48] Repurposed therapies, such as those being tested in clinical trials like LACI-2 (Lacunar Intervention Trial-2) also offer promise.[49] While the LACI-2 trial targeted individuals with a prior lacunar syndrome due to a small subcortical infarct (i.e., individuals within whom the disease had already started to take hold), it would be preferable to target drugs toward those in the long preclinical and prodromal stages of the disease, before significant damage has occurred. Accordingly, as with most other diseases, early biomarkers would be of tremendous value.

### 2.3.3 Why do we need retinal biomarkers of cSVD?

Although retinal imaging is unlikely to become the sole diagnostic tool for cSVD,[25] if retinal biomarkers were discovered, they would offer several advantages as a supplemental test. First, they could enable individuals to adopt early lifestyle modifications to mitigate future risk of deteriorating brain health, with a focus on known risk factors, many of which have available therapies and interventions.[50] Second, if appropriate biomarkers were identified, retinal imaging could be a valuable screening tool. Its low cost and wide availability make it an ideal first step for selecting candidates for clinical trials or determining who should undergo more resource-intensive procedures like brain imaging. Third, retinal imaging findings may reveal

new insights into the underlying disease pathophysiology potentially contributing to identifying new targets for new therapies.[51] Finally, retinal imaging biomarkers could potentially be used as primary or secondary endpoints in clinical trials to quantify the efficacy of therapeutic intervenstions.[25]

In the following section, I will review the current state of biomarker research in cSVD and discuss how cSVD affects the retina, providing potential avenues for early detection.

### 2.3.4 Definition of "biomarker"

Before discussing cSVD biomarkers, which include neuroimaging markers, it will be useful to first define the term "biomarker". A thoughtful 2010 paper defines a biomarker as "a broad subcategory of medical signs – that is, objective indications of medical state observed from outside the patient – which can be measured accurately and reproducibly".[52] This distinction highlights the objective nature of biomarkers, contrasting them with symptoms, which are subjective experiences reported by patients. Within this definition, we can include markers derived from neuroimaging and retinal imaging, as both can provide objective, external measurements of biological processes and can be consistently and accurately measured.

### 2.3.5 Current biomarkers of cSVD

cSVD is typically diagnosed through a combination of clinical evaluation and neuroimaging, with risk factors in mind.[33] Sometimes ancillary techniques such as blood tests and carotid or cardiac ultrasonography are also used. Blood tests largely focus on markers of endothelial dysfunction and blood brain barrier permeability, both of which are known pathological features of cSVD.[5,32,36] For the purpose of this thesis, I will focus on neuroimaging features, which are central to diagnosis and monitoring disease progression.[36] There are four main MRI indicators of cSVD: white matter hyperintensities (WMH), lacunes, microbleeds, and enlarged perivascular spaces (ePVS). These are typically detected with 1.5 – 3-Tesla scanners, however

each type of lesion is best visualised with a specific MRI sequence, which can highlight certain abnormalities more effectively than others (Figure 5).[32]

**White matter hyperintensities** are visible as bright areas on T2-weighted and FLAIR (fluid-attenuated inversion recovery) MRI, and mostly represent axonal loss and demyelination.[53]

**Lacunes** are small (between 3-15 mm in diameter) oval or round shaped cavities typically located in the basal ganglia and white matter.[2] They appear as hypointense (dark) areas on FLAIR, often with a hyperintense (bright) rim.[2] They represent a localised area of cell death caused by a lacunar infarction (a small ischemic stroke) or haemorrhage, that has since been filled with cerebrospinal fluid.

**Cerebral microbleeds** are small haemorrhages (between 2-10 mm in diameter) that result from structural damage to the small vessels. They are best visualised with susceptibility-weighted imaging or T2-weighted gradient echo MRI, where they appear as small round hypointense regions.[2]

**Enlarged perivascular spaces**, also known as Virchow-Robin spaces, are small (typically less than 3 mm in diameter) fluid-filled spaces that surround blood vessels as they penetrate the brain. They are usually located in the basal ganglia, white matter, and along the course of perforating arteries. On FLAIR, perivascular spaces appear as hypointense areas without a surrounding hyperintense rim, helping to distinguish them from lacunes.[2] Perivascular spaces represent the cerebral glymphatic system, helping clear waste fluids and compounds.

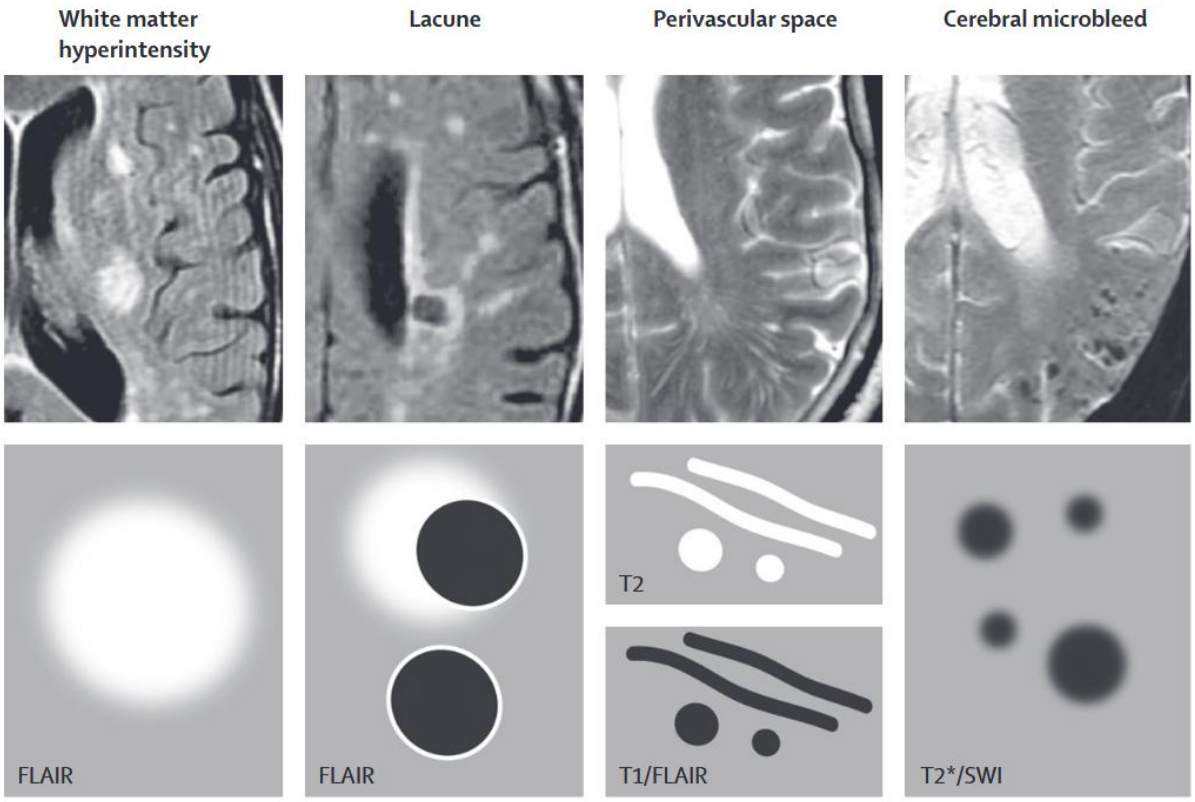


**Figure 5.** The four key MRI indicators of cerebral small vessel disease.[2] Abbreviations: FLAIR (fluid-attenuated inversion recovery); SWI (susceptibility-weighted imaging).

### 2.3.6 Resolution of MRI scans

The resolution of a typical 3T MRI scan is around 1mm.[54] This means that even small MRI-visible lesions represent fairly large-scale damage. In contrast, a colour fundus photograph offers a much finer resolution of around 7 µm,[28] making it potentially more sensitive to detecting smaller, subtle changes that occur during the preclinical or prodromal stages of disease.

### 2.3.7 How does cSVD affect the eye?

To date, there have been no histopathological studies of the retina in cSVD, in either the amyloidal or non-amyloidal forms. Therefore, our current understanding of how cSVD affects the retinal tissue is limited to what we can learn from *in vivo* imaging.

In general, retinal features can be broadly categorised as either vascular or neuronal. Vascular features relate to measurements of blood vessels, encompassing both larger vessels (arteries and veins) and smaller vessels (arterioles, venules, and capillaries). Retinopathies, such as cotton wool spots, hard exudates, microaneurysms, and retinal haemorrhages, signify end-stage damage to the capillaries and are therefore classified as vascular in nature.

#### 2.3.7.1 Vascular Changes

There have been numerous studies investigating retinal vascular changes in cSVD. In population studies, the presence of retinopathy identified through colour fundus photographs has been linked to the presence and progression of white matter hyperintensities and cerebral infarcts.[55–57] Quantitative vessel-based metrics derived from colour fundus photographs, such as fractal dimension (quantifying the complexity of the vascular branching pattern) and arteriolar thickness, have also shown consistent associations with white matter hyperintensities and lacunar infarcts.[58,59] Converging evidence from multiple studies suggests that vascular changes correlate with cSVD, both in terms of diagnosed cSVD and neuroimaging indicators.[25]

#### 2.3.7.2 Neuronal changes

cSVD also affects the retinal layers, which are neuronal. In contrast to vascular measures, neuronal measures have received far less attention. In a recent review of retinal imaging and cSVD, Biffi et al.[51] identified 50 studies that examined retinal vascular features, and six studies that examined retinal layers. In particular, the authors note that RNFL thinning was associated with multiple cSVD disorders – with five associations reported among 4,509 participants.

In addition to examining retinal change in diagnosed cSVD disorders, retinal features can be directly correlated with MRI-based markers of cSVD. Reduced ganglion cell layer (GCL) thickness has been linked to the extent of brain lesions and differs from controls.[60] Thinning of the pRNFL has been associated with white matter hyperintensities,[61] as has

thinning of the ganglion cell-inner plexiform layer (GCIPL).[61] Both RNFL and GCIP thinning have also been found to correlate with WMH.[62] Furthermore, GCIPL thinning has been associated with increased cortical cerebral microinfarcts.[63] Collectively, these studies provide strong evidence that changes in the retinal layers correlate with neuroimaging markers of cSVD.

## 2.4 Parkinson's disease

PD is an age-related neurodegenerative disorder that primarily affects movement but also leads to cognitive decline and dementia in later stages.[3] It is characterised by the progressive loss of dopaminergic neurons in the substantia nigra, resulting in motor symptoms such as tremors, rigidity, and bradykinesia (slowness of movement).[3] In addition to motor symptoms, PD patients commonly suffer from mood and sleep disturbances, depression, and pain.[3,64] In 2016, around 6.1 million people were affected worldwide.[1] Females have a lower incidence than males, although certain aspects of the disease, such as the propensity to develop dyskinesia, can be higher than in males.[65] PD is mostly monogenic, although between 3-5% of cases can be explained by genetic causes.[3] Unlike other neurodegenerative disorders, PD progresses slowly, often spanning decades – there is an average delay of 10 years between the first noticeable symptoms and diagnosis.[66] PD has an enormous impact on the individual and their caregivers, and constitutes a growing socioeconomic burden.[1] Medications such as levodopa can lessen symptoms, but there is currently no cure.

### 2.4.1 Risk factors

A recent case-control study involving 694 cases and 640 controls from six sites identified six risk factors for PD, and three protective factors.[67] The six risk factors were family history of PD, dyspepsia (indigestion), exposure to pesticides, oils, and metals, and general anaesthesia,

whereas the three protective factors were coffee, smoking, and physical activity. Head injury is another well-established risk factor, with evidence gained from professional sports players.[68] In addition, both chronic and acute stress have been shown to exacerbate symptoms.[69] Considering physical activity, the protective effect appears to come from moderate to vigorous exercise, in comparison with light exercise.[70] Alongside coffee and smoking, the "protective effects" of physical activity could potentially be *causal*, supported by their well-documented effects on the central nervous and dopamine systems.[70–73] However, they may also reflect underlying factors, such as higher dopamine levels in smokers or generally healthier lifestyles in more active individuals.[3] Therefore, further research is needed to rule out *reverse* causation, and clarify their role in PD prevention. PD patients should not start smoking.[74]

### 2.4.2 Why do we need biomarkers of Parkinson's disease?

In PD, patients typically become symptomatic after losing between 70-80% of dopaminergic neurons.[75] Given the limited regenerative abilities of such CNS neurons, identifying individuals who have begun to lose dopaminergic neurons but have not yet begun to experience clinical parkinsonism would be of tremendous importance. Like in cSVD and many other conditions, biomarkers for PD could enhance early diagnosis accuracy (enabling better management of the symptoms which maintains quality of life for longer), aid in more precise participant selection for clinical trials, provide indicators of therapeutic success, monitor disease progression, and help differentiate between disease subtypes.[76,77]

A recent perspective suggests that PD may be a multisystem disease, with pathological changes observed in multiple organs, including the colon, salivary glands, and skin.[78] These tissues may offer more accessible biomarker sources than brain scans or cerebrospinal fluid.

### 2.4.3 Current biomarkers of Parkinson's disease

There are four main types of PD biomarkers: clinical, imaging, biochemical, and genetic.[76] Clinical biomarkers, such as motor and non-motor symptoms, provide observable indicators of PD progression, but they often appear only after significant neuronal loss.[3] Imaging biomarkers, including PET and MRI, offer visual insights into dopamine loss and brain changes, but they can be expensive and may not always detect early-stage PD.[64,76] Genetic biomarkers, involving mutations in genes such as LRRK2 or SNCA, help identify at-risk individuals but only account for a limited number of cases, as most PD cases are sporadic rather than hereditary.[3] Biochemical markers offer the most promise for early detection and precision medicine in PD. A recent breakthrough has been the refinement of the α-synuclein seed amplification assay (SAA),[79] which was developed through the multicentre Parkinson's Progression Markers Initiative. This assay detects misfolded α-synuclein, a key protein involved in PD pathology, with high sensitivity and specificity. Findings suggest that α-synuclein SAA could play a crucial role in therapeutic development by identifying pathologically defined subgroups and establishing biomarker-defined at-risk cohorts for earlier interventions.[79]

However, there remains significant potential for retinal biomarkers in PD research. The α-synuclein SAA currently requires the extraction of cerebrospinal fluid, which is an invasive procedure that can cause discomfort, carries a risk of complications, and is not practical for routine or large-scale screening.[80] By contrast, retinal imaging is non-invasive, providing a more patient-friendly approach while still offering valuable insights into the neurodegenerative changes seen in PD. Retinal biomarkers, if found, could complement existing biomarkers, creating an additional avenue for early diagnosis and disease monitoring, especially in cases where invasive procedures like cerebrospinal fluid collection are less practical.

### 2.4.4 How does Parkinson's disease affect the eye?

In the retina, the dopaminergic cells that are characteristically lost in PD are located in the inner nuclear layer and inner plexiform layer.[81] Several histopathological studies have demonstrated a reduction in dopaminergic cells in the retinal layers alongside the presence of phosphorylated α-synuclein.[82,83] These findings have stimulated the search for in vivo biomarkers, particularly using OCT, which can visualise the retinal layers. A 2019 meta-analysis of 1916 patients and 2006 controls across 36 studies found PD patients had significantly thinner retinas compared to age and sex-matched controls.[84] Thinning was observed in the macular region and around the optic disc. In particular, pRNFL thinning was mostly observed superiorly, inferiorly, and temporally, but not nasally. There are no published studies investigating the retinal vasculature as seen on colour fundus photographs and PD. Some studies have examined retinal vasculature using ultra-widefield images, which capture a larger area than conventional fundus images (around 200° compared with around 45°). They suggest that in PD, vessel tortuosity increases and vascular complexity decreases,[85,86] but the evidence is limited due to small sample sizes (38 and 22 PD patients respectively).

## 2.5 Optic disc pallor

So far, I have established that the retina serves as a valuable model for investigating brain health, with evidence suggesting that changes in one organ often reflect changes in the other. Two retinal imaging modalities have also been reviewed along with how the retina is affected in both a cerebrovascular disease (cSVD) and a neurodegenerative disease (PD). In these diseases, retinal neuronal assessments predominantly rely on measures obtained from OCT. However, a less-explored area is the use of neuronal measures derived from fundus images, which are more widely accessible and could provide complementary information to OCT.

Fundus imaging, while not offering the same depth information of OCT, is more commonly available and can still provide valuable insights into retinal structure and health. Given its widespread use, exploring how fundus images can be utilised for neuronal assessments represents a promising avenue for future research. In the following section, I will discuss optic disc pallor as a potential biomarker, which could serve as a non-invasive marker of brain health.

A healthy human retina contains around 1.2 million RGCs, whose axons converge over the neuro-retinal rim (NRR) before exiting the eye through the laminar cribrosa. The NRR is anatomically shaped like a slightly elliptical donut, surrounding the central cup of the optic disc. Its width and thickness vary across the optic disc, being typically broader in the inferior and superior regions compared to the nasal and temporal regions – a configuration known as the "ISNT rule" (Inferior > Superior > Nasal > Temporal).[87] When light strikes the surface of the fundus, it undergoes total internal reflection within the axonal fibres, and a portion of the light is reflected from the capillaries.[12] In a healthy eye (Figure 6B), this gives rise to a yellow-pinkish colour. However, as axonal fibres are lost, total internal reflection is reduced, and the light is less contained, increasing the visibility of the underlying sclera, which appears white (Figure 6A). Additionally, axonal death leads to increased gliosis and reduced vascularity.[11,88,89] These factors combine to make the NRR appear pale.[10] In short, axonal loss causes the NRR to appear pale. In the literature, the term “NRR pallor” is not frequently used. Instead, the terms “optic disc pallor” or “optic nerve head pallor” are more widely used. Hereafter, I will refer to “NRR pallor” as “optic disc pallor”.

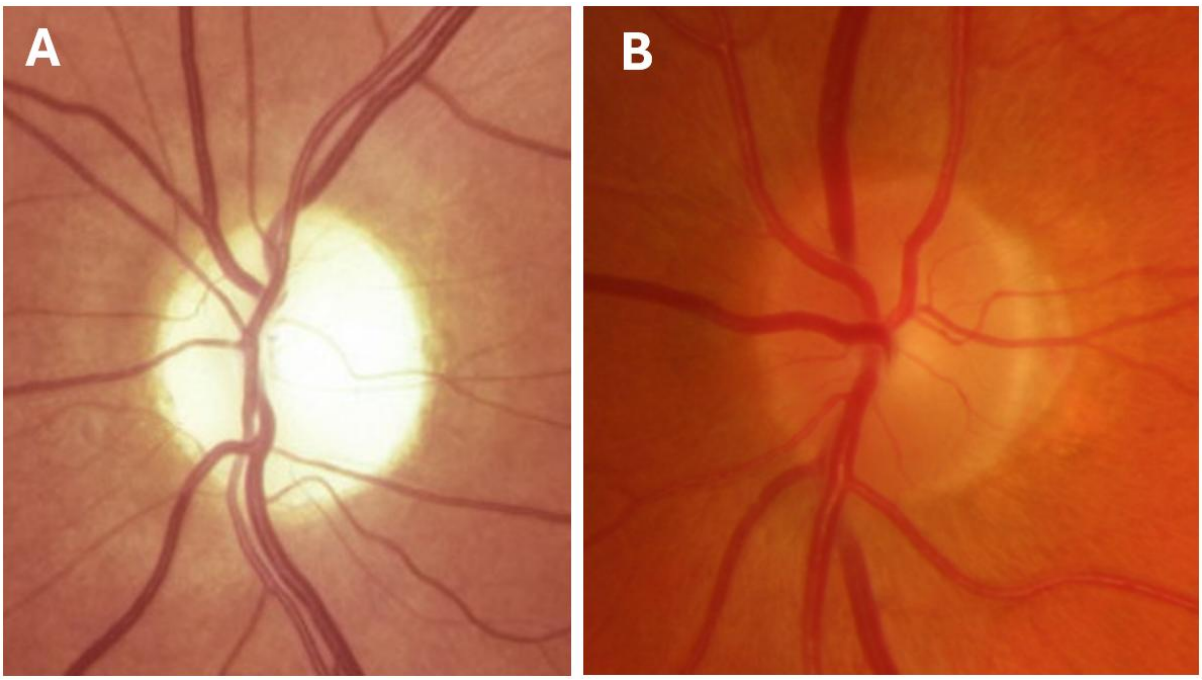


**Figure 6.** A) A pale optic disc from a patient diagnosed with optic atrophy,[11] B) a healthy optic disc.

Optic disc pallor is not a disease in itself, but rather a clinical sign indicating optic atrophy. Optic atrophy occurs in several conditions, including optic neuropathies (e.g., Leber's hereditary optic neuropathy), extrinsic compression (e.g., pituitary adenoma, aneurism), intrinsic optic nerve tumours (e.g., optic nerve glioma, lymphoma), vascular disease (e.g., NAION, central retinal artery occlusion), inflammatory diseases (e.g., multiple sclerosis, meningitis), infections (e.g., Lyme disease, tuberculosis), toxic or nutritional optic neuropathies (e.g., drug addiction, juvenile diabetes), trauma, papilledema, and retinal disease (e.g., retinitis pigmentosa, macula dystrophies).[12] In histopathology, when an RGC axon is severed, the part that leads to the brain disintegrates within a week (anterograde degeneration), however the part connected to the RGC remains visible for up to 4 weeks (retrograde degeneration), after which disintegration is rapid, and complete by 6-8 weeks.[90] Therefore, optic disc pallor typically begins to show around 4-6 weeks after axonal damage,[12,90] indicating the end-stage of one of several disease processes. In clinical practice, a pale optic disc is typically assumed to be caused by a compressive lesion until proven otherwise through further testing (MRI of the visual

pathway and orbits).[12,91] Accurately identifying optic disc pallor can lead to life-saving treatment.

## 2.6 Conclusion

In this chapter, I have outlined the background information necessary to give context to the subsequent chapters of this thesis. This included a discussion of the eye-brain connection and how cSVD and PD might affect the eye and ended with a section on optic disc pallor as a potential and promising non-invasive marker of neurological and cerebrovascular dysfunction. In chapter 3, I will describe the software I developed for quantifying optic disc pallor in fundus images. In subsequent chapters, I will present the application of that software to cSVD and PD.

# Chapter 3

# Developing software to measure optic disc pallor

## 3.1 Introduction

In this chapter, I address the first objective – developing a method of quantifying optic disc pallor in fundus images.

Optic disc pallor is a key clinical sign indicating irreversible damage to the optic nerve or its pathways.[12,88] It largely results from the loss of RGC axons, which is reflected by reduced pRNFL thickness.[12] Given that thinning of the pRNFL is commonly observed in both cSVD and PD,[51,84] optic disc pallor could be a potentially valuable biomarker in studying these diseases, as well as other cerebrovascular and neurodegenerative conditions. However, despite its clinical relevance, there are currently limited methods to quantitatively assess optic disc pallor, and none of these are publicly accessible.[92,93] Here, I aim to fill this critical gap.

Before going further, it is worth noting that most research-stage retinal image analysis toolkits are notoriously challenging to use, often requiring users to perform a series of technical steps. Users typically need to navigate a complex computational process involving cloning a repository, setting up a virtual environment, and processing images via the command line – while dealing with unexpected bugs and technical challenges along the way. While these steps might seem straightforward to researchers with a background in computer science, they can be

completely unfamiliar - and daunting - for many potential users, particularly clinicians, who are often the intended end-users of such software.

With this in mind, I aimed to design my software to be as user-friendly as possible. Aside from installing MATLAB and the necessary packages – both of which can be done with a few clicks – the process is straightforward. Users simply need to set the input folder ("pathIn") containing the images they want to analyse, set the output folder ("pathOut") to save the results, then click "Start." The software then processes the images sequentially. Afterward, the output folder contains a marked-up version of each processed image, alongside a single spreadsheet compiling all the results. I believe this approach reduces the technical barriers to accessing research-stage software, making my tool accessible to a broad range of users.

## 3.2. Acknowledgement of contribution

Charlene Hamid (Lead Ophthalmic Imager and Analyst, Edinburgh Clinical Research Facility, University of Edinburgh) oversaw image acquisition for the PREVENT Dementia study and carried out quality control of the OCT scans and fundus images. Fabian Yii (doctoral student, Centre for Clinical Brain Sciences, University of Edinburgh) annotated the optic disc in a subset of 100 fundus images.

## 3.3. My contribution to this work

I led:

- Generating the idea to quantify optic disc pallor.
- Conducting a review of existing techniques.
- Annotating the fundus images.

- Developing the deep learning-based images segmentation models.
- Developing the image analysis pipeline.
- Deciding which statistical tests to conduct.
- Deciding which covariates to use.
- Performing statistical analysis.
- Creating the tables and figures.
- Drafting the manuscript.
- Incorporating co-authors' comments and finalising the manuscript.
- Writing this chapter.

## 3.4 Published article

tvst

Neuro-Ophthalmology

# PallorMetrics: Software for Automatically Quantifying Optic Disc Pallor in Fundus Photographs, and Associations With Peripapillary RNFL Thickness

**Samuel Gibbon[1,2], Graciela Muniz-Terrera[3], Fabian S. L. Yii[1,2], Charlene Hamid[1], Simon Cox[5], Ian J. C. Maccormick[6,7], Andrew J. Tatham[1,8], Craig Ritchie[1,3], Emanuele Trucco[9], Baljean Dhillon[1,8], and Thomas J. MacGillivray[1,2,4]**

[1] Centre for Clinical Brain Sciences, Edinburgh, UK
[2] Robert O Curle Ophthalmology Suite, Institute for Regeneration and Repair, University of Edinburgh, UK, Edinburgh, UK
[3] Centre for Dementia Prevention, University of Edinburgh, Edinburgh, UK
[4] VAMPIRE Project, Edinburgh Clinical Research facility, University of Edinburgh, Edinburgh, UK
[5] Lothian Birth Cohorts, Department of Psychology, University of Edinburgh, Edinburgh, UK
[6] Centre for Inflammation Research, University of Edinburgh, Edinburgh, UK
[7] Institute for Adaptive and Neural Computation, University of Edinburgh, Edinburgh, UK
[8] Princess Alexandra Eye Pavilion, Chalmers Street, Edinburgh, UK
[9] VAMPIRE Project, Computing (SSEN), University of Dundee, Dundee, UK

**Correspondence:** Samuel Gibbon, Chancellor's Building, The University of Edinburgh, 49 Little France Crescent, Edinburgh EH16 4SB, UK.
e-mail: samuel.gibbon@ed.ac.uk

**Received:** June 8, 2023
**Accepted:** April 10, 2024
**Published:** May 23, 2024

**Keywords:** optic disc pallor; RNFL; optic atrophy; fundus; deep learning

**Citation:** Gibbon S, Muniz-Terrera G, Yii FSL, Hamid C, Cox S, Maccormick IJC, Tatham AJ, Ritchie C, Trucco E, Dhillon B, MacGillivray TJ. PallorMetrics: Software for automatically quantifying optic disc pallor in fundus photographs, and associations with peripapillary RNFL thickness. Transl Vis Sci Technol. 2024;13(5):20, https://doi.org/10.1167/tvst.13.5.20

**Purpose:** We sough to develop an automatic method of quantifying optic disc pallor in fundus photographs and determine associations with peripapillary retinal nerve fiber layer (pRNFL) thickness.

**Methods:** We used deep learning to segment the optic disc, fovea, and vessels in fundus photographs, and measured pallor. We assessed the relationship between pallor and pRNFL thickness derived from optical coherence tomography scans in 118 participants. Separately, we used images diagnosed by clinical inspection as pale ($n = 45$) and assessed how measurements compared with healthy controls ($n = 46$). We also developed automatic rejection thresholds and tested the software for robustness to camera type, image format, and resolution.

**Results:** We developed software that automatically quantified disc pallor across several zones in fundus photographs. Pallor was associated with pRNFL thickness globally ($\beta = -9.81$; standard error [SE] $= 3.16$; $P < 0.05$), in the temporal inferior zone ($\beta = -29.78$; SE $= 8.32$; $P < 0.01$), with the nasal/temporal ratio ($\beta = 0.88$; SE $= 0.34$; $P < 0.05$), and in the whole disc ($\beta = -8.22$; SE $= 2.92$; $P < 0.05$). Furthermore, pallor was significantly higher in the patient group. Last, we demonstrate the analysis to be robust to camera type, image format, and resolution.

**Conclusions:** We developed software that automatically locates and quantifies disc pallor in fundus photographs and found associations between pallor measurements and pRNFL thickness.

**Translational Relevance:** We think our method will be useful for the identification, monitoring, and progression of diseases characterized by disc pallor and optic atrophy, including glaucoma, compression, and potentially in neurodegenerative disorders.

## Introduction

A pale optic disc is the hallmark of nonglaucomatous optic atrophy, which refers to the irreversible loss or damage of retinal ganglion cell axons along the anterior visual pathway.[1] A pale disc has numerous potential causes, including inflammation, ischemia, compression, increased intracranial pressure, toxicity, nutritional deficiency, trauma, hereditary conditions, vascular disease, infection, and retinal disease.[1,2] As such, disc pallor indicates the end stage of one of several disease processes. It begins to show approximately 4 to 6 weeks after axonal damage.[1] In clinical practice, a pale disc is often considered to be due to a compressive lesion until further tests prove otherwise.[1,3] Correctly identifying disc pallor can lead to life-saving treatment.

Pallor can be identified through ophthalmoscopy or fundus photography. However, these methods are limited in that assessing change over time may be difficult, judgment can vary substantially among observers,[4] and the location of pallor is often not recorded consistently.[5] Computational approaches may offer a solution, but efforts have been limited, either requiring special filters during acquisition[6–8] or manual demarcation of the disc.[9,10] The purpose of this study was to develop a fully automatic method of locating and quantifying disc pallor in fundus photographs.

The quantity of retinal ganglion cell axons can be observed directly with optical coherence tomography (OCT), which images the retinal nerve fiber layer (RNFL). Accordingly, we validated the tool by comparing pallor with peripapillary RNFL (pRNFL) thickness from OCT scans in anatomically equivalent zones. Additionally, we tested the software on an image set with clinically diagnosed pallor. Finally, we tested the robustness of the software to camera type, image format, and resolution with a variety of datasets.

## Materials and Methods

### Participants and Image Capture

Several datasets were used in model development and testing (Fig. 1); however, only one dataset (PREVENT) was used for testing the association between pallor and pRNFL thickness. The PREVENT-Dementia study protocol is described elsewhere.[11] Briefly, participants aged 40 to 59 years were recruited through multiple sources from five sites in the UK. Retinal imaging was conducted in a substudy at the Edinburgh site only ($n$ = 123), which included fundus photography centered halfway between the optic disc and the macula (Fig. 2, right), with a nonmydriatic 45° field of view camera (CR-DGi; Canon USA, Inc., Lake Success, NY), and OCT (Heidelberg SPECTRALIS, Heidelberg Engineering, Germany) (Figs. 2 and 4 left most images). The N-site circular scan OCT module was used, set to high speed (1536 A-scans) with a target automatic real-time function of 100. Participants provided written informed consent, and the study was carried out in compliance with the Declaration of Helsinki. Six additional datasets were used in model development and testing (Table 1).

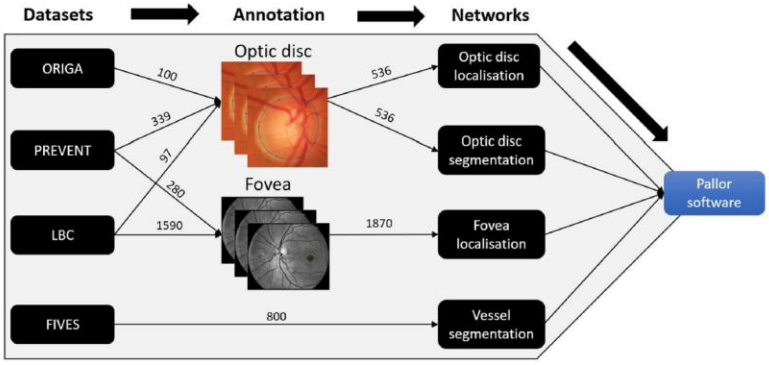


**Figure 1.** Flow of images through annotation, networks, and into the final software.

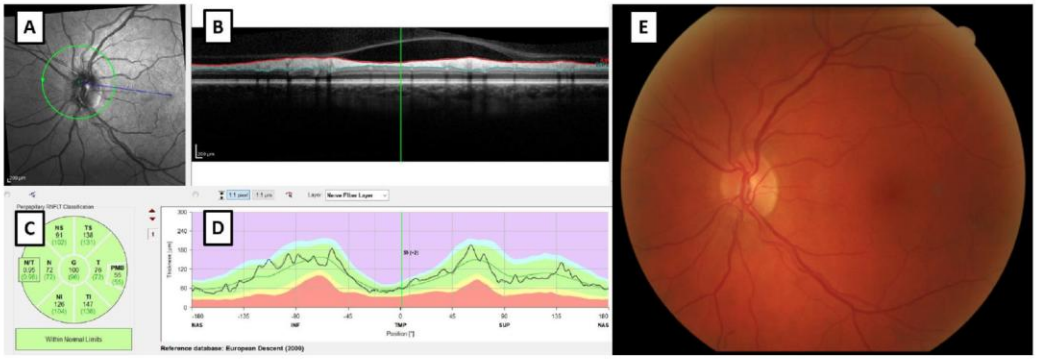


**Figure 2.** (**A**–**D**) Output of the Heidelberg SPECTRALIS peripapillary scan, where (**A**) shows the scan location, (**B**) shows the various layers (thick topmost layer is RNFL), (**C**) shows the measurement zones, and (**D**) shows the normative data (jagged line is the current participant). (**E**) shows the corresponding retinal fundus image.

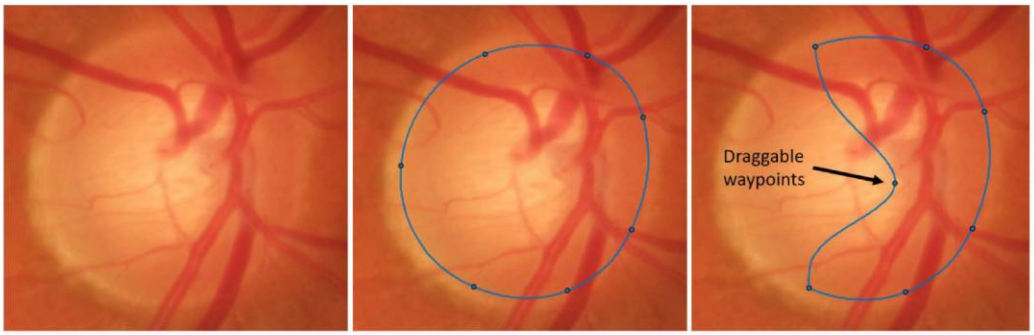


**Figure 3.** Annotation procedure. The annotator loads a full-sized image and zooms into the optic disc. The user then drags the waypoints of a deformable ellipse to the desired location. Additional waypoints can be added by double clicking. The entire shape can also be dragged. Performed in MATLAB with custom-written code.

## Optic Disc Annotation

We annotated the optic disc in 536 images from three datasets (100 ORIGA, 339 PREVENT, 97 LBC). In fundoscopy, it is widely accepted that the disc margin lies at the inner edge of the border tissue, defined as collagenous tissue that arises from the sclera to join Bruch's membrane, forming a scleral cuff or lip between the optic nerve head and the choroid, which gives rise to its characteristic appearance as a yellow–white halo or crescent (Fig. 3).[19,20] Accordingly, the annotation protocol required dragging the waypoints of a deformable ellipse to the inner edge of the border tissue in full-resolution RGB fundus images (Fig. 3). Annotation was performed by a single researcher (author S.G., a PhD student in retinal image analysis), using custom MATLAB code.

To assess interannotator agreement, a second researcher (author F.Y., a PhD student in retinal image analysis and an optometrist) annotated a subset of 100 images (30 ORIGA, 40 PREVENT, 30 LBC) using the same protocol. The agreement metric was the mean intersection over union (mIoU), calculated as the area of overlap divided by the area of union. The mIoU has been shown to be a suitable measure of interannotator agreement for medical image segmentation tasks.[21] The mIoU between the two annotators was 0.942 (94.2%). Overall, F.Y. annotated a smaller area than S.G. (mean number of pixels for all images = 75,844 vs. 84,701); however, this difference was largely driven by a low

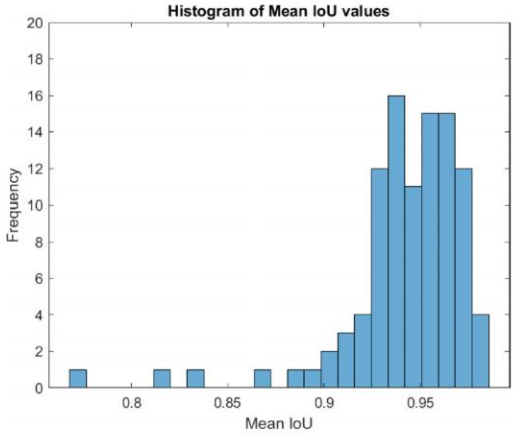


**Figure 4.** Histogram of interannotator agreement.

agreement on a few images (see the histogram in Fig. 4 and examples in Fig. 5).

## Fovea Annotation

We annotated the fovea in 1870 images from the LBC and PREVENT datasets (280 PREVENT, 1590 LBC). The annotation procedure involved dragging a circle with a fixed radius of 150 pixels onto the estimated center of the fovea to generate a binary fovea map, where pixels inside the circle were labelled as fovea and pixels outside labelled as background. The image presented to the annotator was preprocessed to improve visibility by extracting the green channel of the RGB image and contrast was enhanced by performing contrast-limited adaptive histogram equalization. When the fovea was not visible (i.e., owing to poor illumination), the annotator estimated its position relative to the vessel arc of the central arcades and disc. If neither the vessel arc nor the disc was visible, the image was rejected. According to this protocol, 33 of 1623 images were rejected from the LBC, and none were rejected from PREVENT. Annotation was performed by a single researcher (author S.G.) using custom MATLAB code. No second annotator was used. The annotation and procedure are visualized in Figure 6.

## Convolutional Neural Network Architecture and Computing Platform

Based on a 2022 survey of deep learning–based image segmentation,[22] we selected Google's DeepLabv3+ architecture,[23] which was the best performing network for image segmentation among the networks reviewed. DeepLabv3+ incorporates an encoding and decoding phase. The encoder–decoder model has been described elsewhere.[22,23] Briefly, in the encoding phase, information from the input image is extracted and compressed into a feature representation using a backbone convolutional neural network. The decoder then takes this as input to reconstruct the initial representation. The goal of such encoder–decoder architecture is for the model to learn a useful representation of the image. The result is accurate segmentation along object boundaries.[23] DeepLabv3+ can take one of several backbone architectures, including MobileNetv2[24] and Xception.[25] During experimentation, we found that MobileNetv2 produced the best results. Accordingly, we used DeepLabv3+ with a MobileNetv2 backbone pretrained on ImageNet[26] for all models, except vessel segmentation, for which we selected Xception. The values of relevant parameters varied with tasks and are given in the next section.

All models were trained in MATLAB (*version R2022b*; The MathWorks Inc., Natick, MA) using the Deep Learning Toolbox, on a Dell 7820 machine, fitted with an Intel Xeon Silver CPU and a NVIDIA Quadro RTX 5000 GPU, running Windows 10.

## Optic Disc Localization

The optic disc localization network was trained on 536 images from three datasets (100 ORIGA, 339 PREVENT, 97 LBC). In preprocessing, we resized all images and their corresponding labels to 650 × 650 pixels, allowing the whole image to be processed by the network. We then split images into training, validation, and test sets, with a ratio of 80/10/10, yielding 429 images for training, 54 for validation, and 53 for testing. We used the Adam optimizer, the learning rate was constant at 0.0001, and the batch size was 4. During training, validation was carried out after every 100 iterations (approximately every epoch). We applied the following data augmentations to the training images to enhance generalization to unseen data: addition of random color jitter (brightness = 0.3, contrast = 0.3, saturation = 0.3), scaling (between a factor of 0.8 and 1.3), and rotation (between −30° and 30°). To prevent overfitting, we finalized training if the validation loss stopped decreasing or was equal to the previous 10 losses (validation patience).

The aim of the task was to locate the approximate center of the disc. There were far fewer pixels labelled as "disc" than pixels labelled as background (ratio = 1/65), leading to an imbalanced training set.

**Table 1.** Characteristics of Datasets Used in Model Development and Testing

| Variable | PREVENT[12] | LBC 1936[13] | ORIGA[14] | FIVES[15] | RIM-ONE[16] | IDRiD[17] | RFMiD[18] |
|---|---|---|---|---|---|---|---|
| No. of images | 339* | 1623 | 650 | 800 | 169 (v1)485 (v3) | 103 | 92 |
| No. of images rejected | 2 | 33 | 0 | 0 | 0 | 0 | 1 |
| Camera | Canon CR-Dgi | Canon CR-Dgi | Canon CR-Dgi | Topcon TRC-NW8 | Nidek AFC-210 & Kowa WX sD | Kowa VX-10$\alpha$ | TOPCON sD OCT-2000, Kowa VX-10$\alpha$, TOPCON TRC-NW300 |
| FOV | 45 | 45 | – | 50 | Nidek = 45, Kowa = 34 | 50 | 45–50 |
| Resolution | 3072 × 2048 | 2689 × 2186 | 2518 × 2048 | 2048 × 2048 | Between 318 × 318 and 626 × 626 | 4288 × 2848 | Between 2144 × 1424 and 4288 × 2848 |
| Format | BMP | BMP | JPEG | PNG | PNG | JPG | PNG |
| Country | UK | UK | Singapore | China | Spain | India | India |
| Age, years (mean± SD) or range | 51.5 ± 5.5 | 72.5 ± 0.7 | 40–79 | 4–83 | – | – | – |
| Female sex | 57.70% | 49.80% | – | – | – | – | – |
| Purpose of data collection | Cohort study in dementia | Population-based study of cognitive ageing | Population-based study of eye diseases | Enable AI-based methods of vessel segmentation | Glaucoma diagnosis | Diabetic retinopathy | To enable multidisease detection research |

*This number includes images from professional rugby players, a substudy within Edinburgh, which were used in model development, but not analyzed further, partly because OCT was not captured in this group.

LBC 1936, Lothian Birth Cohort 1936; hereafter, LBC; ORIGA, Online Retinal Image Database for Glaucoma Analysis and Research; FIVES, Fundus Image VEssel Segmentation; RIM-ONE, Retinal IMage database for Optic Nerve Evaluation; IDRiD, Indian Diabetic Retinopathy Image Dataset; RFMiD, Retinal Fundus Multi-Disease Image Dataset); FOV, field of view); SD, standard deviation.

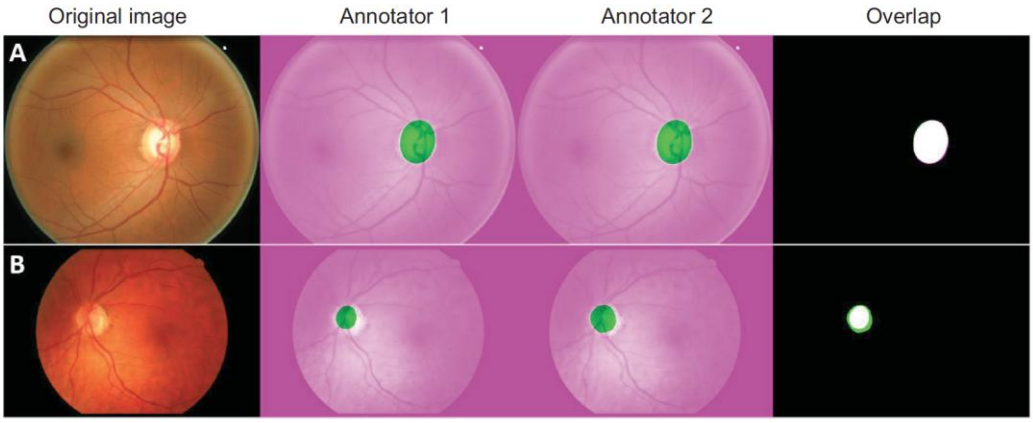


**Figure 5.** Interannotator agreement. (**A**) A high level of agreement. (**B**) A low-level agreement. Annotator 1 (S.G.); annotator 2 (F.Y.).

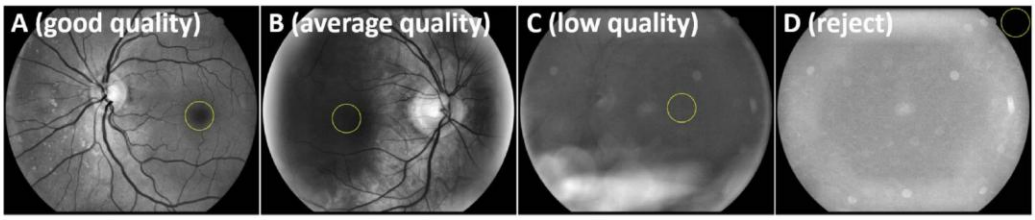


**Figure 6.** Fovea annotation procedure. (**A**) A good quality image, with the fovea clearly visible. (**B**) An area of low illumination over the macula, but the fovea can still be estimated. (**C**) Very low illumination and blur across the image; however. the optic disc and vessel arc are still visible, allowing the fovea to be estimated. (**D**) Neither the vessel arc nor the optic disc is visible; fovea estimation not possible.



With common metrics, a model would perform quite well if all pixels were simply labelled as background. To account for imbalance, we replaced the classification layer with a class weights layer, based on the class distribution of the full image set.

The convergence criterion was met after 3700 iterations (during the 28$^{th}$ epoch). The final validation accuracy was 99.16%. After postprocessing (removing the smallest object where multiple objects were detected), we computed the mean Euclidean distance (mED) in pixels between the ground truth and prediction based on the central points (Fig. 7). The mED in the test set was 2.06 ± 1.21 pixels, which expressed as a percentage of disc size (major axis length) was 2.02% ± 1.2%.

## Optic Disc Segmentation

The optic disc segmentation network was trained on 536 images from three datasets (100 ORIGA, 339 PREVENT, 97 LBC). Input to the network was a 650 × 650 × 3 RGB image, cropped around the disc, plus its corresponding ground truth segmentation. We split images into training, validation, and test sets, with a ratio of 80/10/10, respectively. We used the Adam optimizer, the learning rate was constant at 0.0001, and the batch size was 4. During training, validation was carried out after every 100 iterations (approximately every epoch). Augmentations were applied as before, but with additional levels of random color jitter (brightness = 0.6, contrast = 0.6, saturation = 0.6) and scaling (between a factor of 0.4 and 1.6). As before, class imbalance was high, albeit less than before (ratio ≈ 1/4.17), which we accounted for in the same way. The validation patience was 20. The convergence criterion was met after 16,400 iterations (during the 123rd epoch). The final validation accuracy was 98.79%. The mIoU for the test set (53 images) was 0.959 (95.9%). Two examples from the test set are presented in Figure 8.


**Figure 7.** Disc localization results on the test set. The ground truth is represented by a circle, and the prediction by an asterisk.

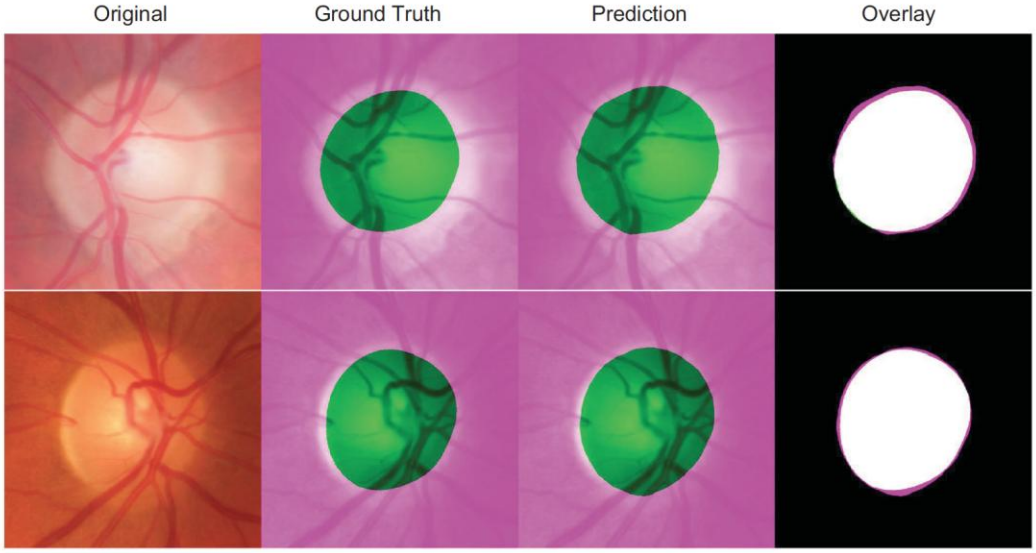


**Figure 8.** Optic disc boundary predictions from the test set.

We carried out external testing on IDRiD and RIM-ONE. Before generating predictions for IDRiD, each input image was resized, while maintaining its aspect ratio, to the median height of the training images. This strategy ensured that, when the image was cropped around the disc, the ratio of disc to background was approximately similar to that of a typical image from the training set. We carried out this step to improve generalizability.

The RIM-ONE dataset contains images that are already cropped around the disc; therefore, we skipped the disc localization stage. Our main performance metric was the mIoU; however, to enable a better comparison with other work, we also provide mean accuracy, defined as TP/(TP + FN), where TP is a true positive and FN is a false negative. We provide a direct comparison with the state of the art for IDRiD; however, for RIM-ONE we applied our network to their most recent data release (release 3). Other networks cited here have only been applied to release 1; therefore, comparative results are indicative only. On IDRiD, our model achieved a mIoU of 0.891, which beat the current state of the art (0.845). On RIM-ONE, we achieved a mIoU of 0.926 for nonglaucomatous

**Table 2.** Comparison of Our OD Segmentation Model to State of the Art

| Method | Year | IDRiD (81 Images) | | RIM-ONE V3 (Nonglaucoma; 313 Images) | | RIM-ONE V3 (Glaucoma; 172 Images) | | RIM-ONE V1 (169 Images) | |
|---|---|---|---|---|---|---|---|---|---|
| | | mAcc | mIoU | mAcc | mIoU | mAcc | mIoU | mAcc | mIoU |
| ResNet + Unet | 2020 | – | – | – | – | – | – | – | 0.925[a] |
| DRNet | 2021 | 0.997 | 0.845 | – | – | – | – | 0.962 | 0.901 |
| Ours | 2022 | 0.899 | 0.891[b] | 0.958 | 0.926[b] | 0.947 | 0.907 | – | – |

ResNet + Unet,[28] DRNet.[29]
[a]Second best score.
[b]Best score.
mAcc, mean accuracy.

eyes, and 0.907 for glaucomatous eyes. A comparative summary is shown in Table 2.

## Fovea Localization

The fovea localization network was trained on 1870 images from the LBC and PREVENT datasets (280 PREVENT, 1590 LBC). In preprocessing, we resized each image to 224 × 224 pixels. Unlike other features, the fovea is often not visible; however, its location can be inferred from its position relative to other salient features, including the vessel arc of the central arcades and the large dark patch covering the macula, which is common in poorly illuminated images. We hypothesized that substantially decreasing the image size would force the network to focus on these features. Therefore, input to the network was a 224 × 224 × 3 RGB image and its corresponding label. Images were split into training, validation, and test sets, with a ratio of 70/10/20, respectively, yielding 1309 images for training, 187 for validation, and 374 for testing. We chose a relatively large (20%) test set for this task as the focus was on generalization. We used the Adam optimizer, the learning rate was constant at 0.0001, and the batch size was 64. During training, validation was carried out after every 20 iterations.

We manually stopped training after 1167 iterations (during epoch 41), when we observed that the model was no longer improving. In postprocessing, we removed the smallest object, where multiple objects were detected. As with the optic disc localization network, we measured performance in the test set by calculating the Euclidian distance between the ground truth and prediction based on their central points. The mED was 3.77 ± 2.71. Expressed as a percentage of image height (224 pixels; disc size was not consistently available owing to image quality), the mED was 1.68% ± 1.11%. Several results from challenging images in the test set are presented in Figure 9.

We carried out external testing on IDRiD (103 images). In addition to providing the mED, we evaluate performance with the 1R criterion,[29] which refers to the radius of the optic disc. The 1R grid is centered on the fovea, and a score of 1 is given if the predicted coordinates lie within a given region (Fig. 10). The mED was 64.38 ± 76.43, and median Euclidean distance was 38.71. Overall, 95.15% of predictions fell within 1R, 86.41% within 0.5 R, 71.84% within 0.25 R, and 4.85% fell outside 1R (failed). The current state of the art for IDRiD is mED 41.87.[28]

## Vessel Segmentation

We trained the vessel segmentation network on 800 images from the FIVES dataset. In preprocessing, we used the optic disc localization network, described elsewhere in this article, to crop each image and its counterpart vessel mask to 650 × 650 pixels centered on the disc. Therefore, input to the network was a 650 × 650 × 3 RGB image and its corresponding label. We split images into training, validation, and test sets, with a ratio of 70/15/15, resulting in 560 images for training, 120 for validation, and 120 for testing. Unlike our previous networks, we used Xception[25] as the backbone, because it generated more accurate segmentations during experimentation. We used the Adam optimizer; the learning rate was 0.0001, which we set to decrease by a factor of 0.1 in a piecewise manner every five epochs. The batch size was 4, and validation was carried out every 100 iterations. Augmentations applied were identical to those used for disc localization.

We manually stopped training after 3561 iterations (during epoch 6), because the model had converged. The final validation accuracy was 97.2%. The mean accuracy on the test set was 95.43% and the mIoU was 0.88. An example of the ground truth and automatic result is presented in Figure 11.

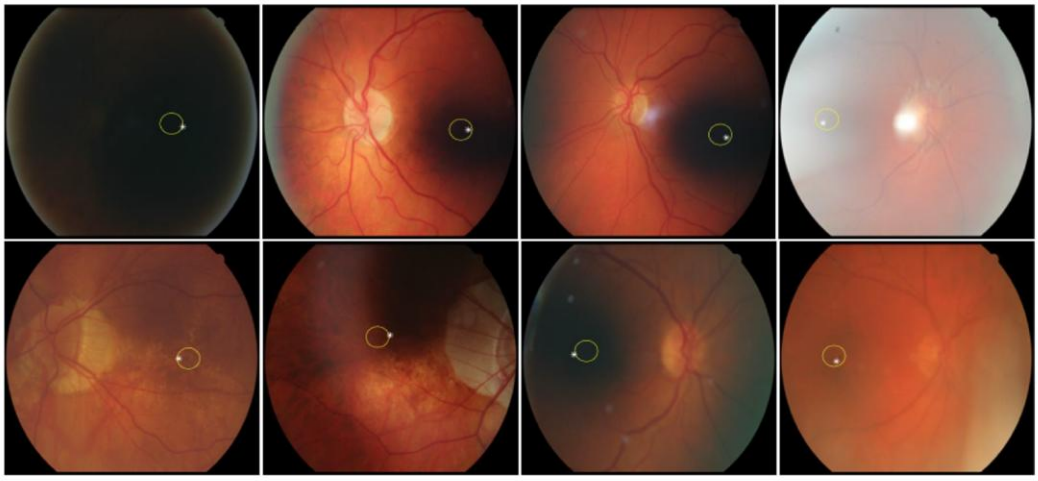

Figure 9. Fovea estimations in challenging images from the test set. The yellow circle represents the ground truth, and the asterisk is the prediction.

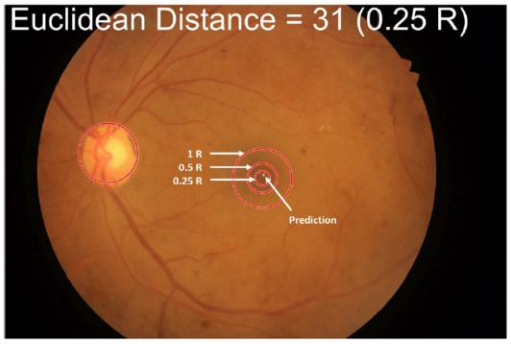


Figure 10. Both Euclidean distance and the 1R criterion were used to evaluate performance in the fovea detection network. The circular 1R grid is centered on the fovea. Image shown is from IDRiD.

## Generating Pallor Measures

To calculate pallor, the software took as input full-size color fundus photographs. In preprocessing, a 300-pixel border of zeros was added to the left and right sides of the image, and the whole image was resized to the median height of the training images (2166 pixels), while maintaining its aspect ratio. Adding the border prevented a cropping failure when the disc was close to or on the border, and resizing helped the model to generalize by ensuring that the input image was approximately equivalent in size to the images the network was trained on.

The disc localization network was used to locate the disc center. Then, the image was cropped to a size of 650 × 650 pixels, with the disc at the center. Next, disc segmentation was performed on the cropped image. Postprocessing of the predicted disc boundary involved keeping the largest object (where multiple objects were detected), filling holes (where holes were detected), and smoothing edges. Edge smoothing consisted of three stages: (1) morphological opening with a disc-shaped structuring element of radius 75, (2) blur with a two-dimensional convolution, and (3) rethreshold to a value of 0.5. (Edge smoothing algorithm taken directly from MATLAB user "Image Analyst", available at https://uk.mathworks.com/matlabcentral/answers/380687-how-to-smooth-rough-edges-along-a-binary-image).

We defined the measurement region as starting at the inner edge of the border tissue and extending a fixed distance of 30 pixels inward. We chose this distance through direct observation as a balance between capturing as much of the neuroretinal rim (NRR) as possible while avoiding the cup. We defined the control region as starting at the outer border of the cropped image and extending a fixed distance of 50 pixels inwards. We chose this distance through direct observation as a compromise between capturing as much of the retina as possible while avoiding the disc and any atrophy. Vessels were detected in the cropped

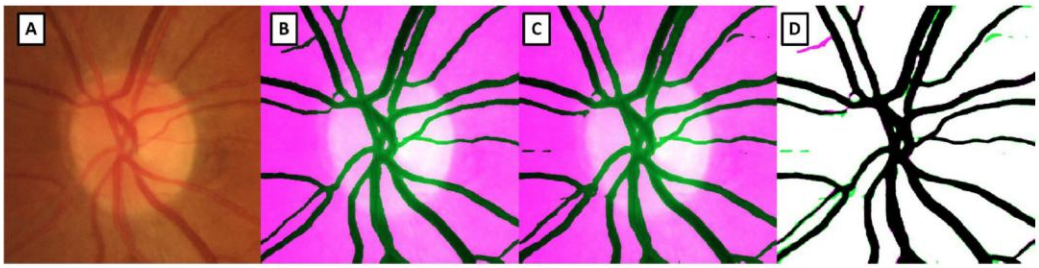


Figure 11. Vessel segmentation. (**A**) Input to the network, (**B**) ground truth, (**C**) automatic result, and (**D**) superposition of false-color image of ground truth and automatic result (false negative = green; false positive = magenta).

image and excluded (vessel pixels replaced with zero) from both the measurement region and the control region.

We then divided the measurement region into zones in accordance with the Heidelberg system for assessing pRNFL thickness. Specifically, the intersection of the optic disc–fovea axis and the measurement region took a value of zero degrees. The temporal zone then extended from 45° to −45°, the temporal inferior from 45° to 90°, and so on. The papillomacular bundle is a special case of the temporal zone, extending from 15° to −15°.

Finally, we calculated pallor based on the ratios of red and green pixel intensities[6,7,10,30,31] between the measurement and control regions. Specifically, we divided the mean of the green channel in the measurement zone by the mean of the red channel in the same zone. The result was then divided by the same measurement in the control region, except using the medians instead of the means. The result was a measure of pallor within each eye, for each zone.

## Statistical Analysis

Data from one eye are correlated with data from the fellow eye.[32] Shuang et al.[33] showed that ignoring this intereye correlation in standard regression models can lead to spurious conclusions. The authors suggest that linear mixed effects modelling with the eye as the unit of analysis should be used. Accordingly, we modelled a random intercept for each person and eye. We adjusted $P$ values for multiple comparisons with the false discovery rate procedure, which accounts for correlation between measurements. Statistical analysis was performed in R (version 4.2.1; www.R-project.org) using the lme4 and LmerTest packages.

To select covariates, we follow the dijunctive cause criterion,[34] which states that covariates should be added if they are causes of the exposure or outcome, or causes of both. Accordingly, the two retinal covariates are disc size and image brightness.

### Disc Size

The NRR must accommodate between 0.9 and 1.5 million retinal ganglion cell axons. In a large disc, the axons can spread out, whereas in a small disc they are more compact. This means that, theoretically, the larger the disc, the paler it will appear, and vice versa. Indeed, we found a correlation between disc size and global pallor ($R^2 = 0.11$).

### Brightness

We defined brightness as the median of all pixels inside the control region, after converting to greyscale, and removing vessels. Although the software controls for image brightness within each eye, light reflectance in the fundus is known to vary depending on the which part of the retina it strikes.[35] Specifically, the proportion of light reflected from the NRR and the background fundus may not remain constant with the level of light entering the pupil through the camera flash. Indeed, we found a correlation between brightness in the control region and global pallor ($R^2 = 0.12$).

## Interocular Variability

We assessed interocular differences in pallor for each zone and propose a new measure, namely, interocular pallor variability, defined as the sum of absolute differences from all six zones.

## Detecting Pallor in the RFMiD Dataset

We tested the results of our software on 92 images from the RFMiD dataset (images taken from the training set), one-half of which had been labelled as

optic disc pallor and one-half as disease risk = 0 by ophthalmologists from the RFMiD group. To assess group differences, we performed unpaired two-sampled Wilcoxon tests.

### Testing the Software for Robustness to Camera System, Format, and Resolution

Among different countries, clinics, and research institutions, there is considerable heterogeneity in the technical aspect of retinal fundus images, including (i) the camera (e.g., Topcon, Canon), (ii) image resolution and image size, and (iii) file format (e.g., JPG, PNG, TIFF). To test the resilience of our system to these factors, a dataset was constructed containing images captured by various imaging systems, with different resolutions and formats. In addition, details pertaining to the field of view, centering protocol, and dilation were also noted. We chose 5 sets of 10 images from a total of 4 datasets (G1020[36], MESSIDOR[37] PREVENT, and REFUGE[38]). All these datasets, except for PREVENT, are accessible publicly. The task focus was on whether images could be processed successfully, not on how the software copes with images of varying levels of quality. Accordingly, we selected images with sufficient quality (broadly even illumination, free of major pathology). We judged the results by visual inspection, according to whether the software correctly (a) located the fovea, (b) located and segmented the disc, (c) rotated the image along the optic disc-fovea axis, and (d) segmented the vessels. We also recorded the computation time for each batch to assess whether processing time differed by dataset.

### Developing a Set of Automatic Rejection Criteria

If there was insufficient information in an image to localize the disc or fovea, the image failed at the stage of processing. These images were usually very overexposed or underexposed (i.e., near totally white or black, respectively), or contained excessive blur. However, in most cases, the software processed the image, even when the quality was very low. To enable processing on large datasets, we aimed to develop a set of criteria through which such images could be rejected automatically. That is, although the images have been processed successfully, they are clearly not suitable for further analysis. For this task we used the LBC dataset, which contains images of varying levels of quality. We propose two automatic rejection criteria: disc eccentricity and control region brightness.

1. *Eccentricity* is the ratio of the distance between the center of an ellipse fitted onto the disc, and the major axis length, where 0 is a circle, and 1 is a line.
2. *Control region brightness* is the median of all pixels inside the control region, after converting to greyscale, and removing vessels.

By visual inspection, we aimed to develop conservative thresholds that would reject only the poorest quality images, or cases in which the software clearly failed for another reason (e.g., severe pathology).

## Results

The software takes less than 3 seconds to process a single image and outputs several key visualizations (Fig. 12) alongside tabular data.

### Quality Control and Sample Derivation

The sample derivation is illustrated in Figure 13. After quality control, concurrent fundus images and OCT scans were available for 118 participants (226 eyes). Three fundus images were rejected owing to segmentation error and low illumination (author S.G.; visual inspection) (Supplementary Fig. S1), and 13 OCT scans were excluded for reasons including clipping (4 images), improper centering (4 images), high myopia ($\leq -5$ diopters; 2 images), poor segmentation (3 images), poor illumination (1 image), and signs of pathology (5 images). Pathologies in OCT included epiretinal membrane, excessive peripapillary atrophy, and tilted discs. OCT quality control was carried out by C.H., an ophthalmic imager and analyst, via manual inspection of the images through the Heidelberg platform.

### Summary Statistics

Image characteristics are summarized in Table 3, alongside basic demographics. Histograms showed that pallor was normally distributed (Supplementary Fig. S2).

Pallor was highest temporally and lowest nasally. Mean pallor was lower when considering all zones in the measurement region (global pallor; $1.37 \pm 0.18$) than when considering the entire disc (mean, $1.43 \pm 0.2$). In all measurement zones, pallor was numerically higher in the left eye compared with the right eye. pRNFL was thickest in both polar zones (superiorly and inferiorly), which was in accordance with typical findings.[39] Unlike pallor, pRNFL was not systemati-

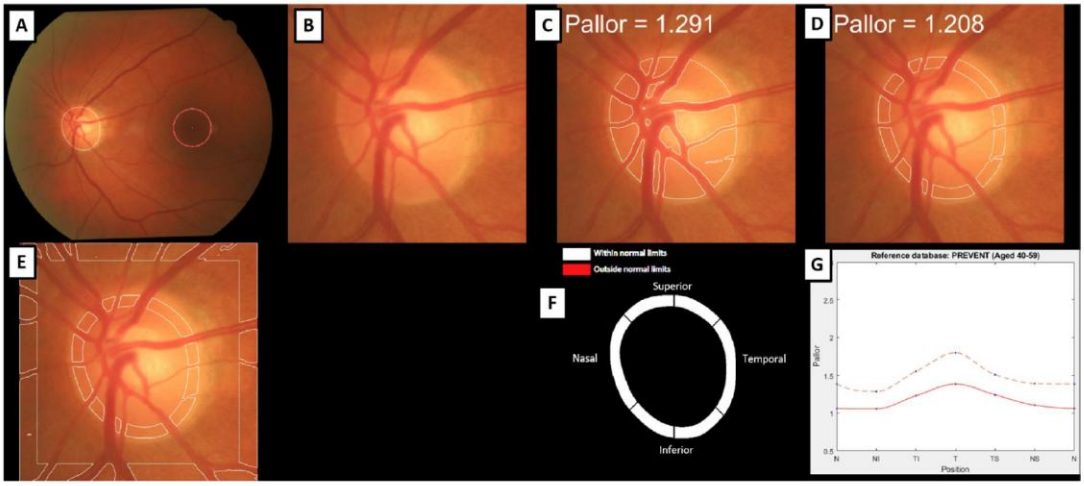


**Figure 12.** Core visualizations of the software. (**A**) Disc and fovea localization are used to rotate the image along the optic disc–fovea line. (**B**) Cropped optic disc. (**C**) Segmented disc excluding vessels. (**D**) Measurement region excluding vessels. (**E**) measurement and control region (outer square) excluding vessels. (**F**) Alert system (region lights up red if a limit is exceeded). (**G**) Dashed line represents 1 standard deviation above the mean of all participants in PREVENT, red line is the current participant.

cally different between the eyes. Boxplots of pallor and pRNFL by zone and eye are presented in Figure 14.

## Associations Between pRNFL Thickness and Pallor

After adjusting for age, sex, disc area, control region brightness, and multiple comparisons, we observed statistically significant associations between pRNFL thickness and pallor globally ($\beta = -9.81$; SE = 3.16; $P < 0.05$), in the temporal inferior zone ($\beta = -29.78$; SE = 3.32; $P < 0.01$), and with the nasal/temporal ratio ($\beta = 0.88$; SE = 0.34; $P < 0.05$). Pallor in the measurement region was more discriminative than pallor measured in the whole disc ($\beta = -8.22$; SE = 2.92; $P < 0.05$). We also found an association between pRNFL thickness and pallor in the temporal-superior zone ($\beta = -17.29$; SE = 7.83; $P < 0.05$); however, this significance did not survive correction for multiple comparisons. Results are summarized in Table 4.

## Interocular Pallor Variability

In the PREVENT dataset, data from both eyes were available for 108 participants. For global pallor, we measured a mean unit difference of 0.10 ± 0.07 between the eyes. To put this into context, global pallor ranges from 0.87 to 1.90. This result means that, although interocular difference is evident, measurements from one eye in a person are broadly similar to measurements from the fellow eye. We also observed differences between zones, for example, the greatest difference between the left and right eyes was observed in the temporal region (mean, 0.13 ± 0.1). The general pattern of pallor being high temporally and low nasally was preserved between the eyes (Fig. 15). In Figure 16 (right), pallor is higher in the right eye than the fellow eye in the nasal zone, but higher in the left eye than the fellow eye in the temporal zone. To capture this zone-to-zone variability, we take the sum of absolute differences from all six zones. By contrast, in Figure 16 (left), pallor is higher in all zones in the left eye.

## Assessing Pallor in the RFMiD Dataset

Of 92 images (46 pallor, 46 controls) in the RFMiD dataset (training set), which contained a patient group (diagnosed optic disc pallor) and healthy controls, the fovea localization module failed in one patient image and was subsequently rejected, despite accurate disc segmentation. Accordingly, analysis was carried out on 45 images labelled as pallor and 46 healthy controls.

Predicted pallor was substantially higher in the patient group compared with the control group for all zones. For example, the mean global pallor in the control group was 0.98 ± 0.09 compared with 1.23 ± 0.14 in the patient group, and this difference was statis-

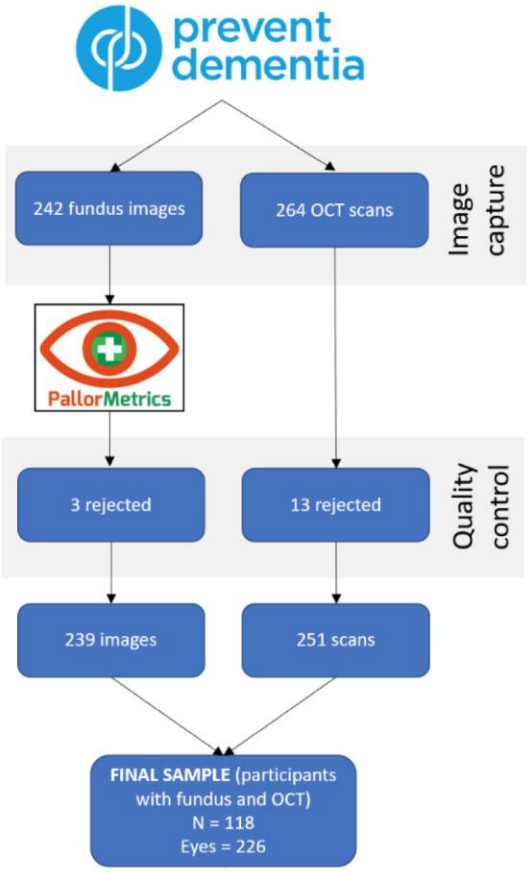


Figure 13. Sample derivation flowchart.

tically significant (Wilcoxon unpaired signed rank test: $W = 208$; $P < 10^{-11}$; $R = 0.73$) (Table 5). There was no evidence of significant difference in the nasal/temporal ratio between the groups (control group mean, 0.9 ± 0.07; patient group mean, 0.9 ± 0.05), reflecting the diffuse nature of pallor identified in the images. One example from each group is presented visually in Figure 17.

### Robustness to Camera System, Format, and Resolution

We tested the software on five different datasets (none of which were used in model development) containing images captured with five different camera systems (from three manufacturers), three different image formats, and resolutions ranging from 1634 × 1623 to 3072 × 2048. Judged by visual inspection, as per the criteria described in the Methods section, the methodology successfully processed all 50 images from all 5 datasets. Technical characteristics of the images are summarized in Table 6, and one example from each dataset is presented in Figure 18. Computation time was highest for the MESSIDOR dataset (2.9 seconds per image) and lowest for the REFUGE Canon dataset (2.5 seconds per image).

### Developing a Set of Automatic Rejection Criteria

Of 1584 images from the LBC dataset, 13 failed processing for reasons including excessive blur, optic disc outside field of view, and overexposure and underexposure. Rejection thresholds were set based on visual inspection of the remaining 1571 images. Using our best judgment, thresholds for rejecting images were set at greater than 0.65 for eccentricity at greater than 0.65 and less than 50 for brightness of the control region. Examples of images that exceed these thresholds are presented in Figure 19. Summary statistics for images exceeding the proposed thresholds for both LBC and PREVENT are summarized in Table 7.

## Discussion

We have presented a fully automatic method of quantifying optic disc pallor in color fundus photographs. In approximately 3 seconds per image, the software generates tabular data and visualizations capturing key measurements and summative properties. In particular, the software generates a global pallor metric, as well as metrics for seven zones, in accordance with the Spectralis OCT peripapillary scan. The software proved robust to camera system, image format, and resolution in our experiments and generates several metrics that can be used to filter out challenging or low-quality images, thereby allowing for application to large datasets.

In similar work, Yang et al.[30] developed a fully automatic pallor quantification system that operates on standard fundus photographs. However, their work has some limitations. For example, vasculature is included in their measurement region. This factor may be problematic, because vessel appearance is known to change with disease. For example, in hypertensive retinopathy, the arteriolar light reflex is accentuated,[40] in retinal vasculitis a white cuff is visible around vessels,[41] and, although rare, in lipemia retinalis, vessels appear creamy.[42] In addition, zones in Yang

**Table 3.** Demographics, Covariates, Pallor, and pRNFL Thickness in Microns by Zone and Eye

| | Eye | | |
|---|---|---|---|
| | Left | Right | Overall |
| *N* (participants) | | | 118 |
| *N* (eyes) | (*n* = 112) | (*n* = 114) | (*N* = 226) |
| Age, years | 51.5 ± 5.60 | 51.4 ± 5.67 | 51.4 ± 5.63 |
| Sex (female) | 68 (60.7) | 68 (59.6) | 136 (60.2) |
| Disc area | 75,300 ± 16,400 | 72,400 ± 14,500 | 73,900 ± 15,500 |
| Luminance | 93.1 ± 19.5 | 90.1 ± 18.8 | 91.6 ± 19.1 |
| Temporal | | | |
| Pallor | 1.62 ± 0.24 | 1.54 ± 0.22 | 1.58 ± 0.23 |
| RNFL | 69.3 ± 13.8 | 73.8 ± 13.1 | 71.6 ± 13.6 |
| RNFL missing | 5 (4.5) | 6 (5.3) | 11 (4.9) |
| Temporal inferior | | | |
| Pallor | 1.42 ± 0.19 | 1.34 ± 0.19 | 1.38 ± 0.19 |
| RNFL | 139 ± 19.7 | 141 ± 22.7 | 140 ± 21.2 |
| RNFL missing | 5 (4.5) | 6 (5.3) | 11 (4.9) |
| Nasal inferior | | | |
| Pallor | 1.16 ± 0.14 | 1.12 ± 0.14 | 1.14 ± 0.14 |
| RNFL | 113 ± 21.9 | 112 ± 22.1 | 113 ± 22.0 |
| RNFL missing | 5 (4.5) | 6 (5.3) | 11 (4.9) |
| Nasal | | | |
| Pallor | 1.25 ± 0.16 | 1.19 ± 0.15 | 1.22 ± 0.18 |
| RNFL | 74.7 ± 16.2 | 76.9 ± 18.9 | 75.8 ± 17.6 |
| RNFL missing | 6 (5.4) | 7 (6.1) | 13 (5.8) |
| Nasal superior | | | |
| Pallor | 1.27 ± 0.16 | 1.20 ± 0.15 | 1.23 ± 0.16 |
| RNFL | 111 ± 18.9 | 98.6 ± 18.8 | 105 ± 19.8 |
| RNFL missing | 6 (5.4) | 7 (6.1) | 13 (5.8) |
| Temporal superior | | | |
| Pallor | 1.36 ± 0.19 | 1.30 ± 0.18 | 1.33 ± 0.19 |
| RNFL | 135 ± 17.3 | 135 ± 16.9 | 135 ± 17.0 |
| RNFL missing | 5 (4.5) | 6 (5.3) | 11 (4.9) |
| PMB | | | |
| Pallor | 1.68 ± 0.25 | 1.59 ± 0.23 | 1.63 ± 0.25 |
| RNFL | 53.9 ± 13.1 | 55.6 ± 9.04 | 54.7 ± 11.2 |
| RNFL missing | 6 (5.4) | 9 (7.9) | 15 (6.6) |
| Global | | | |
| Pallor | 1.41 ± 0.18 | 1.34 ± 0.17 | 1.37 ± 0.18 |
| RNFL | 98.1 ± 8.03 | 98.2 ± 8.12 | 98.2 ± 8.06 |
| RNFL missing | 6 (5.4) | 7 (6.1) | 13 (5.8) |
| Nasal/temporal ratio | | | |
| Pallor | 0.77 ± 0.07 | 0.78 ± 0.08 | 0.78 ± 0.07 |
| RNFL | 1.13 ± 0.34 | 1.08 ± 0.36 | 1.10 ± 0.35 |
| RNFL missing | 7 (6.3) | 10 (8.8) | 17 (7.5) |
| Whole disc | | | |
| Pallor | 1.46 ± 0.201 | 1.39 ± 0.185 | 1.43 ± 0.196 |

Values are mean ± SD or number (%).
PMB, papillomacular bundle.

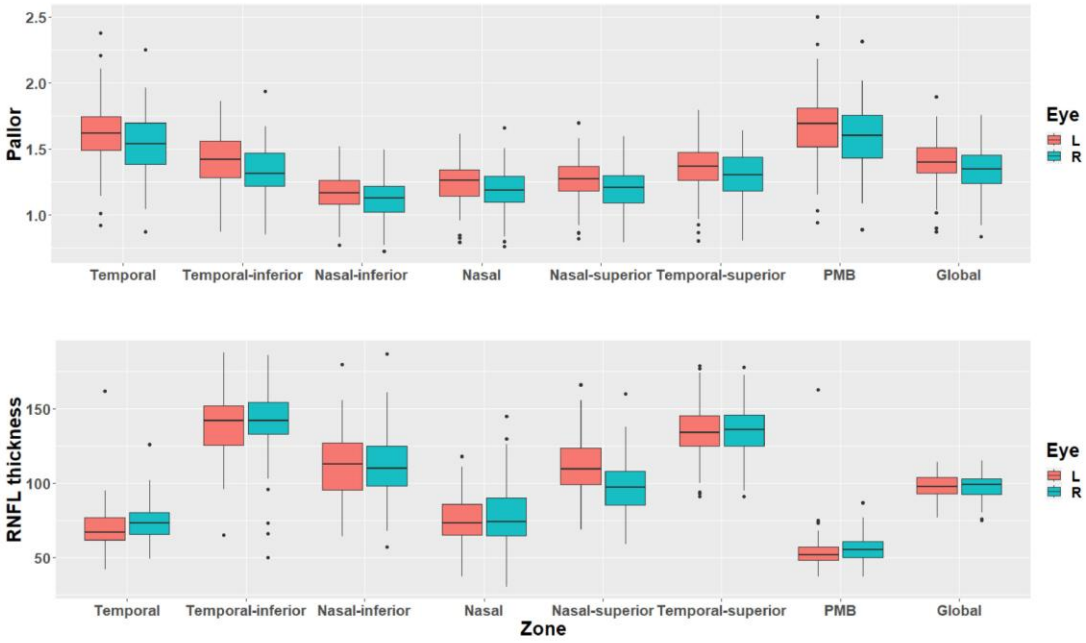


Figure 14. Boxplots representing pallor and pRNFL thickness values by zone and eye. $N = 118$ (114 right eyes, 112 left eyes).

et al.'s work (clock-hour locations) were not defined by their spatial relation to the fovea, making it difficult to compare measurements accurately across different images or to make sectoral comparisons to OCT. Our approach addresses these limitations by (a) detecting vessels and excluding them from both the measurement and control region and (b) rotating the image along the optic disc–fovea axis before analysis.

In other similar work, Gonzalez-Hernandez et al.[31] developed a fully automated system to assess hemoglobin content in the optic disc (Laguna-ONhE; Optic Nerve Head Evaluation), which partly explains pallor. As with Yang et al.'s system, the Laguna software did not define the measurement zone in relation to the fovea. However, unlike Yang et al. and the current study, Laguna does attempt to segment the optic cup. Although this strategy carries the advantage of capturing the entire NRR (where possible), it may fail when the cup is not visible, which is often the case in fundus photographs. Indeed, numerous studies show that segmenting the cup is difficult,[4,27,43,44] although recent work has been more successful[45]; moreover, it is difficult to establish ground truth given interobserver variability in locating the extent of optic disc cupping. For this reason, we chose instead to define the measurement region in accordance with Yang et al. at a fixed distance inward from the disc margin, sacrificing potential accuracy for robustness.

We investigated the relationship between pallor and pRNFL thickness in participants for whom concurrent data were available. Controlling for age, sex, disc area, control region brightness, and multiple comparisons, we found statistically significant associations between pallor and global pRNFL thickness, with a significant association also observed in the temporal-inferior and temporal-superior zones and in the temporal-nasal ratio. pRNFL thinning (as measured with OCT) is associated with several negative health outcomes, including glaucoma,[46] increased cardiovascular risk,[47] Alzheimer's disease, mild cognitive impairment,[48] future cognitive decline,[49] increased risk of dementia,[50] small vessel disease,[51] and stroke.[52] However, OCT is not yet widely available. Our approach generates measures of disc pallor that are associated with pRNFL thickness from simple color fundus photographs, which are much more widely available, potentially enabling the detection and monitoring of the progression of diseases that involve pRNFL loss with this imaging technology.

**Table 4.** Linear Mixed Effects Regression Models of pRNFL Thickness Predicted by Pallor in Equivalent Zones

| | Coefficients | | |
|---|---|---|---|
| Zone | *β (SE)* | *P* Value | *P* Value (Adjusted for FDR) |
| Global | −9.81 (3.16) | 0.002** | 0.011* |
| Temporal | −2.89 (4.68) | 0.538 | 0.724 |
| Temporal-inferior | −29.78 (8.32) | 0.000*** | 0.004** |
| Nasal-inferior | 5.92 (13.09) | 0.652 | 0.724 |
| Nasal | −4.7 (9.2) | 0.610 | 0.724 |
| Nasal-superior | −7.92 (9.85) | 0.422 | 0.704 |
| Temporal-superior | −17.29 (7.83) | 0.028* | 0.057 |
| PMB | −0.03 (3.72) | 0.994 | 0.994 |
| Global pRNFL ~ pallor in whole disc | −8.22 (2.92) | 0.005** | 0.018* |
| Nasal-temporal ratio | 0.88 (0.34) | 0.011* | 0.028* |

Random intercepts are modelled for each subject and eye. Models are adjusted for age, sex, disc area, and image brightness.
*$P < 0.05$.
**$P < 0.01$.
***$P < 0.001$.
FDR, false discovery rate; PMB, papillomacular bundle.

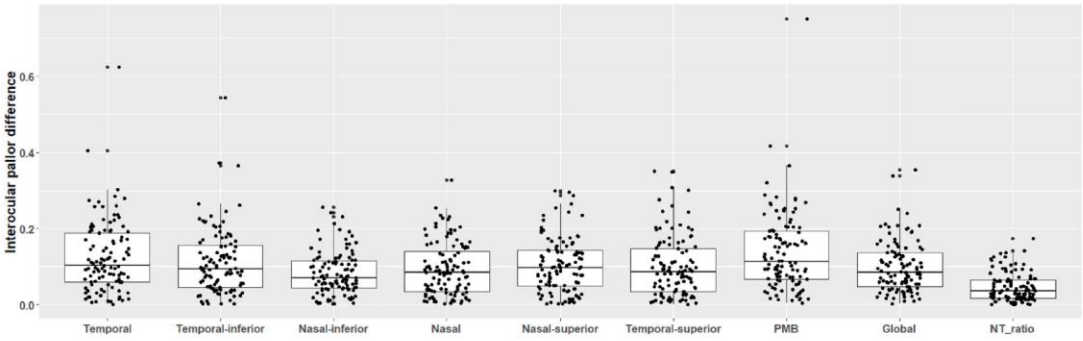


**Figure 15.** Boxplots representing the difference in pallor between the eyes of a participant ($N = 108$).

Aside from its association with pRNFL thickness, the ability to quantify pallor may have additional value in differentiating the etiology of structural changes to the optic nerve head; for example, in differentiating glaucomatous and nonglaucomatous optic neuropathy. Although pRNFL thinning is seen in both conditions, cupping rather than pallor is typical of glaucomatous optic neuropathy, and the presence of clinically apparent pallor often triggers investigations for nonglaucomatous causes, including potential magnetic resonance imaging of the anterior visual pathway.[6,53]

In all zones, pallor was slightly lower in the right eye compared with the left eye, and this finding largely corresponded with pRNFL thickness measured in equivalent zones. This observation is in agreement with other studies that found the RNFL to be consistently thicker in the right eye.[54–57] Cameron et al.[58] discussed the importance of interocular symmetry in health and disease, pointing out that the emergence of asymmetry may alert the ophthalmologist that glaucoma should be considered. Further, they review several studies that attempt to create thresholds for when RNFL asymmetry may be clinically meaningful for glaucoma diagnosis and progression. This observation further suggests that our measure of symmetry (interocular pallor variability), may find usefulness in glaucoma detection and diagnosis.

Another important use case for the software could be the identification, monitoring and progression of

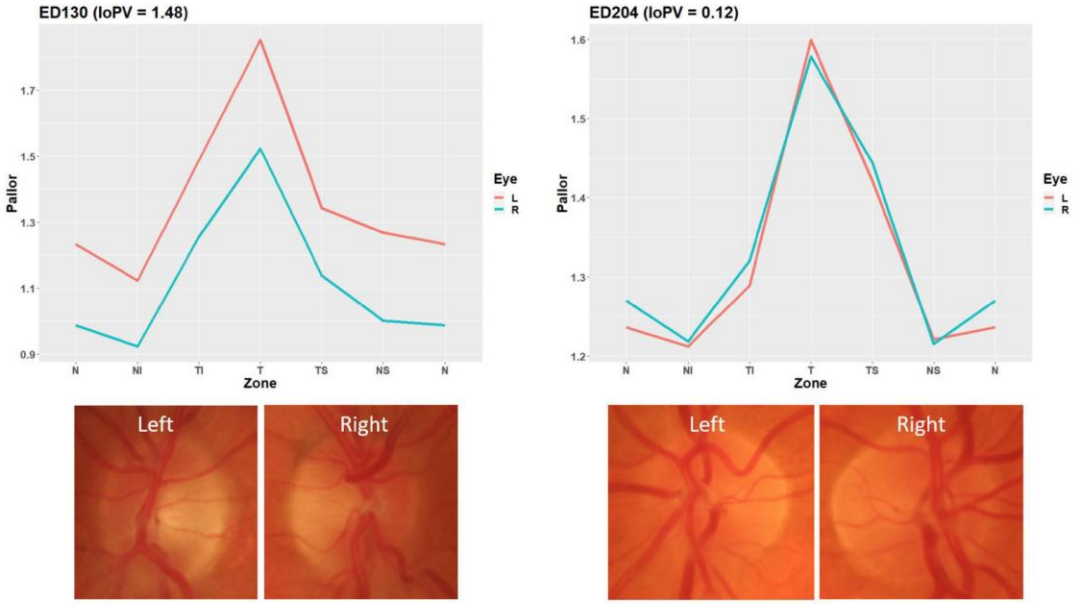


**Figure 16.** Parallel plots from two participants showing interocular differences in pallor by zone (nasal pallor is repeated on either side of each plot for aesthetics). I, inferior; IoPV, interocular pallor variability; N, nasal; S, superior; T, temporal.

**Table 5.** Unpaired Wilcoxon Signed Rank Test Results Comparing Eyes Labelled as Having Pallor vs Controls in the RMFiD Dataset

| Zone | Group, Mean ± SD | | Wilcoxon Test | | |
|---|---|---|---|---|---|
| | Control | Pallor | *W* | *P Value* | *R* (Effect Size) |
| Temporal | 1.06 ± 0.12 | 1.32 ± 0.15 | 195 | $<10^{-10}$ | 0.7 |
| Temporal-inferior | 0.95 ± 0.09 | 1.2 ± 0.13 | 118 | $<10^{-12}$ | 0.76 |
| Nasal-inferior | 0.91 ± 0.09 | 1.15 ± 0.13 | 143 | $<10^{-11}$ | 0.74 |
| Nasal | 0.95 ± 0.1 | 1.18 ± 0.14 | 161 | $<10^{-11}$ | 0.73 |
| Nasal-superior | 0.93 ± 0.09 | 1.14 ± 0.13 | 176 | $<10^{-11}$ | 0.72 |
| Temporal-superior | 0.97 ± 0.1 | 1.24 ± 0.15 | 151 | $<10^{-11}$ | 0.74 |
| PMB | 1.08 ± 0.12 | 1.34 ± 0.16 | 208 | $<10^{-10}$ | 0.69 |
| Global | 0.98 ± 0.09 | 1.23 ± 0.14 | 164 | $<10^{-11}$ | 0.73 |
| Global pRNFL ~ whole disc pallor | 1.03 ± 0.11 | 1.26 ± 0.15 | 217 | $<10^{-10}$ | 0.68 |
| Nasal-temporal ratio | 0.9 ± 0.07 | 0.9 ± 0.05 | 1063 | 0.82 | 0.02 |

Note: We chose not to correct for multiple comparisons here owing to the very low *P* values.
PMB, papillomacular bundle; SD, standard deviation of the mean.

compressive optic neuropathy, whereby a compressive lesion anywhere along the optic nerve or anterior visual pathway (anterior to the lateral geniculate body) causes axons to die, resulting in optic atrophy/pallor.[59] The ability to quantify sectoral pallor may provide additional value. For example, compression to the optic chiasm can cause pallor in the temporal and nasal zones—a condition known as band or bow tie atrophy.[60] Therefore, the pattern of optic disc pallor may further help localization of the lesion. Of particular relevance may be the detection of optic pathway gliomas (OPGs), which predominantly affect children (mean age at presentation, 8.8 years).[61] Assessment of vision is crucial in diagnosis; however, young children

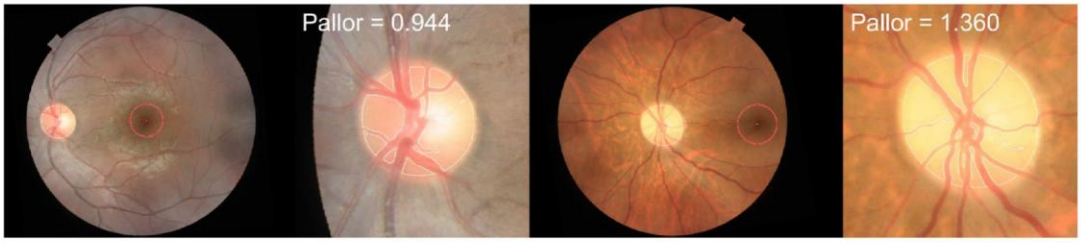


**Figure 17.** Intermittent stages of the pallor software on two images from the RFMiD dataset, one diagnosed by two ophthalmologists as having optic disc pallor (*right*) and a healthy control (*left*).

**Table 6.** Technical Characteristics of the Datasets Used to Assess How the Software Deals With Images Captured With a Range of Different Camera Systems, Resolutions, and Formats

| Dataset | Format | Camera | Resolution | FOV | Centering | Dilation | Computation Time per Image (Seconds) |
|---|---|---|---|---|---|---|---|
| G1020 | JPG | Topcon TRC-NW8 | Between 1944 × 2108 and 2426 × 3007 | 45° | Mixed | Yes | 2.8 |
| MESSIDOR | TIFF | Topcon TRC-NW6 | 2240 × 1488 | 45° | Mixed | Yes | 2.9 |
| PREVENT (follow-up images) | BMP | Canon CR-Dgi | 3072 × 2048 | 45° | Posterior pole | No | 2.7 |
| REFUGE (Canon) | JPG | Canon CR-2 | 1634 × 1634 | – | Posterior pole | – | 2.5 |
| REFUGE (Zeiss) | JPG | Zeiss Visucam 500 | 2124 × 2056 | – | Posterior pole | – | 2.6 |

FOV, field of view.

will often not complain of vision loss, and instead present at a later stage with headache or pain.[62] Given that disc pallor is present in approximately 60% of cases,[61,62] it is feasible that OPG could be detected automatically through routine fundus imaging, which is not typically viewed by an ophthalmologist. Further research should investigate the association between optic disc pallor, as measured with the current software, and various types of compressive optic neuropathy.

Disc pallor is also an important measure of chemotherapy success in pediatric OPGs,[63] with the authors suggesting that the degree of pallor could be important. Indeed, complementary work investigating the visual outcomes of childhood OPG treated with radiotherapy found that severe disc pallor (compared with mild) at diagnosis or follow-up may be associated with a negative prognosis.[64] Further work could reevaluate such existing studies, substituting clinical notes on pallor for the continuous measures generated by our software (depending on the availability of fundus images). However, care should be taken if investigating changes in pallor, because it rarely improves[63]; therefore, the direction of change will almost always be one way.

OCT is the gold standard for assessing RNFL loss. However, compared with fundus, imaging it is costly, requires greater operator training, and is less prevalent. Furthermore, to avoid movement artefacts to which OCT is prone, such as those cause by ocular saccades, blinks, changes in head position, or respiratory movements,[65] patients must maintain a steady focus on a fixed point for several tens of seconds. Therefore, obtaining a high-quality OCT can be particularly challenging in individuals who may struggle with prolonged focus and steadiness, such as children,[66] the

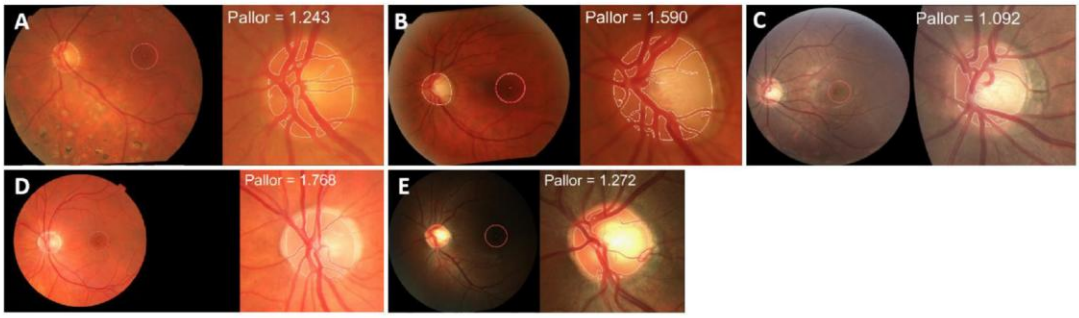


**Figure 18.** Robustness to camera system, format, and resolution results. (**A**) G1020, (**B**) MESSIDOR, (**C**) REFUGE Canon, (**D**) MESSIDOR, and (**E**) REFUGE Zeiss. Image to the left shows disc segmentation and fovea localization in the whole image, image to the right shows disc segmentation in closer detail. Pallor value shown is for the whole disc.

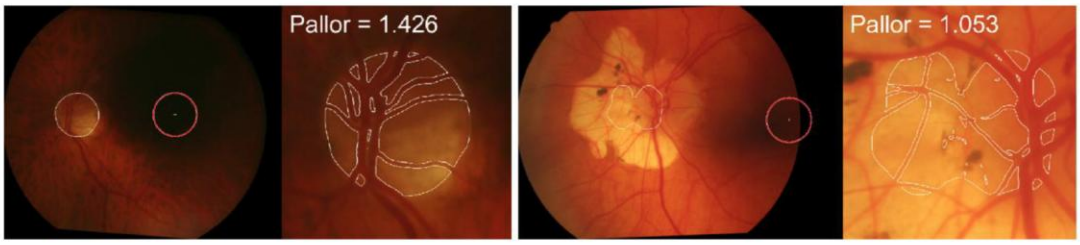


**Figure 19.** Automatic image rejection based on exceeding set thresholds for luminance (left) and eccentricity (right). We acknowledge that the image to the right was a failure of the software to correctly identify the disc margin owing to excessive chorioretinal atrophy.

**Table 7.** Automatic Image Rejection Thresholds

| Criterion | Threshold | LBC | | PREVENT | |
|---|---|---|---|---|---|
| | | Mean ± SD | Images Over Threshold (*n*, %) | Mean ± SD | Images Over Threshold (*n*, %) |
| Eccentricity | >0.65 | 0.39 ± 0.11 | 22 (1.4) | 0.4 ± 0.1 | 2 (0.6) |
| Luminance | <50 | 110.21 ± 26.24 | 18 (1.15) | 90.56 ± 18.62 | 9 (2.85) |

SD, standard deviation.

frail elderly, or those with movement disorders. Owing to the speed of acquisition, fundus imaging is more likely to be successful in these groups. Pallor derived from fundus photographs could provide an indicator that further examination is required, and could be a good alternative in groups where OCT scanning is not feasible.

Strengths of the current study included the networks' ability to segment the optic disc to the inner edge of the border tissue accurately. The disc margin is marked differently depending on the imaging modality through which it is observed. In OCT, the margin is marked at Bruch's membrane opening,[20] whereas in clinical ophthalmoscopy and fundus photography, it is defined as the inner edge of the border tissue.[20] There are many deep learning–based disc segmentation algorithms (for a review see Hasan et al.[28]); however, most systems are trained on one or more of four open-source image sets, namely IDRiD, RIMONE, DRISHTI-GS,[67] and DRIVE.[68] This factor may be problematic for our requirement, because, on close inspection of ground truth segmen-

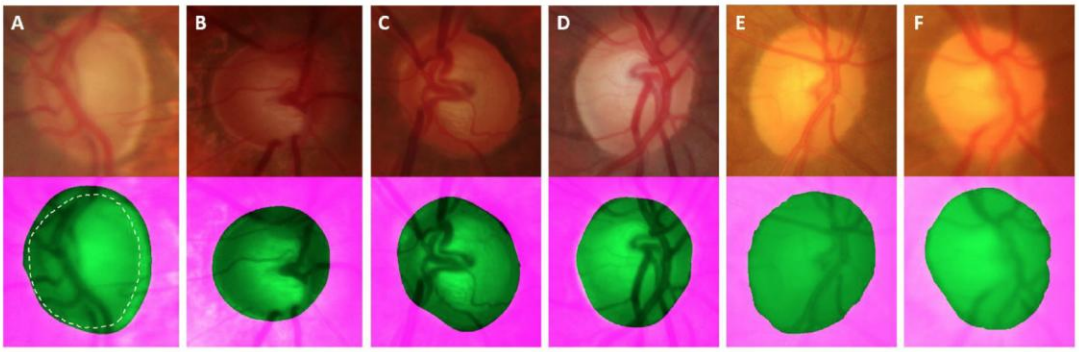


**Figure 20.** Examples from RIM ONE (glaucoma = **A**–**B**, nonglaucoma = **C**–**D**) and IDRiD (**E**–**F**), where the disc margin is overestimated according to a clinical definition. The ground truth (according to the original annotations) is marked in pink. The dashed line in (**A**) represents where we perceive the margin to be. In (**A**), the space between the dashed line and the start of the pink represents label noise.

tations in IDRiD and RIMONE, we observed a noticeable departure from what we perceived to be the clinically defined margin (Fig. 20). We believe this could be the result of averaging multiple annotations from different individuals to arrive at a ground truth, in which there is considerable disagreement. Such disagreements may have arisen owing to the annotators either marking the boundary clinically, or inferring Bruch's membrane opening–based information, for example, the bend of vessels at the rim. Although disagreement between multiple annotators provides an important measure of confidence that must be considered when assessing an automatic system, averaging multiple annotations can lead to label noise.

A recent study on label noise in medical image segmentation demonstrated that, although state-of-the-art networks are somewhat robust to unbiased or random noise, they are sensitive to biased noise.[69] Indeed, we observed that RIMONE and IDRiD may contain biased noise, whereby the clinically defined disc boundary is overestimated systematically with respect to where we perceive the clinical margin to lie. It is, therefore, possible that deep learning–based models trained on these datasets will systematically overestimate the clinically defined boundary. The significance of this factor for automatic segmentation programs would depend on the application. For example, the VAMPIRE software,[70] which is concerned with obtaining vessel-based measurements, requires that the disc be estimated as a best fit ellipse, in which case the precise boundary is less important. However, our work required greater precision, because sharp changes in color at the border would erroneously affect pallor metrics. Another use case that may benefit from a more precisely defined disc margin is measuring the cup to disc ratio/profile in glaucoma,[71] because an overestimated rim could erroneously widen the profile, leading to a false positive (missing glaucoma).

Another strength of the current study is the robustness of the fovea detection network, which, in our experiments, gives good estimates even for very challenging images (Fig. 9). Additionally, locating the fovea helps the software to determine which eye (left or right) is being processed and allows for accurate zone placement. Last, the study had the advantage of using mixed effects modelling, which enabled the use of data from both eyes, thereby increasing statistical power.

The current study has several limitations. First, disc appearance is affected by physiological factors, chiefly the media opacity of the lens, but also potentially the richness of the capillary net supplying the optic nerve. Lens status was not available for the patients included in our study; therefore, we could not distinguish the pallor caused by optic atrophy from pseudopallor (nonpathological paleness, most notably caused by cataract extraction).[2] Further validation work should be carried out to assess the extent to which the current pallor metrics are affected by worsening cataract and cataract removal. In the meantime, information on cataract status and other potential causes of pseudopallor should be included as covariates where possible, particularly with older individuals. With regard to perfusion, in future studies it would be interesting to examine the relationship between OCT angiography measures of vessel density and pallor measured using the software to determine whether density of the capillary net might be a confound-

ing factor in grading pallor, or if the software could potentially be useful for evaluating changes to the optic nerve head caused by reduced optic nerve head perfusion.

Another limitation is that pallor quantification was affected somewhat by the brightness of the control region (which itself is largely determined by pigmentation—a factor that varies among individuals. To overcome this issue, we added control region brightness as a covariate in all statistical models. Although this approach may be acceptable for research studies with multiple participants, for clinical insight into a single image, normative data with a wide range of relevant parameters would be required to determine the extent to which pigmentation affects the measure.

With regard to peripapillary atrophy, we selected the control region to include as much of the background retina as possible, while minimizing the inclusion of any atrophy. Further, we used median values when calculating the overall control region brightness, which helped to mitigate the effect of any included atrophy. However, if the control region of an image contains a significant portion of atrophy, the image should be rejected, because the pallor metrics may be unreliable (there were no such cases in the PREVENT dataset).

Another limitation is that three of the four networks (disc localization and segmentation, and fovea localization) were partly trained on PREVENT images. This overlap calls into question the generalizability of the software. However, we point to internal (test set) and external testing carried out on all three networks, which show excellent generalizability. Nonetheless, further research should aim to replicate the finding that disc pallor is associated with pRNFL thickness in a novel dataset.

A final limitation was the lack of association between pRNFL thickness and pallor in five of the seven zones. In similar work, but using clinical notes (e.g., pallor absent/present), Aleman et al.[5] observed that the association between pallor and pRNFL thickness is optimal only when significant thinning has occurred. This may help explain the lack of associations in five zones in the current study, as participants in the PREVENT cohort are relatively healthy; global mean pRNFL was thick (98.2 ± 8.3 µm) in comparison with normative data (90 µm in Whites[72] and 94 µm in a multiethnic cohort),[72] although thinner than in individuals from Ghana (102 µm).[73]

Further research should aim to replicate the current findings in a larger sample, generate normative data, and test for associations with cardiovascular risk factors and disease.

## Conclusions

A pale disc indicates irreversible damage to the anterior visual pathway and is present in numerous diseases. We present an automatic, artificial intelligence–enabled method that is fast, easy to use, robust, and suitable for application to large datasets. We found associations between pallor and pRNFL thickness, suggesting that disc pallor derived from fundus photographs may act as a proxy for pRNFL. We think our method will be useful for the identification and monitoring of the progression of diseases characterized by disc pallor and optic atrophy, including glaucoma, compression, and potentially in neurodegenerative disorders.

## Acknowledgments

The authors thank all the PREVENT-Dementia participants for kindly donating their time.

Supported by the UK Biotechnology and Biological Sciences Research Council EASTBIO Doctoral Training Programme.

Disclosure: **S. Gibbon**, None; **G. Muniz-Terrera**, None; **F.S.L. Yii**, None; **C. Hamid**, None; **S. Cox**, None; **I.J.C. Maccormick**, None; **A.J. Tatham**, None; **C. Ritchie**, None; **E. Trucco**, None; **B. Dhillon**, None; **T.J. MacGillivray**, None

## References

1. Ahmad SS, Kanukollu VM. Optic Atrophy. In: *StatPearls*. St Petersburg, FL: StatPearls Publishing; 2022. Accessed August 29, 2022. http://www.ncbi.nlm.nih.gov/books/NBK559130/.
2. Osaguona VB. Differential diagnoses of the pale/white/atrophic disc. *Community Eye Health*. 2016;29(96):71–74..
3. Ahmad SS, Kanukollu VM. Optic atrophy. *Handbook of Pediatric Retinal OCT and the Eye-Brain Connection*. Ner York: Elsevier; 2022:292–295, doi:10.1016/B978-0-323-60984-5.00064-0.
4. O'Neill EC, Danesh-Meyer HV, Kong GXY, et al. Optic disc evaluation in optic neuropathies: the optic disc assessment project. *Ophthalmology*. 2011;118(5):964–970, doi:10.1016/j.ophtha.2010.09.002.
5. Aleman TS, Huang J, Garrity ST, et al. Relationship between optic nerve appearance and retinal nerve fiber layer thickness as explored with spec-

tral domain optical coherence tomography. *Transl Vis Sci Technol*. 2014;3(6):4, doi:10.1167/tvst.3.6.4.

6. Ramm L, Schwab B, Stodtmeister R, et al. Assessment of optic nerve head pallor in primary open-angle glaucoma patients and healthy subjects. *Curr Eye Res*. 2017;42(9):1313–1318, doi:10.1080/02713683.2017.1307415.
7. Vilser W, Nagel E, Seifert BU, Riemer T, Weisensee J, Hammer M. Quantitative assessment of optic nerve head pallor. *Physiol Meas*. 2008;29(4):451–457, doi:10.1088/0967-3334/29/4/003.
8. Assad A, Caprioli J. Digital image analysis of optic nerve head pallor as a diagnostic test for early glaucoma. *Graefes Arch Clin Exp Ophthalmol*. 1992;230(5):432–436, doi:10.1007/BF00175928.
9. Nakano E, Hata M, Oishi A, et al. Quantitative comparison of disc rim color in optic nerve atrophy of compressive optic neuropathy and glaucomatous optic neuropathy. *Graefes Arch Clin Exp Ophthalmol*. 2016;254(8):1609–1616, doi:10.1007/s00417-016-3366-2.
10. Kang S, Kim US. Using ImageJ to evaluate optic disc pallor in traumatic optic neuropathy. *Korean J Ophthalmol KJO*. 2014;28(2):164–169, doi:10.3341/kjo.2014.28.2.164.
11. Ritchie CW, Ritchie K. The PREVENT study: a prospective cohort study to identify mid-life biomarkers of late-onset Alzheimer's disease. *BMJ Open*. 2012;2(6):e001893, doi:10.1136/bmjopen-2012-001893.
12. Ritchie CW, Ritchie K. The PREVENT study: a prospective cohort study to identify mid-life biomarkers of late-onset Alzheimer's disease. *BMJ Open*. 2012;2(6):e001893, doi:10.1136/bmjopen-2012-001893.
13. Taylor AM, Pattie A, Deary IJ. Cohort profile update: the Lothian birth cohorts of 1921 and 1936. *Int J Epidemiol*. 2018;47(4):1042–1060, doi:10.1093/ije/dyy022.
14. Zhang Z, Yin FS, Liu J, et al. ORIGA(-light): an online retinal fundus image database for glaucoma analysis and research. *2010 Annual International Conference of the IEEE Engineering in Medicine and Biology*, Buenos Aires, Argentina. 2010;2010:3065–3068, doi:10.1109/IEMBS.2010.5626137.
15. Jin K, Huang X, Zhou J, et al. FIVES: a fundus image dataset for artificial intelligence based vessel segmentation. *Sci Data*. 2022;9(1):475, doi:10.1038/s41597-022-01564-3.
16. Fumero F, Alayon S, Sanchez JL, Sigut J, Gonzalez-Hernandez M. RIM-ONE: an open retinal image database for optic nerve evaluation. In: *2011 24th International Symposium on Computer-Based Medical Systems (CBMS)*. 2011:1–6, doi:10.1109/CBMS.2011.5999143.
17. Porwal P, Pachade S, Kamble R, et al. Indian Diabetic Retinopathy Image Dataset (IDRiD): a database for diabetic retinopathy screening research. *Data*. 2018;3(3):25, doi:10.3390/data3030025.
18. Pachade S, Porwal P, Thulkar D, et al. Retinal fundus multi-disease image dataset (RFMID): A dataset for multi-disease detection research. *Data*. 2021;6(2):1–14, doi:10.3390/data6020014.
19. Strouthidis N, Yang H, Reynaud J, et al. Comparison of clinical and spectral domain optical coherence tomography optic disc margin anatomy. *Invest Ophthalmol Vis Sci*. 2009;50(10):4709–4718, doi:10.1167/iovs.09-3586.
20. Chauhan BC, Burgoyne CF. From clinical examination of the optic disc to clinical assessment of the optic nerve head: a paradigm change. *Am J Ophthalmol*. 2013;156(2):218–227.e2, doi:10.1016/j.ajo.2013.04.016.
21. Yang F, Zamzmi G, Angara S, et al. Assessing inter-annotator agreement for medical image segmentation. *IEEE Access Pract Innov Open Solut*. 2023;11:21300–21312, doi:10.1109/access.2023.3249759.
22. Minaee S, Boykov Y, Porikli F, Plaza A, Kehtarnavaz N, Terzopoulos D. Image segmentation using deep learning: a survey. *IEEE Trans Pattern Anal Mach Intell*. 2022;44(7):3523–3542, doi:10.1109/TPAMI.2021.3059968.
23. Chen LC, Zhu Y, Papandreou G, Schroff F, Adam H. Encoder-decoder with Atrous separable convolution for semantic image segmentation. *Proceedings of the European Conference on Computer Vision (ECCV). arXiv*. 2018;1802.02611. Published online August 22, 2018, doi:10.48550/arXiv.1802.02611.
24. Sandler M, Howard A, Zhu M, Zhmoginov A, Chen LC. MobileNetV2: inverted residuals and linear bottlenecks. *arXiv*. 2019;1801.04381 [cs.CV]. Published online March 21, 2019, doi:10.48550/arXiv.1801.04381.
25. Chollet F. Xception: deep learning with depthwise separable convolutions. *arXiv*. 2017;1610.02357 [cs.CV]. Published online April 4, 2017, doi:10.48550/arXiv.1610.02357.
26. Deng J, Dong W, Socher R, Li LJ, Li K, Fei-Fei L. ImageNet: a large-scale hierarchical image database. In: *2009 IEEE Conference on Computer Vision and Pattern Recognition*. 2009:248–255, doi:10.1109/CVPR.2009.5206848.

27. Yu S, Xiao D, Frost S, Kanagasingam Y. Robust optic disc and cup segmentation with deep learning for glaucoma detection. *Comput Med Imaging Graph*. 2019;74:61–71, doi:10.1016/j.compmedimag.2019.02.005.
28. Hasan MdK, Alam MdA, Elahi MdTE, Roy S, Martí R. DRNet: Segmentation and localization of optic disc and Fovea from diabetic retinopathy image. *Artif Intell Med*. 2021;111:102001, doi:10.1016/j.artmed.2020.102001.
29. Al-Bander B, Al-Nuaimy W, Williams BM, Zheng Y. Multiscale sequential convolutional neural networks for simultaneous detection of fovea and optic disc. *Biomed Signal Process Control*. 2018;40:91–101, doi:10.1016/j.bspc.2017.09.008.
30. Yang HK, Oh JE, Han SB, Kim KG, Hwang JM. Automatic computer-aided analysis of optic disc pallor in fundus photographs. *Acta Ophthalmol (Copenh)*. 2019;97(4):e519–e525, doi:10.1111/aos.13970.
31. Gonzalez-Hernandez M, Gonzalez-Hernandez D, Perez-Barbudo D, Rodriguez-Esteve P, Betancor-Caro N, de la Rosa MG. Fully automated colorimetric analysis of the optic nerve aided by deep learning and its association with perimetry and oct for the study of glaucoma. *J Clin Med*. 2021;10(15):3231, doi:10.3390/jcm10153231.
32. MacGillivray TJ, Cameron JR, Zhang Q, et al. Suitability of UK Biobank Retinal Images for Automatic Analysis of Morphometric Properties of the Vasculature. *PLoS One*. 2015;10(5):e0127914, doi:10.1371/JOURNAL.PONE.0127914.
33. Shuang YG, Maguire MG, Glynn R, Rosner B. Tutorial on biostatistics: linear regression analysis of continuous correlated eye data. *Ophthalmic Epidemiol*. 2017;24(2):130–140, doi:10.1080/09286586.2016.1259636.
34. VanderWeele TJ. Principles of confounder selection. *Eur J Epidemiol*. 2019;34(3):211–219, doi:10.1007/s10654-019-00494-6.
35. Berendschot TTJM, DeLint PJ, van Norren D. Fundus reflectance—historical and present ideas. *Prog Retin Eye Res*. 2003;22(2):171–200, doi:10.1016/S1350-9462(02)00060-5.
36. Bajwa MN, Singh GAP, Neumeier W, Malik MI, Dengel A, Ahmed S. G1020: a benchmark retinal fundus image dataset for computer-aided glaucoma detection. *arXiv*. 2020;2006.09158 [eess.IV]. Published online May 28, 2020, doi:10.48550/arXiv.2006.09158.
37. Decencière E, Zhang X, Cazuguel G, et al. Feedback on a publicly distributed image database: the messidor database. *Image Anal Stereol*. 2014;33(3):231–234, doi:10.5566/ias.1155.
38. Orlando JI, Fu H, Breda JB, et al. REFUGE challenge: a unified framework for evaluating automated methods for glaucoma assessment from fundus photographs. *Med Image Anal*. 2020;59:101570, doi: 10.1016/j.media.2019.101570.
39. Camejo L, Noecker RJ. CHAPTER 14 - Optic nerve imaging. In: Stamper RL, Lieberman MF, Drake MV, eds. *Becker-Shaffer's Diagnosis and Therapy of the Glaucomas* (Eighth Edition). St. Louis: Mosby; 2009:171–187, doi:10.1016/B978-0-323-02394-8.00014-0.
40. Wong TY, Mitchell P. Hypertensive retinopathy. *N Engl J Med*. 2004;351(22):2310–2317, doi:10.1056/NEJMra032865.
41. Abu El-Asrar AM, Herbort CP, Tabbara KF. Differential diagnosis of retinal vasculitis. *Middle East Afr J Ophthalmol*. 2009;16(4):202–218, doi:10.4103/0974-9233.58423.
42. Kumar J, Wierzbicki AS. Lipemia retinalis. *N Engl J Med*. 2005;353(8):823–823, doi:10.1056/NEJMicm040437.
43. Fu H, Cheng J, Xu Y, Wong DWK, Liu J, Cao X. Joint optic disc and cup segmentation based on multi-label deep network and polar transformation. *IEEE Trans Med Imaging*. 2018;37(7):1597–1605, doi:10.1109/TMI.2018.2791488.
44. Sevastopolsky A. Optic disc and cup segmentation methods for glaucoma detection with modification of U-Net convolutional neural network. *Pattern Recognit Image Anal*. 2017;27(3):618–624, doi:10.1134/S1054661817030269.
45. Meng Y, Zhang H, Zhao Y, et al. Graph-based region and boundary aggregation for biomedical image segmentation. *IEEE Trans Med Imaging*. 2022;41(3):690–701, doi:10.1109/TMI.2021.3123567.
46. Leung CKS, Choi N, Weinreb RN, et al. Retinal nerve fiber layer imaging with spectral-domain optical coherence tomography: pattern of RNFL defects in glaucoma. *Ophthalmology*. 2010;117(12):2337–2344, doi:10.1016/j.ophtha.2010.04.002.
47. Chen Y, Yuan Y, Zhang S, et al. Retinal nerve fiber layer thinning as a novel fingerprint for cardiovascular events: results from the prospective cohorts in UK and China. *BMC Med*. 2023;21(1):24, doi:10.1186/s12916-023-02728-7.
48. Thomson KL, Yeo JM, Waddell B, Cameron JR, Pal S. A systematic review and meta-analysis of retinal nerve fiber layer change in dementia, using optical coherence tomography. *Alzheimers*

*Dement Diagn Assess Dis Monit*. 2015;1(2):136–143, doi:10.1016/j.dadm.2015.03.001.

49. Ko F, Muthy ZA, Gallacher J, et al. Association of retinal nerve fiber layer thinning with current and future cognitive decline: a study using optical coherence tomography. *JAMA Neurol*. 2018;75(10):1198–1205, doi:10.1001/jamaneurol.2018.1578.
50. Mutlu U, Colijn JM, Ikram MA, et al. Association of retinal neurodegeneration on optical coherence tomography with dementia: a population-based study. *JAMA Neurol*. 2018;75(10):1256–1263, doi:10.1001/jamaneurol.2018.1563.
51. Biffi E, Turple Z, Chung J, Biffi A. Retinal biomarkers of cerebral small vessel disease: a systematic review. *PLoS One*. 2022;17(4):e0266974..
52. Wang D, Li Y, Wang C, et al. Localized retinal nerve fiber layer defects and stroke. *Stroke*. 2014;45(6):1651–1656, doi:10.1161/STROKEAHA.113.004629.
53. Conn FL. When glaucomatous damage isn't glaucoma. Accessed April 17, 2023. https://www.reviewofophthalmology.com/article/when-glaucomatous-damage-isnt-glaucoma.
54. Hwang YH, Song M, Kim YY, Yeom DJ, Lee JH. Interocular symmetry of retinal nerve fibre layer thickness in healthy eyes: a spectral-domain optical coherence tomographic study. *Clin Exp Optom*. 2014;97(6):550–554, doi:10.1111/cxo.12218.
55. Dalgliesh JD, Tariq YM, Burlutsky G, Mitchell P. Symmetry of retinal parameters measured by spectral-domain OCT in normal young adults. *J Glaucoma*. 2015;24(1):20, doi:10.1097/IJG.0b013e318287ac2f.
56. Yang M, Wang W, Xu Q, Tan S, Wei S. Interocular symmetry of the peripapillary choroidal thickness and retinal nerve fibre layer thickness in healthy adults with isometropia. *BMC Ophthalmol*. 2016;16(1):182, doi:10.1186/s12886-016-0361-7.
57. Budenz DL. Symmetry between the right and left eyes of the normal retinal nerve fiber layer measured with optical coherence tomography (an AOS thesis). *Trans Am Ophthalmol Soc*. 2008;106:252–275..
58. Cameron JR, Megaw RD, Tatham AJ, et al. Lateral thinking – interocular symmetry and asymmetry in neurovascular patterning, in health and disease. *Prog Retin Eye Res*. 2017;59:131–157, doi:10.1016/j.preteyeres.2017.04.003.
59. Rodriguez-Beato FY, De Jesus O. Compressive optic neuropathy. In: *StatPearls*. St Petersburg, FL: StatPearls Publishing; 2023. Accessed April 17, 2023. http://www.ncbi.nlm.nih.gov/books/NBK560583/.
60. Monteiro MLR. Optical coherence tomography analysis of axonal loss in band atrophy of the optic nerve. *Br J Ophthalmol*. 2004;88(7):896–899, doi:10.1136/bjo.2003.038489.
61. Fried I, Tabori U, Tihan T, Reginald A, Bouffet E. Optic pathway gliomas: a review. *CNS Oncol*. 2013;2(2):143–159, doi:10.2217/cns.12.47.
62. Huang M, Patel J, Patel BC. Optic Nerve Glioma. In: *StatPearls*. St Petersburg, FL: StatPearls Publishing; 2023. Accessed April 18, 2023. http://www.ncbi.nlm.nih.gov/books/NBK557878/.
63. Fisher MJ, Loguidice M, Gutmann DH, et al. Visual outcomes in children with neurofibromatosis type 1–associated optic pathway glioma following chemotherapy: a multicenter retrospective analysis. *Neuro-Oncol*. 2012;14(6):790–797, doi:10.1093/neuonc/nos076.
64. Campagna M, Opocher E, Viscardi E, et al. Optic pathway glioma: long-term visual outcome in children without neurofibromatosis type-1. *Pediatr Blood Cancer*. 2010;55(6):1083–1088, doi:10.1002/pbc.22748.
65. Chhablani J, Krishnan T, Sethi V, Kozak I. Artifacts in optical coherence tomography. *Saudi J Ophthalmol*. 2014;28(2):81–87, doi:10.1016/j.sjopt.2014.02.010.
66. Lee H, Proudlock FA, Gottlob I. Pediatric optical coherence tomography in clinical practice—recent progress. *Invest Ophthalmol Vis Sci*. 2016;57(9):OCT69–OCT79, doi:10.1167/iovs.15-18825.
67. Sivaswamy J, Krishnadas SR, Datt Joshi G, Jain M, Syed Tabish AU. Drishti-GS: retinal image dataset for optic nerve head (ONH) segmentation. In: *2014 IEEE 11th International Symposium on Biomedical Imaging (ISBI)*, Beijing, China. 2014:53–56, doi:10.1109/ISBI.2014.6867807.
68. Staal J, Abramoff MD, Niemeijer M, Viergever MA, van Ginneken B. Ridge-based vessel segmentation in color images of the retina. *IEEE Transactions on Medical Imaging*. 2024;23(4):501–509, doi:10.1109/TMI.2004.825627.
69. Vorontsov E, Kadoury S. Label Noise in Segmentation Networks: Mitigation Must Deal with Bias. In: Engelhardt S, Oksuz I, Zhu D, et al., Eds. *Deep Generative Models, and Data Augmentation, Labelling, and Imperfections*. Lecture Notes in Computer Science. New York: Springer International Publishing; 2021:251–258, doi:10.1007/978-3-030-88210-5_25.
70. Mookiah MRK, Hogg S, MacGillivray T, Trucco E. On the quantitative effects of compression of retinal fundus images on morphometric vascular measurements in VAMPIRE. *Comput Methods*

*Programs Biomed*. 2021;202:105969, doi:10.1016/j.cmpb.2021.105969.

71. MacCormick IJC, Williams BM, Zheng Y, et al. Correction: Accurate, fast, data efficient and interpretable glaucoma diagnosis with automated spatial analysis of the whole cup to disc profile (PLoS One (2019) 14:1 (e0209409) DOI: 10.1371/journal.pone.0209409). *PLoS One*. 2019;14(4):1–20, doi:10.1371/journal.pone.0215056.
72. Knight OJ, Girkin CA, Budenz DL, Durbin MK, Feuer WJ, Cirrus OCT Normative Database Study Group. Effect of race, age, and axial length on optic nerve head parameters and retinal nerve fiber layer thickness measured by Cirrus HD-OCT. *Arch Ophthalmol*. 2012;130(3):312–318, doi:10.1001/archopthalmol.2011.1576.
73. Ocansey S, Abu EK, Owusu-Ansah A, et al. Normative values of retinal nerve fibre layer thickness and optic nerve head parameters and their association with visual function in an African population. *J Ophthalmol*. 2020;2020:e7150673, doi:10.1155/2020/7150673.

## 3.5 Conclusion

In this chapter, I have presented software, *PallorMetrics*, that automatically measures optic disc pallor in fundus images globally and in several zones akin to those used by contemporary OCT scanners. The software processes each image in under one second, with processing time increasing to approximately three seconds when generating marked-up images. The software was validated by demonstrating associations between measurements of pallor and pRNFL thickness in a dataset that contained both fundus images and OCT scans of the pRNFL in the same eyes. We also confirmed that pallor was higher in individuals with clinically diagnosed pallor compared to healthy controls in an external dataset. Additionally, we demonstrated that the software was robust across a variety of retinal images, capable of handling different camera systems, resolutions, and formats (e.g., JPEG, PNG). I believe that this versatility is essential if *PallorMetrics* is to be applied across diverse clinical settings and imaging setups.

In the published article, we described a preliminary method of automatically rejecting images. In the next chapter, I describe the development of a more thorough method of automatically performing quality control, which is essential for the efficient processing of large datasets.

# Chapter 4

# Developing automatic quality control methods for *PallorMetrics*

## 4.1 Introduction

In the previous chapter, I described a method of automatically quantifying optic disc pallor in fundus images, *PallorMetrics*.[94] However, as with other automated image processing pipelines for fundus images,[95] some form of automatic quality control is necessary to ensure accurate and reliable analysis when processing datasets. In this chapter, I describe two methods to address this need, aimed at both enhancing efficiency in handling large datasets and mitigating selection bias that might result from manual quality control in smaller datasets. Therefore, this chapter continues to address the first objective – developing a method of quantifying optic disc pallor.

Other automated pipelines that process fundus images, such as AutoMorph,[95] tend to rely on external methods to filter out poor quality images *prior* to processing. The most widely used filtering method is MCFNet,[96] a deep learning-based network trained on the EyeQ dataset that labels images as either Good, Useable, or Reject. More recent iterations, such as QuickQual,[97] provide a continuous measure of quality – from 0 (good) to 1 (bad). These metrics evaluate image quality by considering all pixels across the entire image. However, in many

fundus images, artefacts are only present in the periphery, and the optic disc is often preserved. In *PallorMetrics*, as long as the optic disc and the surrounding area are clearly visible, the image can still be successfully processed, making poor quality in other regions less relevant. This means that some images marked as reject by MCFNet would still be useable for optic disc measurements (see Figure 4.1 for an example). Quality control, therefore, largely depends on the intended use case. For example, when assessing vessel-based metrics like fractal dimension, it is important to ensure clear visibility of the vasculature across the entire retina. In contrast, for optic disc-based measurements, peripheral quality is inconsequential. With this in mind, I set *PallorMetrics* up to process all available images and perform quality control on the processed results, rather than rejecting images before processing.

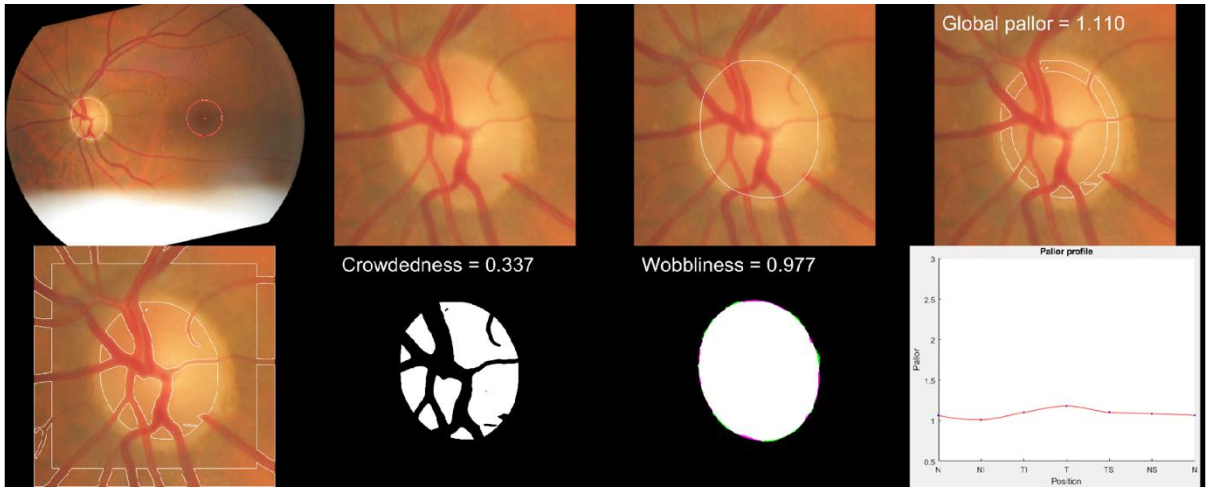


**Figure 4.1.** Visual output of *PallorMetrics* for a single image from the LBC 1936 dataset.[98] While this image would be classified as "Reject" by MCFNet due to photographic artefact, the optic disc is unaffected, therefore *PallorMetrics* is still able to process the image successfully.

## 4.2 Methods

I collated 1,485 fundus images from 12 different datasets (Table 4.1), all except three (PREVENT Dementia, LBC 1936, UK Biobank) are publicly available. My goal was to create

a heterogeneous dataset by selecting images with varying quality, a broad range of pathologies, and different resolutions. To get an idea of the distribution of quality in the dataset, I initially measured quality using QuickQual.[97] According to QuickQual, the images show a wide range of quality scores (Mean = 0.45, SD = 0.30; see Figure 4.2 for histogram). Pathologies present in the datasets include but are not limited to glaucoma, diabetic retinopathy, age-related macular degeneration, drusen, pathological myopia, cataract, and retinal disease. I selected the first ~100 images from each dataset according to their alphabetically sorted filenames. The full range of image resolutions was from 320 × 316 to 5184 × 3456 pixels, however only 2 images had a resolution of 320 × 316, the rest were at least 1444 × 1444.

**Table 4.1.** Dataset characteristics.

| **Dataset** | **Description** | **Number of images** | **Image format** | **Resolution (in pixels)** |
|---|---|---|---|---|
| ORIGA[99] | Primarily used for glaucoma detection and analysis. | 99 | JPG | 2495 × 2048 |
| MESSIDOR[100] | Primarily used for diabetic retinopathy research. | 100 | PNG | 2240 × 1488 |
| UK Biobank[101] | Large UK based cohort. | 104 | PNG | 2048 × 1536 |
| PREVENT Dementia[102] | Mid-life adults at increased risk of dementia. | 100 | PNG | 3072 × 2048 |
| Kaggle cataract dataset[103] | Used for detecting cataract. | | | |
| *Normal* | | 100 | PNG | mixed |
| *Glaucoma* | | 100 | PNG | mixed |
| *Cataract* | | 100 | PNG | mixed |
| *Retinal disease* | | 100 | PNG | mixed |
| IDRiD[104] | Primarily used for diabetic retinopathy research. | 81 | PNG | 4288 × 2848 |
| LBC 1936[98] | Elderly (all aged ~ 72) UK based “healthy” cohort. | 100 | PNG | 2689 × 2186 |
| PAPILA[105] | Primarily used for optic disc and cup segmentation. | 100 | JPG | 2576 × 1934 |
| G1020[106] | Primarily used for glaucoma detection. | 100 | JPG | mixed |
| FIVES[107] | Primarily used for vessel segmentation. | 100 | PNG | 2048 × 2048 |
| Kaggle ODIR-5K[108] | Contains multiple retinal disease labels. | 101 | JPG | 2592 × 1728 |
| RFMiD[109] | Contains multiple retinal disease labels. | 100 | PNG | 2144 × 1424 |

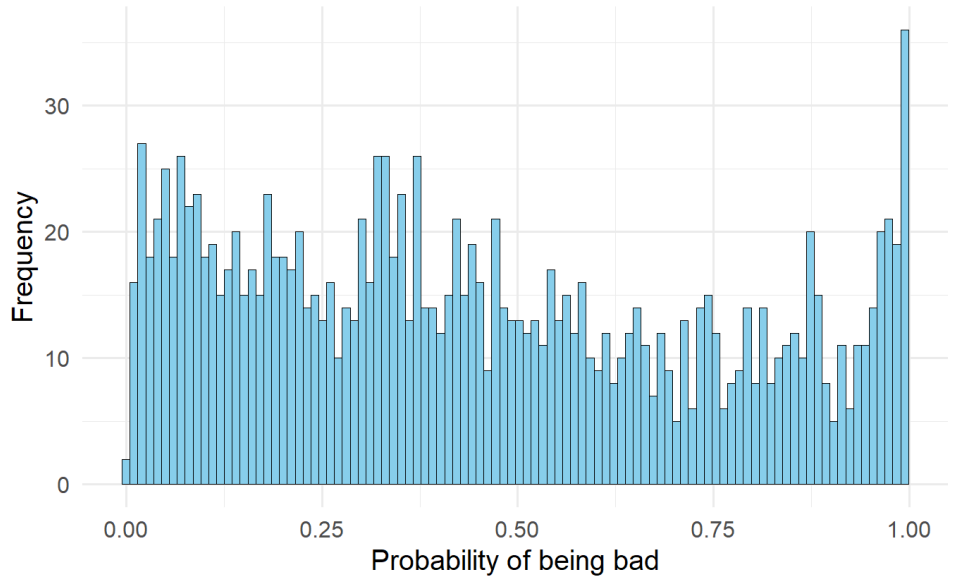


**Figure 4.2.** Histogram of quality scores from QuickQual. A higher score equates to worse quality.

### 4.2.1 Procedure for rejecting processed images

I passed all 1,485 images in the collated dataset to the *PallorMetrics* software. The software failed to process 4 images (0.3%; Figure 4.3). I visually inspected the remaining 1,481 processed images for quality. In this procedure, I marked each processed image as either *keep* or *reject* (0, 1). The rejection criteria were:

- Was the optic disc located and segmented successfully?
- Was the fovea located successfully?
- Was the image properly rotated along the disc-fovea axis?
- Were the vessels segmented successfully?
- Was there even exposure over the optic disc?
- Did peripapillary atrophy extend excessively into the control region?

According to this protocol, 326 images were marked as *reject* (22.0%).

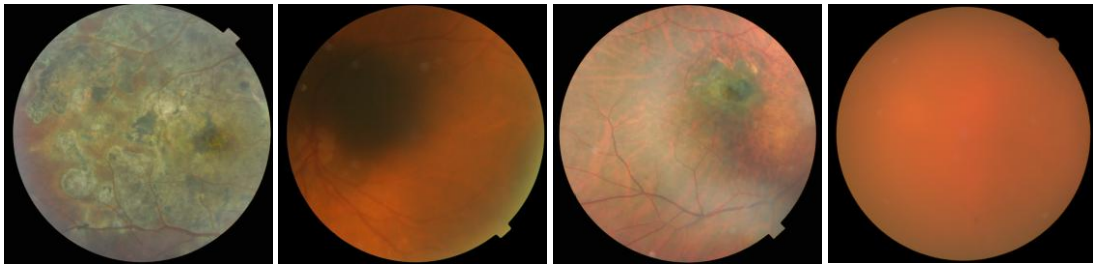

**Figure 4.3.** Four images out of 1,485 failed processing. Images that fail processing are returned to the results folder in their original form with the filename appended with "_proc_error". In the tabular data, the field "proc_error" is marked "1", and all other variables ar filled with "NA".

In Figure 4.4, I present two examples of processed images, one marked as *keep*, and the other marked as *reject*.

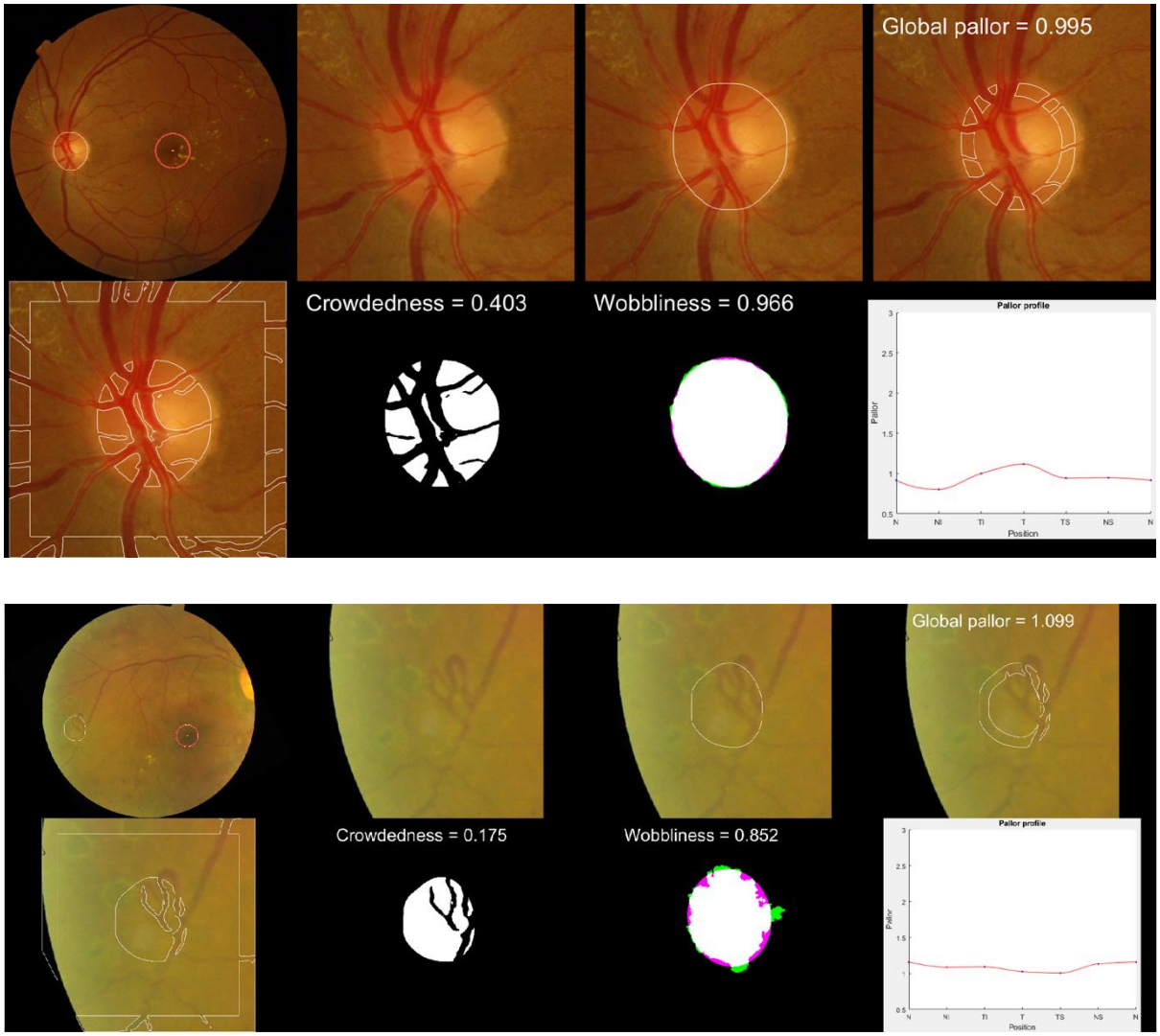


**Figure 4.4.** Examples of processed images labelled as keep (top) and reject (bottom).

### 4.2.2 Rejection rates and quality by dataset

To evaluate whether certain datasets had a higher likelihood of being labelled as *reject*, I constructed a bar plot displaying the frequency of rejection labels across datasets (Figure 4.5). Additionally, I included a reference bar plot illustrating the distribution of quality scores from QuickQual. Compared to the QuickQual score, I observed a high rejection rate for the PAPILA images (67.0%). The discrepancy is likely due to the smaller field of view (30°) of these images compared to the others in the dataset, which typically had a broader field of view (~45°). This means that *PallorMetrics* is not reliable with images with a small field of view and represents an opportunity for improvement. A high reject rate was observed for images with cataracts, which cause the image to appear blurry/hazy. However, this was to be expected and agrees with the corresponding QuickQual score. When considering the PREVENT Dementia images, a particularly high-quality set of images that are largely free of pathology, a very low rejection rate was observed, even though the QuickQual score was relatively high. This discrepancy is likely because *PallorMetrics* is mainly concerned with measurements in and around the optic disc, the quality of which is usually preserved in colour fundus photographs, even when artifacts are present elsewhere in the image. By contrast, QuickQual was designed to assess the image as a whole. These observations further highlight the need for more nuanced methods of assessing fundus image quality that consider anatomical features separately and can be tailored to the specific requirements of the user.

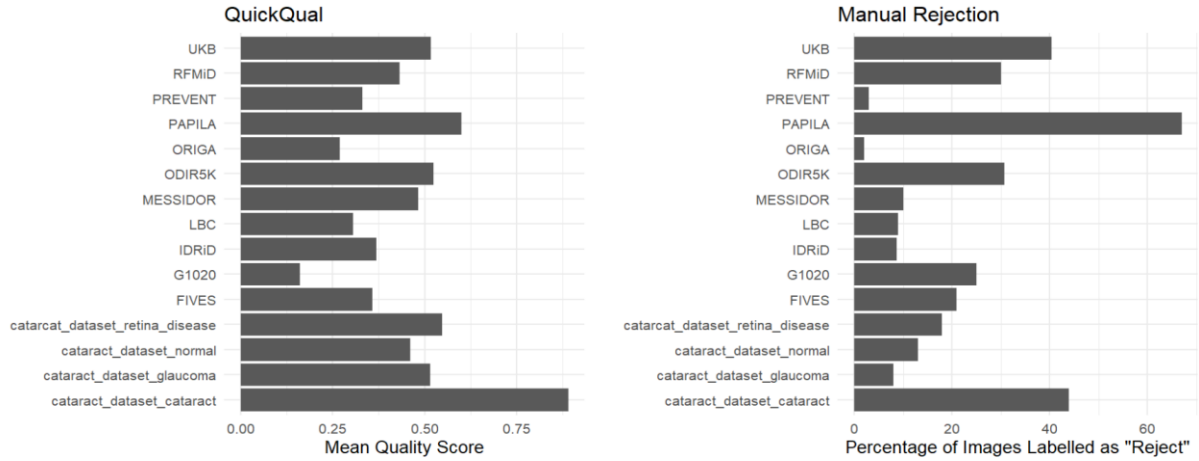


**Figure 4.5.** Bar plots comparing mean quality scores, and the percentage of processed images labelled as “reject”, by dataset.

### 4.2.3 Features used for rejecting processed images

Alongside the measurements of pallor described in the Chapter 3, *PallorMetrics* computes several additional features such as *optic disc diameter*, and the *distance between the optic disc and the fovea*. I also computed a set of experimental features such as *optic disc crowdedness* and *hypoplasia*. While these additional features are not yet validated, they can still be used to help assess quality, as described below. The full set of features generated by *PallorMetrics* is presented in Table 4.2.

**Table 4.2.** Full set of features generated by *PallorMetrics*.

| Name | Type | Description |
|---|---|---|
| proc_error | [0,1] | Processing error. Image failed at point of processing. If "visualise == 1", original image will be returned to the output directory appended with "proc_error". |
| Eye | [left, right] | Algorithmically defined, based on x-axis location of optic disc relative to fovea. |
| pal_T* | Float | Temporal pallor |
| pal_TI* | Float | Temporal-inferior pallor |
| pal_NI* | Float | Nasal-inferior pallor |
| pal_N* | Float | Nasal pallor |
| pal_NS* | Float | Nasal-superior pallor |
| pal_TS* | Float | Temporal-superior pallor |
| pal_PMB | Float | Pallor in the papillomacular bundle |
| pal_G* | Float | Global pallor (from the entire measurement region) |
| pal_NT_ratio* | Float | Nasal Pallor divided by Temporal pallor |
| pal_disc | Float | Pallor in the whole disc, including the cup |
| disc_area | Float | Disc area |
| distance* | Float | Length in pixels between the disc centre and the fovea |

| | | |
|---|---|---|
| eccentricity* | [0-1] | Zero is a perfect circle, 1 is a line. The higher the value, the more eccentric. |
| vessel_mass* | Float | Total number of pixels classified as "vessel" inside the cropped square around the disc |
| crowdedness* | [0-1] | The ratio of vessels to disc area. The higher the value, the more crowded. |
| DD | Float | Disc diameter |
| DM | Float | Distance from temporal edge of disc to macular/fovea |
| hypoplasia | Float | DD/DM |
| wobbliness* | Float | The Intersection over Union (IoU) between the predicted disc and an estimated ellipse. |
| torsion | Degrees | Degrees between the major axis of the optic disc and the vertical meridian. |
| ovality | [0-1] | Ovality of the optic disc. Minor axis length of the disc / major axis length of the disc. |
| tilt | [0,1] | 1 if torsion > 15 & ovality < 0.8, else zero. |
| cont_int* | Float | Control region intensity. Median of green pixels in the control region / median of red pixels in the control region. |

**Note:** Features used for automated quality control are marked with an asterisk.

One feature, *wobbliness*, was particularly good at classifying segmentation error. As described in Table 2, *wobbliness* is the intersection over union (IoU) between the predicted disc and an estimated ellipse. In a fundus image where the disc border is unclear, the disc segmentation network will struggle to delineate the border, as would a human. This results in a splat-like shape, demonstrated by the jagged white shape in Figure 4.6G. By contrast, the shape in Figure 4.6D-F represents the smoothed version of the jagged shape, and the ellipse in Figure 4.6G is the fitted ellipse. A low value for *wobbliness* is therefore a strong indicator that the disc segmentation failed, and the image should be rejected (thresholds are specified in Table 3).

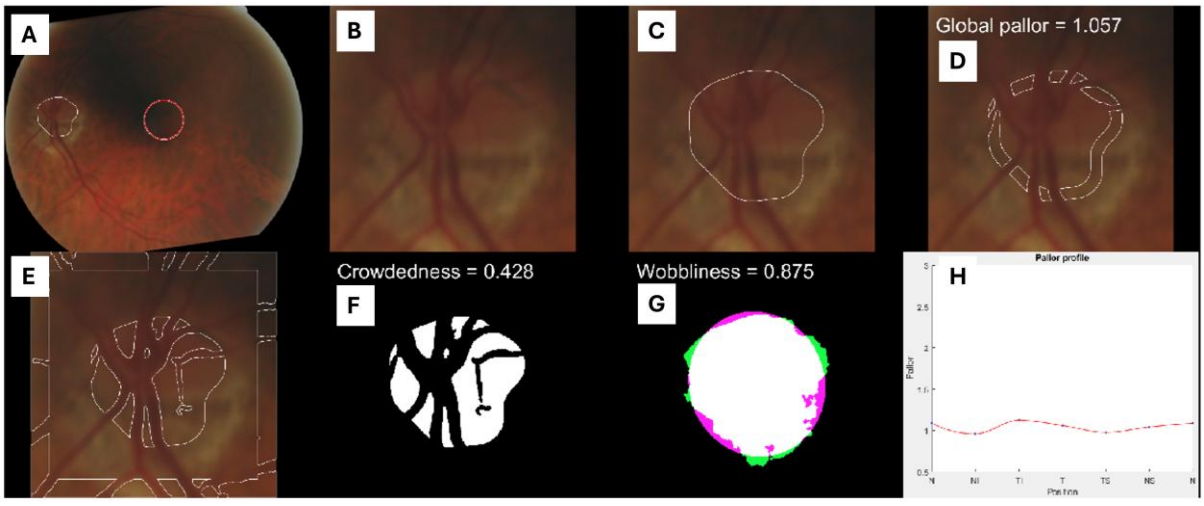


**Figure 4.6.** A processed image from the LBC 1936 dataset. A) Predicted location of optic disc and macula. B) Cropped optic disc. C) Predicted and smoothed optic disc border. D) Predicted measurement region. E) Predicted measurement and control

region with vessels excluded. F) Wobbliness measure. G) The jagged shape is the raw prediction from the deep-learning network. The smooth shape is a fitted ellipse around the prediction. The white and pink colours are the difference between the two, and are used to calculate the wobbliness measure (Intersection over Union). H) Profile of measured pallor values in different zones.

From the full set of features, I selected 14 to develop the automated quality control. I limited the selection to 14 because some features were too highly correlated. For instance, *distance*, *DM*, and *hypoplasia* are all derived from the distance between the optic disc and fovea, so only one metric was needed. Similarly, *tilt* is calculated from both *ovality* and *torsion*, and *ovality* is another way of measuring *eccentricity*. Furthermore, *tilt* was binary and showed little variation. Using these 14 continuous metrics generated by the software, I developed two quality control methods. In the first, I manually set thresholds based on overlapping histograms (section 4.2.4). In the second, I trained a range of machine learning classifiers to predict the binary outcome: *keep* or *reject* (section 4.2.5).

### 4.2.4 Quality control method 1: Manually selected thresholds

I manually selected thresholds for rejecting images based on the distributions of the 14 continuous measures generated by the software. For each measure, I overlaid the distributions of *keep* and *reject*, and selected thresholds that aimed to capture the non-overlapping *reject* datapoints in the tails of the distribution (Figure 4.7).

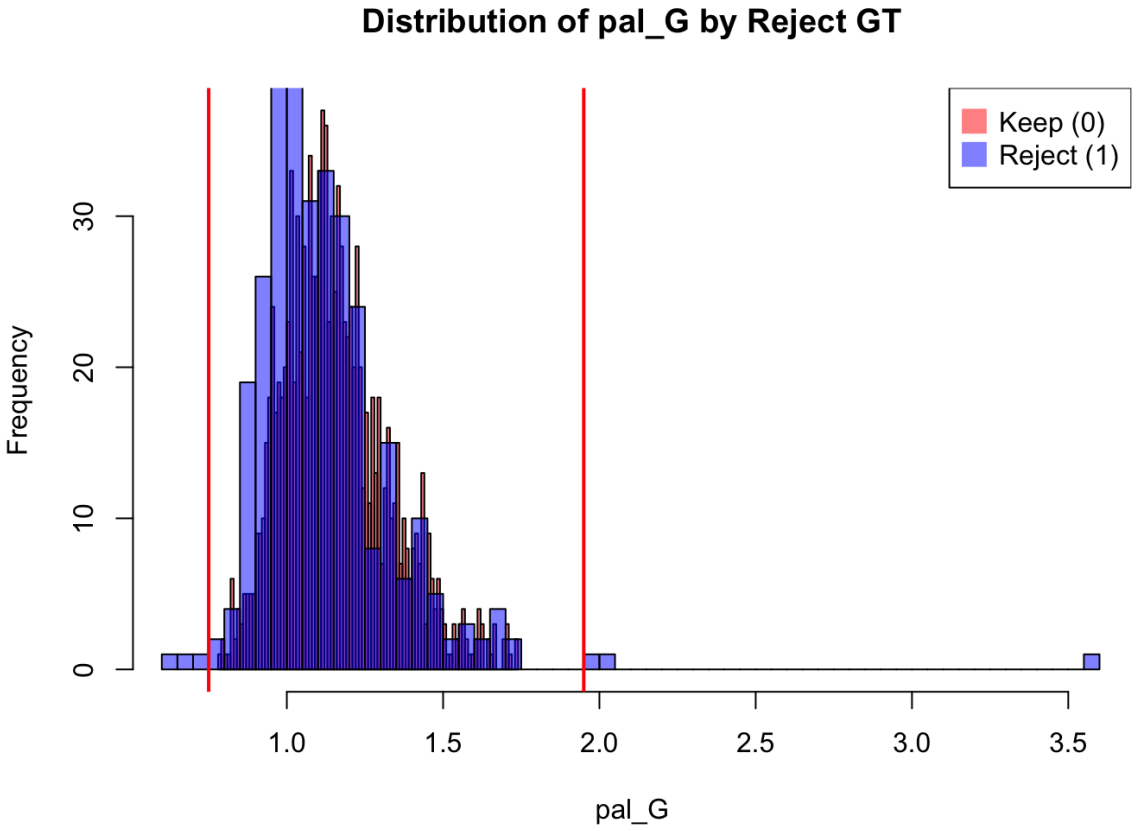


**Figure 4.7.** Overlaid distributions of global pallor in processed images that I manually marked as *keep* or *reject*. Vertical red lines represent the manually selected upper and lower thresholds. Similar plots for all other features are presented in Supplementary Figure x. **Abbreviations:** pal_G (Global Pallor); GT (Ground Truth).

Manual selection may have biases; however, it allowed for nuanced consideration of each metric's unique distribution. The thresholds are specified in Table 4.3. Based on these thresholds, a classification model does reasonably well, with an AUC (area under the curve) of 0.81, correctly classifying 208 images as *reject* (14.0%). The confusion matrix and full range of statistics are presented alongside results for the second method in Figure 4.7 and Table 4.4.

**Table 4.3.** Manually selected thresholds for keeping or rejecting a processed image.

| Metric | Thresholds | Number of images outside threshold (N, %) |
|---|---|---|
| Pallor | | |
| *Global* | 0.75 – 1.95 | 6 (0.4%) |
| *Temporal* | 0.75 – 2.1 | 9 (0.6%) |
| *Temporal-inferior* | 0.7 – 1.85 | 7 (0.5%) |
| *Nasal-inferior* | 0.7 – 1.6 | 12 (0.8%) |
| *Nasal* | 0.7 – 1.7 | 9 (0.6%) |

| | | |
|---|---|---|
| *Nasal-superior* | 0.65 – 1.65 | 6 (0.4%) |
| *Temporal-superior* | 0.75 – 1.8 | 7 (0.5%) |
| *NT Ratio* | 0.6 – 1.15 | 22 (1.5%) |
| Crowdedness | < 0.25 | 73 (4.9%) |
| Wobbliness | < 0.92 | 178 (12.0%) |
| Disc-fovea distance | < 330 pixels | 19 (1.0%) |
| Eccentricity (of disc) | > 0.75 | 4 (0.3%) |
| Vessel mass | < 52,000 pixels | 58 (4.0%) |
| Control region intensity | 0.2 – 1.0 | 4 (0.3%) |

**Abbreviations:** NT (nasal-temporal); IoU (intersection over union).

### 4.2.5 QC Method 2: Machine learning classifier

I trained a wide range of traditional machine learning classifiers (e.g., decision trees, support vector machines, neural networks) using MATLAB's "Classification Learner" (The MathWorks, Inc., Natick, Massachusetts, United States). The outcome was the binary ground truth label *keep* or *reject* (0, 1). The predictors were the same 14 metrics listed in Table 4.3. I trained with 5-fold cross validation. I chose validation accuracy as the main performance metric because it has been shown to provide a robust assessment of classifier performance across different machine learning models, and effectively measures the ability of each model to generalise to new, unseen data.[110] The best model was a "coarse decision tree", which achieved a validation accuracy of 92.8% and an AUC of 0.88, correctly classifying 261 images as *reject* (17.6%). Confusion matrices comparing the two methods are presented in Figure 4.7. Performance metrics for the two classification methods are presented in Table 4.4.

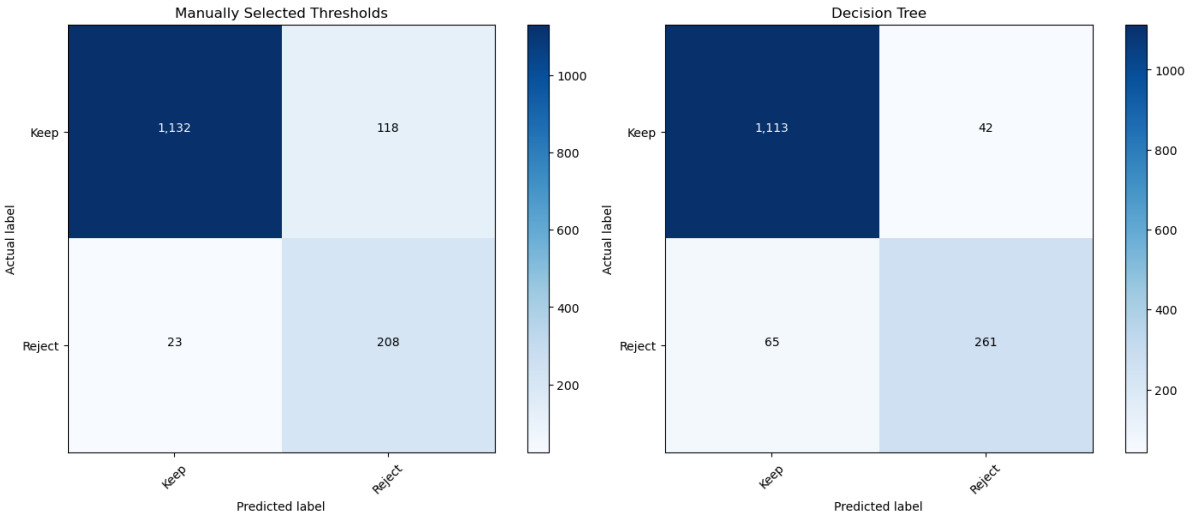

**Figure 4.7.** Confusion matrices comparing the two methods of automated quality control.

**Table 4.4.** Classification statistics for the two methods of automated quality control.

| Measure | Derivations | Thresholds | Decision tree |
|---|---|---|---|
| Sensitivity | TPR = TP / (TP + FN) | **0.9801** | 0.9448 |
| Specificity | SPC = TN / (FP + TN) | 0.638 | **0.8614** |
| Precision | PPV = TP / (TP + FP) | 0.9056 | **0.9636** |
| Negative Predictive Value | NPV = TN / (TN + FN) | **0.9004** | 0.8006 |
| False Positive Rate | FPR = FP / (FP + TN) | 0.362 | **0.1386** |
| False Discovery Rate | FDR = FP / (FP + TP) | 0.0944 | **0.0364** |
| False Negative Rate | FNR = FN / (FN + TP) | **0.0199** | 0.0552 |
| Accuracy | ACC = (TP + TN) / (P + N) | 0.9048 | **0.9278** |
| F1 Score | F1 = 2TP / (2TP + FP + FN) | 0.9414 | **0.9541** |
| Matthews Correlation Coefficient | TP*TN - FP*FN / sqrt((TP+FP)*(TP+FN)*(TN+FP)*(TN+FN)) | 0.7059 | **0.7849** |

**Abbreviations:** TP (True Positive); FN (False Negative); FP (False Positive); TN (True Negative). **Notes:** Best score in bold type.

## 4.3 Discussion

I have presented two methods of automatically performing quality control for the *PallorMetrics* software. Based on a collated set of 1,485 images from 12 different datasets that represent a range of heterogeneity in terms of image resolution, field of view, quality, and pathology, the manual threshold method achieved an AUC of 0.81, and the decision tree achieved an AUC of 0.88. Overall, the decision tree method achieved a more balanced split compared to the manual threshold method. However, the manual threshold method demonstrated greater sensitivity, a higher negative predictive value (NPV), and a lower false negative rate. Despite these advantages, the decision tree outperforms the manual method on most other performance metrics. Due to its higher NPV, which indicates its ability to correctly reject more images, the threshold method can be considered more conservative.

An important consideration when choosing between these rejection methods is how well the data is suited for statistical analysis. Many statistical tests, particularly those involving linear regression, are sensitive to the presence of outliers, which can skew results and lead to unreliable estimates.[111] In linear regression, for example, even a single outlier can

disproportionately influence the estimate.[111] Therefore, handling outliers, either by removing or transforming them, is often necessary before conducting statistical analyses. With the manual threshold method, all outliers are systematically removed, offering a potential advantage for downstream data analysis, as the resulting dataset is less likely to be influenced by extreme values.

Ultimately, the choice between these rejection methods will depend on the user's specific goals and priorities – whether they value a more conservative approach with fewer false negatives or prefer a broader, more balanced classification from the decision tree. In most cases, I would recommend the manual threshold method, which removes outliers.

## 4.4 Conclusion

In this chapter, I have described two methods for automatically marking images processed by *PallorMetrics* as pass or reject. One method works by using manually derived cut-off points, and the other uses a machine learning classifier. These methods have been integrated into the *PallorMetrics* software, and the results are stored alongside other outputted variables. Automated quality control is essential for applying *PallorMetrics* to large datasets, where manual inspection of the processed images, or manually demarcating the optic disc, might be impractical.

# Chapter 5

# Optic disc pallor and cerebral small vessel disease

## 5.1 Introduction

Having successfully developed a novel method of quantifying optic disc pallor in fundus images, and establishing a robust method of automatic quality control, I now move to address the second objective of this thesis – exploring optic disc pallor in a cerebrovascular condition.

As discussed in Chapter 2, one highly prevalent cerebrovascular condition is cSVD – an age-related disease affecting the small blood vessels of the central nervous system, leading to stroke, dementia, and cognitive decline.[31–33] cSVD is commonly detected via MRI, which reveals key indicators including lacunes, microbleeds, white matter hyperintensities, and enlarged perivascular spaces.[32] However, owing to cost and availability, MRI is not suitable for mass screening. The retina, sharing similarities with the brain, may offer a more accessible alternative for detecting signs of cSVD.[20,25,51] Retinal layer thinning has been linked to cSVD prevalence and progression,[112–115] however, no work has yet explored optic disc pallor in cSVD. Here, I present a publication that tests for associations between optic disc pallor and both pRNFL thickness and four MRI markers of cSVD.

Data from the PREVENT Dementia study – a multi-centre prospective cohort conducted across five UK sites (Cambridge, Edinburgh, Oxford, London, and Dublin), collecting brain and retinal imaging alongside health, demographic, and cognitive variables at

approximately 2-year intervals[29,102] – was used. The PREVENT cohort consists of healthy, mid-life participants (aged 40-59 years). A key design feature is the intentional oversampling of individuals with a family history of dementia, with about half of the participants having an increased genetic risk. It is important to note that the PREVENT participants do not have a cSVD diagnosis. Instead, they represent a population with subtle markers associated with cSVD while being otherwise healthy. This cohort therefore provides a unique opportunity to investigate ocular and brain changes in individuals who may be in the very early prodromal stage of dementia. At the start of my PhD, the second wave of data collection had recently commenced.

## 5.2. Acknowledgement of contribution

Within the PREVENT study, Prof. John O'Brien led the neuroimaging arm, Dr Tom MacGillivray led retinal imaging arm, and Prof. Craig Ritchie was the Chief Investigator. For the publication included in this chapter, Dr Audrey Low generated the MRI measurements and identified participants with incidental findings. Ms Charlene Hamid acquired and processed the OCT scans and extracted the pRNFL measurements, including identifying abnormalities and performing quality control. I would like to express my gratitude to all researchers, participants, and support staff who made this work possible. All authors reviewed and commented on the manuscript.

## 5.3. My contribution to this work

I led:

- Generating the research question, and study design featured in the paper.
- Conducting a literature review.
- Processing of retinal images including quality control.

- Combining datasets from different arms of the PREVENT Dementia study (MRI, retinal, clinical).
- Deciding which statistical tests to conduct.
- Deciding which covariates to use.
- Performing the data and statistical analysis.
- Creating the tables and figures.
- Drafting the manuscript.
- Incorporating co-authors' comments and finalising the manuscript.
- Writing this chapter.

## 5.4. Published article

Received: 21 February 2024 | Revised: 5 July 2024 | Accepted: 16 July 2024

DOI: 10.1002/dad2.12633

Alzheimer's & Dementia®
Diagnosis, Assessment & Disease Monitoring

RESEARCH ARTICLE

# Association of optic disc pallor and RNFL thickness with cerebral small vessel disease in the PREVENT-Dementia study

Samuel Gibbon[1,2] | Audrey Low[3] | Charlene Hamid[1,2] | Megan Reid-Schachter[1,2] | Graciela Muniz-Terrera[4] | Craig W. Ritchie[1] | Emanuele Trucco[5] | Baljean Dhillon[1,2,6] | John T. O'Brien[3] | Thomas J. MacGillivray[1,2,7]

[1]Centre for Clinical Brain Sciences, Chancellor's Building, Edinburgh, UK

[2]Robert O Curle Ophthalmology Suite, Institute for Regeneration and Repair, Edinburgh, UK

[3]Department of Psychiatry, School of Clinical Medicine, University of Cambridge, Cambridge, UK

[4]Heritage College of Osteopathic Medicine, Ohio University, Athens Campus, Athens, Ohio, USA

[5]VAMPIRE project, Computing (SSEN), University of Dundee, Queen Mother Building, Dundee, UK

[6]Princess Alexandra Eye Pavilion, Edinburgh, UK

[7]Edinburgh Imaging, The Queen's Medical Research Institute, University of Edinburgh, Edinburgh, UK

**Correspondence**
Samuel Gibbon, Centre for Clinical Brain Sciences, Chancellor's Building, 49 Little France Crescent, Edinburgh EH16 4SB, UK.
Email: samuel.gibbon@ed.ac.uk

## Abstract

**INTRODUCTION:** We tested associations between two retinal measures (optic disc pallor, peripapillary retinal nerve fiber layer [pRNFL] thickness) and four magnetic resonance imaging markers of cerebral small vessel disease (SVD; lacunes, microbleeds, white matter hyperintensities, and enlarged perivascular spaces [ePVSs]).

**METHODS:** We used PallorMetrics to quantify optic disc pallor from fundus photographs, and pRNFL thickness from optical coherence tomography scans. Linear and logistic regression assessed relationships between retinal measures and SVD markers. Participants ($N = 108$, mean age 51.6) were from the PREVENT Dementia study.

**RESULTS:** Global optic disc pallor was linked to ePVSs in the basal ganglia in both left ($\beta = 0.12$, standard error [SE] = 0.05, $P < 0.05$) and right eyes ($\beta = 0.13$, SE = 0.05, $P < 0.05$). Associations were also noted in different disc sectors. No pRNFL associations with SVD markers were found.

**DISCUSSION:** Optic disc pallor correlated with ePVSs in the basal ganglia, suggesting retinal examination may be a useful method to study brain health changes related to SVD.

KEYWORDS
cerebral small vessel disease, dementia, magnetic resonance imaging, optic disc pallor, retina

## Highlights

- Optic disc pallor is linked to enlarged perivascular spaces in basal ganglia.
- There is no association between peripapillary retinal nerve fiber layer thickness and cerebral small vessel disease markers.
- Optic disc examination could provide insights into brain health.
- The sample included 108 midlife adults from the PREVENT Dementia study.

## 1 | INTRODUCTION

Cerebral small vessel disease (SVD) is an age-related condition affecting the arterioles, venules, and capillaries of the central nervous system, and is a major cause of stroke, dementia, and cognitive decline.[1–3] SVD can be detected in the brain using magnetic resonance imaging (MRI). The most widely recognized MRI-visible features of SVD include lacunes, microbleeds, white matter hyperintensities (WMHs), and enlarged perivascular spaces (ePVSs).[1–4] Due to high cost and low availability, MRI is not suited for mass screening. Instead, the retina, owing to its homology with the brain,[5] and the relative ease with which images can be acquired, has become a target for biomarker discovery in SVD.[6,7] One such promising imaging modality is optical coherence tomography (OCT), which can capture the peripapillary retinal nerve fiber layer (pRNFL), a thinning of which represents a loss of retinal ganglion cells/axons and is associated with SVD[8–10] and dementia.[11] However, the resolution of current OCT devices and the repeatability of scanning and analysis may not have sufficient sensitivity to discern subtle changes in the preclinical stages of dementia.[12,13] Recently, we developed PallorMetrics,[14] an alternative for studying pRNFL based on measuring optic disc pallor in fundus photographs, on the premise that a pale disc may indicate loss or degeneration of the pRNFL. In this study, we explore the associations between both pRNFL thickness and continuous measures of optic disc pallor with four MRI-derived markers of SVD (lacunes, microbleeds, WMHs, ePVSs).

**RESEARCH IN CONTEXT**

1. **Systematic review**: We reviewed the literature on the relationship between optic disc pallor, retinal nerve fiber layer thickness, and markers of cerebral small vessel disease (SVD). While retinal health is known to reflect brain health, few studies have specifically linked optic disc pallor to SVD markers.
2. **Interpretation**: We found a significant association between increased optic disc pallor and enlarged perivascular spaces in the basal ganglia. This suggests that optic disc pallor could be an early indicator of SVD, supporting the use of retinal imaging as a non-invasive method for detecting brain health issues like stroke and dementia.
3. **Future directions**: Future research should confirm these associations in larger, more diverse populations, investigate the mechanisms linking optic disc pallor and SVD, and evaluate retinal imaging as an adjunctive tool for assessing brain health. Longitudinal studies are needed to see if changes in optic disc pallor can predict SVD progression and subsequent cognitive decline.

## 2 | METHODS

### 2.1 | Participants and image capture

The PREVENT Dementia study protocol has been described elsewhere.[15] Briefly, 700 participants aged 40 to 59, enriched for family history of dementia (targeted 50% with family history), were recruited from five sites in the UK and Ireland. Brain MRI was performed on 648 participants using 3T Siemens Scanners (Verio, Skrya, and Prisma); sequence and acquisition parameters have been described in detail previously.[16,17] Briefly, for the 3D T1-weighted (T1w) magnetization-prepared rapid acquisition gradient echo images, there were 160 slices, a repetition time (TR) of 2300 ms, an echo time (TE) of 2.98 ms, a 9° flip angle, and a $1 \times 1 \times 1$ mm$^3$ voxel size. The T2-weighted (T2w) scans involved 32 slices, a TR of 1500 ms, a TE of 80 ms, a 150° flip angle, and a voxel size of $0.69 \times 0.69 \times 4$ mm$^3$. For fluid-attenuated inversion recovery (FLAIR) images, there were 27 slices, a TR of 9000 ms, a TE of 94 ms, a 150° flip angle, and a voxel size of $0.43 \times 0.43 \times 4$ mm$^3$. Susceptibility-weighted imaging (SWI) scans used 72 slices, a TR of 28 ms, a TE of 20 ms, a 15° flip angle, and a voxel size of $0.72 \times 0.72 \times 1.2$ mm$^3$.

Retinal imaging was a substudy conducted at the Edinburgh site only.[18] Exclusion criteria included participants with current or previous ocular disease such as glaucoma, macular degeneration, diabetic retinopathy, uveitis, vitreous hemorrhage, ischemic optic neuropathy, optic neuritis or other optic nerve diseases, or those who had undergone previous ocular surgery such as cataract surgery or retinal surgery. Retinal fundus photographs were captured using a non-mydriatic camera (CR-DGi; Canon USA, Inc.), with a 45° field of view. The protocol was to capture the posterior pole, with an image centered halfway between the macula and the optic disc. OCT was captured with a Heidelberg SPECTRALIS machine (Heidelberg Engineering) using the N-site peripapillary module set to high speed (1536 A-scans), with a target Automatic Real Time-function (ART) of 100. Participants provided written informed consent, and the study was carried out in compliance with the Declaration of Helsinki. Due to reasons including device/computer error, imaging room availability, poor cooperation, small pupil size, and participant feeling unwell, it was not always possible to capture both fundus images and OCT of each eye from each participant (Figure 1, top bar). After quality control (detailed in the section "Quality control") and the removal of four participants with incidental MRI findings (previously screened[17]), concurrent fundus images and OCT scans were available for 108 participants (207 eyes; Figure 1).

### 2.2 | SVD quantification

SVD quantification for the PREVENT Dementia cohort has been described elsewhere.[16,17] Briefly, ePVSs were assessed separately in the basal ganglia and centrum semiovale in T2w MRI using a validated rating scale.[19] Scores ranged from 0 to 4 based on the number of lesions: 0 (none), 1 (1–10), 2 (11–20), 3 (21–30), 4 (> 40). ePVSs in the midbrain were dichotomized as 0 (absent) or 1 (present). Cerebral

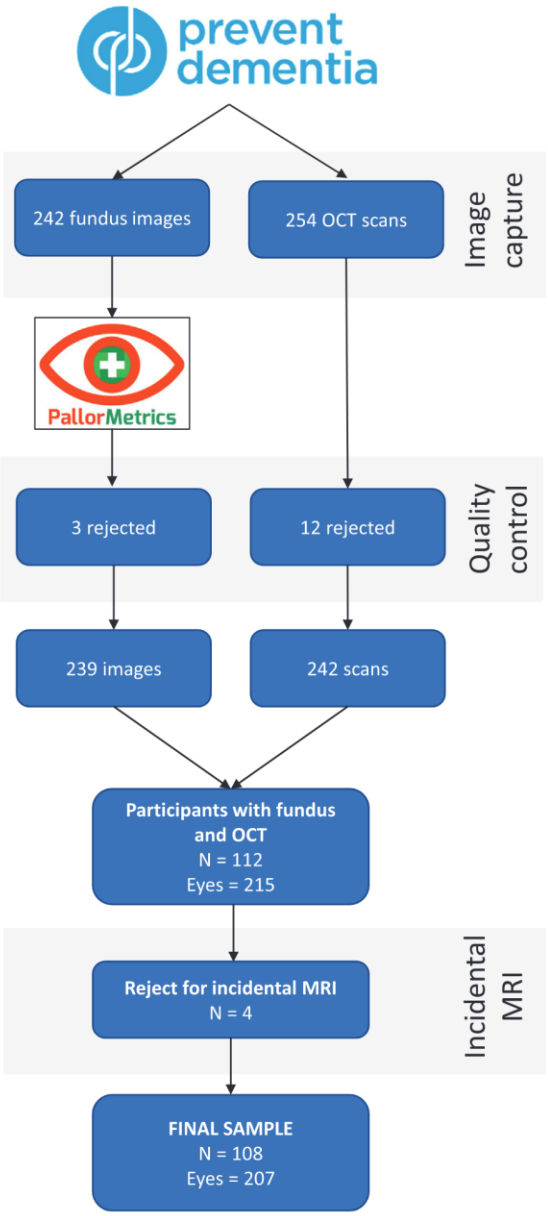


**FIGURE 1** Participant selection flowchart. OCT, optical coherence tomography

microbleeds were assessed separately in the lobar (centrum semiovale) and deep (basal ganglia, thalamus) regions on SWI MRI, and cross-checked against T1w and T2w MRI using a validated scale.[20] Scores were binarized as 0 (absent) or 1 (present in one or both regions). Similarly, lacunes were assessed in the same regions but in T1w, T2w, and FLAIR MRI[4] and binarized in the same manner. Each SVD marker was evaluated by a single rater and a subset (20%) by a second rater. Inter-rater reliability (Cohen kappa) was good: 0.74 for cerebral microbleeds, 0.92 for lacunes, and 0.85 for ePVSs.

WMH total lesion volume was measured according to a protocol described elsewhere.[16] Briefly, in a semi-automated manner, gray matter, white matter, and cerebrospinal fluid were segmented from T1w images to create a binary mask. This mask was then registered to, and subtracted from, the corresponding FLAIR images. All WMH lesion masks were visually inspected and manually corrected for misclassifications. WMH volume was extracted from lesion masks, providing global WMH volume and regional volumes (periventricular WMH, deep WMH). WMH volume was then cube-root transformed.

## 2.3 | Optic disc pallor quantification

Optic disc pallor was measured automatically in color fundus photographs using previously validated software, PallorMetrics.[14] Briefly, a deep learning–based approach was used to localize the fovea and segment the optic disc to the inner edge of the border tissue (Figure 2A, C). A measurement region was defined to start at the disc border and extend 30 pixels inward (Figure 2D). Zones were placed over the measurement region in accordance with the Heidelberg SPECTRALIS peripapillary scan (Figure 2F). Specifically, the intersection of the fovea–optic disc axis with the measurement region was given a value of 0° (Figure 2A). The temporal zone extended from −45° to 45°, the temporal superior from −45° to −90°, and so on. The papillomacular bundle (PMB; a thick bundle of axons originating in the macula that is responsible for central, sharp vision) is a special case of the temporal zone, extending from −15° to 15°. Finally, pallor was measured as a function of red/green light reflectance in each zone with respect to a control region (Figure 2E). The resulting pallor values are dimensionless, and the disc area is in pixels.

## 2.4 | Quality control

Of 242 fundus images presented to the Pallor software, three were subsequently rejected due to: segmentation error (two images) and abnormal disc presentation (one image; Figure S1 in supporting information). Of 254 OCT scans, 12 were rejected due to one or more of improper centering (four scans), clipping (four scans), high myopia (≥ −5D; two scans), poor segmentation (three scans), poor illumination (one scan), and signs of pathology (five scans). Pathologies included excessive peripapillary atrophy, excessively tilted discs, and epiretinal membrane. OCT quality control was conducted by an ophthalmic imager and analyst (author C.H.) via manual inspection of the scans through the Heidelberg Engineering HeyEx device software platform.

## 2.5 | Statistical analysis

To minimize false positives, our approach was 2-fold. First, we tested for associations between each SVD marker and global pallor and global

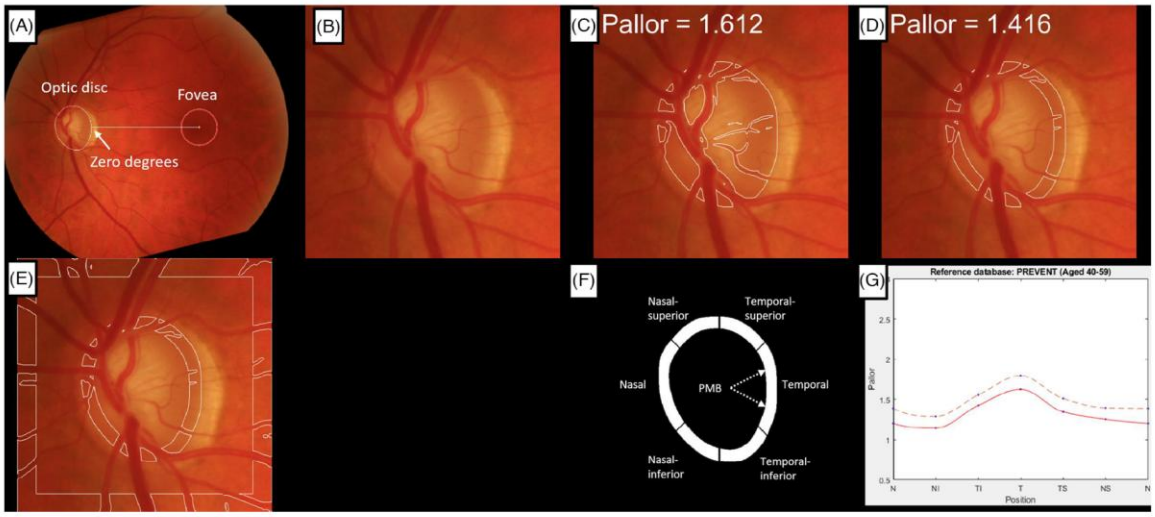


**FIGURE 2** Visual output of the pallor software for a single image. A, Full image rotated along the optic disc-fovea axis. B, Cropped optic disc. C, Segmented whole disc with pallor value. D, Segmented measurement region with global pallor value. E, Measurement and control region. F, Zones and alert system (region turns red if a limit is exceeded). G, Dashed line represents one standard deviation above the mean of all participants, red line is the current participant. Notes: Vessels are excluded in (C), (D), and (E)

pRNFL thickness. When a significant association was found, we then proceeded to test for associations with all eight zonal measures of pallor and pRNFL (seven zones + nasal/temporal ratio). Second, we tested the left and right eyes independently and only considered a finding genuine if it was significant in both eyes. We treated ePVS as a continuous variable—with a range of 0–4 (we did not have access to the full count). We used linear regression for continuous SVD markers (WMH, ePVS), and logistic regression for binary markers (lacunes, microbleeds). Our decision to treat ePVS as continuous was motivated in part due to the limitations of ordinal logistic regression (the main alternative to linear modeling for this case), which can be difficult to interpret and assumes proportional odds, in part to maintain alignment with previous work,[16,17] which also treats ePVS as continuous, and in part to make it easier for readers to compare coefficients across multiple SVD markers. Nonetheless, we acknowledge that linear models may have power limitations in the current context. All models were adjusted for age, sex, history of hypertension, fasting cholesterol, body mass index, and smoking status (current, ex, never). Pallor measurements may be affected by differences in retinal magnification as a result of varying axial length and disc area.[14] Given that disc area is a correlate of axial length,[21] we opted to control for disc area in our models. We further acknowledge that mixed effect models may have been preferable as they can account for the nested structure of eyes within participants and allow the use of all datapoints in a single model; however, the small sample size and a relatively large number of covariates precluded their use. Only three participants were current smokers, so we collapsed "current" with "ex," and only three participants had diabetes, so we did not include diabetes as a covariate. All continuous variables were standardized. Rows containing missing values (detailed in Table 1) were excluded at the point of analysis. Analyses were conducted in R (version 4.2.1; www.R-project.org).

## 2.6 | Data availability

Data are available upon reasonable request from the PREVENT-Dementia study team https://preventdementia.co.uk/.

## 3 | RESULTS

The final sample had a mean age of 51.6 years (standard deviation [SD] = 5.5) and contained a higher proportion of females (62.8%). Scores from SVD markers were similar between the left and right eyes. Demographics and study variables are summarized in Table 1, and visualizations from the pallor software for a single fundus image are presented in Figure 2.

We observed evidence of significant associations between ePVSs in the basal ganglia and global pallor in both the left eye (standardized $\beta$; $\beta = 0.12$ [standard error (S)E = 0.05], $P < 0.05$), and the right eye ($\beta = 0.13$ [SE = 0.05], $P < 0.05$). By zone, we found associations between ePVSs in the basal ganglia and disc pallor in the temporal ($\beta = 0.11$ [SE = 0.05], $P < 0.05$), temporal–inferior ($\beta = 0.11$ [SE = 0.05], $P < 0.05$), nasal–inferior ($\beta = 0.11$ [SE = 0.05], $P < 0.05$), nasal ($\beta = 0.12$ [SE = 0.05], $P < 0.05$), nasal–superior ($\beta = 0.13$ [SE = 0.05], $P < 0.05$) and PMB ($\beta = 0.11$ [SE = 0.05], $P < 0.05$) zones in the left eye, and the temporal ($\beta = 0.13$ [SE = 0.05], $P < 0.05$], temporal–inferior ($\beta = 0.15$ [SE = 0.05], $P < 0.01$), nasal ($\beta = 0.10$ [SE = 0.05], $P < 0.05$), nasal–superior ($\beta = 0.13$ [SE = 0.05], $P < 0.05$), and PMB ($\beta = 0.13$ [SE = 0.05], $P < 0.05$)

**TABLE 1** Demographics and study variables by zone and eye.

| | Eye | | |
|---|---|---|---|
| | *Left* | *Right* | *Overall* |
| *N* (participants) | | | 108 |
| *N* (eyes) | 102 | 105 | 207 |
| **Age** | 51.6 (5.6) | 51.6 (5.5) | 51.6 (5.5) |
| **Sex (female)** | 64 (62.7%) | 66 (62.9%) | 130 (62.8%) |
| **Hypertension diagnosis** | 8 (7.8%) | 8 (7.6%) | 16 (7.7%) |
| **BMI** | 28.7 (5.8) | 28.5 (5.9) | 28.6 (5.8) |
| **Cholesterol** | 5.47 (1.1) | 5.42 (1.0) | 5.44 (1.0) |
| **Smoking** | | | |
| Current | 2 (2.0%) | 2 (1.9%) | 4 (1.9%) |
| Ex | 36 (35.3%) | 37 (35.2%) | 73 (35.3%) |
| Non | 63 (61.8%) | 65 (61.9%) | 128 (61.8%) |
| **White matter hyperintensities** | | | |
| Total | 2.72 (3.2) | 2.7 (3.2) | 2.71 (3.2) |
| Deep | 1 (1.26) | 0.99 (1.24) | 0.99 (1.24) |
| Periventricular | 1.72 (2.2) | 1.71 (2.2) | 1.72 (2.2) |
| **Enlarged perivascular spaces** | | | |
| Count | | | |
| Basal ganglia | 12 (11.8%) | 11 (10.5%) | 23 (11.1%) |
| 0 | | | |
| 1 | 76 (74.5%) | 79 (75.2%) | 155 (74.9%) |
| 2 | 12 (11.8%) | 13 (12.4%) | 25 (12.1%) |
| Centrum semiovale | | | |
| 0 | 12 (11.8%) | 11 (10.5%) | 23 (11.1%) |
| 1 | 62 (60.8%) | 63 (60.0%) | 125 (60.4%) |
| 2 | 17 (16.7%) | 20 (19.0%) | 37 (17.9%) |
| 3 | 8 (7.8%) | 8 (7.6%) | 16 (7.7%) |
| 4 | 1 (1.0%) | 1 (1.0%) | 2 (1.0%) |
| Midbrain (present) | 61 (59.8%) | 64 (61.0%) | 125 (60.4%) |
| **Lacunes (present)** | 13 (12.7%) | 15 (14.3%) | 28 (13.5%) |
| **Microbleeds (present)** | 21 (20.6%) | 22 (21.0%) | 43 (20.8%) |
| **Optic disc pallor** | | | |
| Global | 1.40 (0.18) | 1.34 (0.17) | 1.37 (0.18) |
| Temporal | 1.62 (0.24) | 1.55 (0.23) | 1.58 (0.24) |
| Temporal–inferior | 1.42 (0.20) | 1.34 (0.19) | 1.38 (0.20) |
| Nasal–inferior | 1.16 (0.14) | 1.12 (0.14) | 1.14 (0.14) |
| Nasal | 1.24 (0.16) | 1.18 (0.16) | 1.21 (0.16) |
| Nasal–superior | 1.27 (0.16) | 1.20 (0.15) | 1.23 (0.16) |
| Temporal–superior | 1.36 (0.19) | 1.31 (0.18) | 1.33 (0.18) |
| PMB | 1.68 (0.25) | 1.60 (0.24) | 1.64 (0.25) |
| Nasal/temporal ratio | 0.769 (0.06) | 0.771 (0.08) | 0.770 (0.07) |
| **RNFL thickness** | | | |
| Global | 98.2 (8.2) | 98.3 (8.1) | 98.3 (8.1) |
| Temporal | 69.7 (13.6) | 74.5 (13.2) | 72.1 (13.6) |
| Temporal–inferior | 140 (19.5) | 141 (22.9) | 141 (21.2) |

(Continues)

**TABLE 1** (Continued)

| | Eye | | |
|---|---|---|---|
| | *Left* | *Right* | *Overall* |
| Nasal–inferior | 114 (22.1) | 112 (22.5) | 113 (22.3) |
| Nasal | 74.3 (16.3) | 76.3 (19.0) | 75.3 (17.7) |
| Nasal–superior | 111 (19.3) | 98.7 (18.8) | 105 (20.0) |
| Temporal–superior | 135 (17.4) | 135 (17.0) | 135 (17.1) |
| PMB | 54.2 (13.2) | 56.1 (9.1) | 55.1 (11.3) |
| Nasal/temporal ratio | 1.11 (0.3) | 1.06 (0.4) | 1.08 (0.3) |
| **Retinal covariates** | | | |
| Disc area | 75,700 (15,700) | 73,600 (14,200) | 74,600 (14,900) |

*Notes*: All values are mean (standard deviation) or N (%). Missing data (variable, number of participants): Hypertension diagnosis (2), body mass index (4), cholesterol (8), smoking status (2), diabetes (2), white matter hyperintensities (4), enlarged perivascular spaces (4), lacunes (4), microbleeds (6), global pRNFL (2), nasal pRNFL (2), nasal–superior pRNFL (2), papillomacular bundle RNFL (4), nasal/temporal ratio pRNFL (6).
Abbreviations: BMI, body mass index; NT, nasal/temporal; PMB, papillomacular bundle; pRNFL, peripapillary retinal nerve fiber layer thickness.

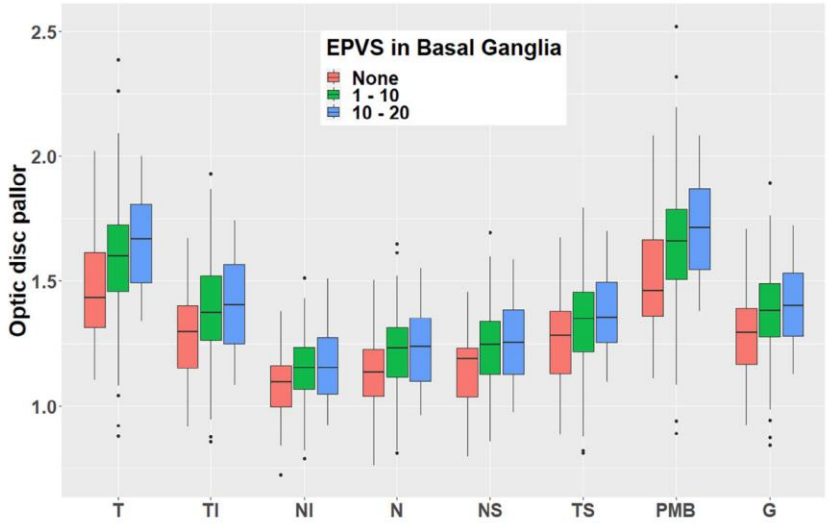


**FIGURE 3** Grouped box plot showing the relationship between the number of EPVSs in the basal ganglia and optic disc pallor by zone. Data aggregated from both eyes. EPVSs, enlarged perivascular spaces; G, global; I, inferior; N, nasal; S, superior; T, temporal

zones in the right eye. There was no evidence of pallor being associated with any other MRI markers. Similarly, we observed no evidence of associations between pRNFL thickness and any of the MRI markers. Results are summarized in Table 2 and presented graphically in Figure 3.

## 4 | DISCUSSION

Independent of covariates, we found that disc pallor, but not pRNFL thickness, was significantly associated with ePVSs in the basal ganglia globally, and in several zones. These associations were found independently in the left and right eyes. ePVSs are commonly observed in SVD pathologies[22,23] and have been associated with increased age and cardiovascular risk factors,[24] inflammation,[25] blood–brain barrier dysfunction,[26] cognitive decline and dementia,[27,28] and other MRI features of SVD,[23,24] yet they are difficult and costly to measure. Here, we provide evidence that increasing paleness of the optic disc, measured automatically in conventional retinal fundus images, is associated with ePVSs in the brain.

Previous research has established a connection between MRI-derived markers of SVD and parameters measured from fundus images showing the retinal vasculature.[7,29–33] For example, studies have discovered that ePVSs are associated with changes in retinal vessel

**TABLE 2** Linear (WMH, ePVS) and logistic (lacunes, microbleeds) regression results for each eye.

| | | | Eye | | | |
|---|---|---|---|---|---|---|
| | | | *Left* | | *Right* | |
| | Retinal zone | Imaging modality | *β (SE)/odds ratio (CI)* | *P value* | *β (SE)/odds ratio (CI)* | *P value* |
| **White matter hyperintensities** | | | | | | |
| Total | *Global* | Fundus | 0.10 (0.11) | 0.377 | 0.05 (0.11) | 0.648 |
| | | OCT | −0.08 (0.10) | 0.453 | −0.03 (0.10) | 0.781 |
| Periventricular | *Global* | Fundus | 0.06 (0.11) | 0.596 | 0.03 (0.11) | 0.803 |
| | | OCT | −0.07 (0.10) | 0.576 | −0.02 (0.10) | 0.866 |
| Deep | *Global* | Fundus | 0.14 (0.11) | 0.198 | 0.08 (0.11) | 0.482 |
| | | OCT | −0.08 (0.11) | 0.440 | −0.04 (0.10) | 0.691 |
| **Enlarged perivascular spaces** | | | | | | |
| Basal ganglia | *Global* | Fundus | 0.12 (0.05) | **0.020*** | 0.13 (0.05) | **0.141*** |
| | | OCT | −0.04 (0.05) | 0.408 | −0.03 (0.05) | 0.538 |
| | *Temporal* | Fundus | 0.11 (0.05) | **0.022*** | 0.13 (0.05) | **0.013*** |
| | *Temporal–Inferior* | Fundus | 0.11 (0.05) | **0.015*** | 0.15 (0.05) | **0.008**** |
| | *Nasal–Inferior* | Fundus | 0.11 (0.05) | **0.026*** | 0.09 (0.05) | 0.082 |
| | *Nasal* | Fundus | 0.12 (0.05) | **0.016*** | 0.10 (0.05) | **0.042*** |
| | *Nasal–Superior* | Fundus | 0.13 (0.05) | **0.013*** | 0.13 (0.05) | **0.013*** |
| | *Temporal–Superior* | Fundus | 0.09 (0.05) | 0.067 | 0.10 (0.05) | 0.064 |
| | *PMB* | Fundus | 0.11 (0.05) | **0.023*** | 0.13 (0.05) | **0.014*** |
| | *NT ratio* | Fundus | −0.01 (0.05) | 0.783 | −0.04 (0.04) | 0.379 |
| Midbrain | *Global* | Fundus | 1.34 (0.82–2.25) | 0.249 | 1.04 (0.61–1.75) | 0.884 |
| | | OCT | 0.82 (0.51–1.30) | 0.400 | 0.90 (0.56–1.43) | 0.650 |
| Centrum sem. | *Global* | Fundus | 0.01 (0.09) | 0.881 | 0.06 (0.09) | 0.522 |
| | | OCT | 0.03 (0.09) | 0.761 | 0.03 (0.08) | 0.698 |
| **Lacunes** | *Global* | Fundus | 1.49 (0.77–3.05) | 0.247 | 1.20 (0.63–2.36) | 0.576 |
| | | OCT | 1.29 (0.68–2.56) | 0.445 | 1.44 (0.79–2.72) | 0.245 |
| **Microbleeds** | *Global* | Fundus | 0.87 (0.47–1.56) | 0.638 | 0.87 (0.48–1.54) | 0.624 |
| | | OCT | 1.21 (0.70–2.16) | 0.501 | 1.37 (0.82–2.39) | 0.248 |

*Note*: All models were adjusted for age, sex, diagnosed hypertension, cholesterol, body mass index, and smoking status. Pallor/fundus models were additionally adjusted for disc size.

Abbreviations: CI, confidence interval; ePVS, enlarged perivascular space; NT, nasal/temporal; OCT, optical coherence tomography; PMB, papillomacular bundle; SE, standard error of the mean; WMH, white matter hyperintensity.

*$P < 0.05$

**$P < 0.01$.

thickness[32,33] and reduced fractal dimension.[33] However, there has been less focus on investigating the relationship between SVD and neuronal retinal measures. To the best of our knowledge, no other studies have explored the relationship between SVD and optic disc appearance in terms of its color or pallor. However, a limited body of work has linked SVD with pRNFL thinning in conditions such as cerebral amyloid angiopathy[8] and cerebral autosomal dominant arteriopathy with subcortical infarcts and leukoencephalopathy (CADASIL) [9,10] although it is worth noting that an increase in pRNFL has also been observed in CADASIL.[34] Our research supports these findings and suggests that optic disc pallor may be more sensitive than pRNFL as an indicator of SVD.

Out of four MRI markers tested, only ePVSs in the basal ganglia were associated with an ocular measure. One reason could be statistical power. Indeed, non-significant associations all suggested a positive association (see Table 2), so an effect may have emerged given more data. Alternatively, the observed association between increasing disc pallor and ePVSs suggests that disc pallor may be a surrogate for another pathology. Perivascular spaces/channels are the anatomical basis of the recently proposed glymphatic system,[35–38] a brain-wide waste clearance system responsible for eliminating metabolites and soluble proteins from the central nervous system. Impaired glymphatic function has been associated with multiple neurological disorders,[37,39] including worsening radiological features of SVD.[40–42]

Importantly, there is a growing body of research supporting the existence of an ocular glymphatic system[38,43–47] that is likely continuous with the glymphatic system of the brain,[48] extending to the visual pathway (including the retina and optic nerve). Indeed, several studies have highlighted the potential role of ocular glymphatic dysfunction in optic nerve disorders, such as glaucoma and hydrocephalus (see Kasi et al.[48] for a review). This suggests that the ocular glymphatic system may play a crucial role in normal optic nerve function, and impairment could lead to ocular dysfunction, including the loss of retinal ganglion cells and subsequent RNFL thinning.[49]

In our study, we observed an association between brain ePVS and increasing paleness of the optic disc, which itself is believed to be driven by RNFL loss. As a result, we propose that optic disc pallor may serve as a marker of glymphatic dysfunction affecting both the brain and visual pathway. In particular, our findings align with previous research which found that impaired glymphatic function in the brain may be uniquely linked to increased ePVS in the basal ganglia, but not the centrum semiovale.[42] Further work should investigate the effect of glymphatic function on optic disc appearance.

Although optic disc pallor is an indirect measure of pRNFL thickness, in the current study we observed associations between ePVS and disc pallor but not between ePVS and pRNFL thickness. There are two potential reasons for this apparent discrepancy. First, disc pallor can reflect not only the loss of nerve fibers but also gliosis,[50] axonal degeneration, and other changes within the optic nerve head, which might be more directly related to the presence of ePVSs. By contrast, pRNFL measurements are specifically focused on axonal thickness and may not capture these broader changes. Furthermore, disc pallor indicates chronic, longstanding optic nerve damage, which may be more aligned with the cumulative effects of chronic SVD as evidenced by ePVSs. By contrast, pRNFL thickness changes can occur more rapidly in response to acute insults and may not reflect the chronicity of the underlying pathology as sensitively as optic disc pallor.

Strengths of this study include: (1) the concomitant use of fundus images and OCT scans to investigate multiple brain-based SVD markers; (2) the use of novel, automated software to quantify optic disc pallor; and (3) that significant associations were found independently in the left and right eyes.

Limitations of this study include its cross-sectional design, which precluded us from inferring causality or investigating change over time. In addition, the sample was majority female (62.8%) and White British in ethnicity, which may limit generalizability to a wider population. Finally, it should be noted that there are several other metrics available for quantifying ePVS burden including length, width, volume, sphericity, and orientation,[23] which may have allowed for further insight into the associations between brain health and disc pallor. Future research should aim to replicate the current results in a larger and more diverse sample.

## 5 | CONCLUSION

ePVSs are a hallmark feature of SVD, yet they are difficult and costly to measure. Our study suggests that increasing paleness of the optic disc may be linked to the presence of ePVSs in the basal ganglia. Our findings emphasize the value of retinal fundus imaging as a convenient and promising avenue for investigating changes in brain health associated with SVD. Further research in this direction could shed more light on the complex interplay between retinal measures and SVD, ultimately contributing to our understanding of neurodegenerative diseases.

## ACKNOWLEDGMENTS

We would like to thank the PREVENT Dementia participants for kindly donating their time. This research was conducted as part of the doctoral studies of Samuel Gibbon, who is supported by the Biotechnology and Biological Sciences Research Council (BBSRC), a UK government body.

## CONFLICT OF INTEREST STATEMENT

S. Gibbon, A. Low, C. Hamid, M. Reid-Schachter, G. Muniz-Terrera, C. Ritchie, E. Trucco, J. T. O'Brien, and T. J. MacGillivray report no disclosures relevant to the manuscript. B. Dhillon received an educational grant from Apellis Pharmaceuticals in 2023. Author disclosures are available in the supporting information.

## CONSENT STATEMENT

All participants provided written informed consent, and the study was carried out in compliance with the Declaration of Helsinki.

## ORCID

*Samuel Gibbon* https://orcid.org/0000-0002-5485-7523

## REFERENCES

1. Cannistraro RJ, Badi M, Eidelman BH, Dickson DW, Middlebrooks EH, Meschia JF. CNS small vessel disease: a clinical review. *Neurology*. 2019;92(24):1146-1156. doi:10.1212/WNL.0000000000007654
2. Wardlaw JM, Smith C, Dichgans M. Small vessel disease: mechanisms and clinical implications. *Lancet Neurol*. 2019;18(7):684-696. doi:10.1016/S1474-4422(19)30079-1
3. Li Q, Yang Y, Reis C, et al. Cerebral small vessel disease. *Cell Transplant*. 2018;27(12):1711-1722. doi:10.1177/0963689718795148
4. Wardlaw JM, Smith EE, Biessels GJ, et al. Neuroimaging standards for research into small vessel disease and its contribution to ageing and neurodegeneration. *Lancet Neurol*. 2013;12(8):822-838. doi:10.1016/S1474-4422(13)70124-8
5. Patton N, Aslam T, MacGillivray T, Pattie A, Deary IJ, Dhillon B. Retinal vascular image analysis as a potential screening tool for cerebrovascular disease: a rationale based on homology between cerebral and retinal microvasculatures. *J Anat*. 2005;206(4):319-348. doi:10.1111/j.1469-7580.2005.00395.x
6. Kashani AH, Asanad S, Chan JW, et al. Past, present and future role of retinal imaging in neurodegenerative disease. *Prog Retin Eye Res*. 2021;83:100938. doi:10.1016/j.preteyeres.2020.100938
7. Biffi E, Turple Z, Chung J, Biffi A. Retinal biomarkers of cerebral small vessel disease: a systematic review. *PLoS One*. 2022;17(4):e0266974.
8. van Etten ES, de Boer I, Steenmeijer SR, et al. Optical coherence tomography detects retinal changes in hereditary cerebral amyloid angiopathy. *Eur J Neurol*. 2020;27(12):2635-2640. doi:10.1111/ene.14507
9. Parisi V, Pierelli F, Coppola G, et al. Reduction of optic nerve fiber layer thickness in CADASIL. *Eur J Neurol*. 2007;14(6):627-631. doi:10.1111/j.1468-1331.2007.01795.x

10. Rufa A, Pretegiani E, Frezzotti P, et al. Retinal nerve fiber layer thinning in CADASIL: an optical coherence tomography and MRI study. *Cerebrovasc Dis*. 2011;31(1):77-82. doi:10.1159/000321339
11. Mutlu U, Colijn JM, Ikram MA, et al. Association of retinal neurodegeneration on optical coherence tomography with dementia: a population-based study. *JAMA Neurol*. 2018;75(10):1256-1263. doi:10.1001/jamaneurol.2018.1563
12. MacGillivray T, McGrory S, Pearson T, Cameron J. Retinal imaging in early Alzheimer's disease. *Neuromethods*. 2018;137:199-212. doi:10.1007/978-1-4939-7674-4_14
13. Yang H, Lee HS, Bae HW, Seong GJ, Kim CY, Lee SY. Effect of image quality fluctuations on the repeatability of thickness measurements in swept-source optical coherence tomography. *Sci Rep*. 2020;10(1):13897. doi:10.1038/s41598-020-70852-y
14. Gibbon S, Muniz-Terrera G, Yii FSL, et al. PallorMetrics: software for automatically quantifying optic disc pallor in fundus photographs, and associations with peripapillary RNFL thickness. *Transl Vis Sci Technol*. 2024;13(5):20. doi:10.1167/tvst.13.5.20
15. Ritchie CW, Ritchie K. The PREVENT study: a prospective cohort study to identify mid-life biomarkers of late-onset Alzheimer's disease. *BMJ Open*. 2012;2(6):e001893. doi:10.1136/bmjopen-2012-001893
16. Low A, Prats-Sedano MA, McKiernan E, et al. Modifiable and non-modifiable risk factors of dementia on midlife cerebral small vessel disease in cognitively healthy middle-aged adults: the PREVENT-Dementia study. *Alzheimers Res Ther*. 2022;14(1):154. doi:10.1186/s13195-022-01095-4
17. Low A, Prats-Sedano MA, Stefaniak JD, et al. CAIDE dementia risk score relates to severity and progression of cerebral small vessel disease in healthy midlife adults: the PREVENT-Dementia study. *J Neurol Neurosurg Psychiatry*. 2022;93(5):481-490. doi:10.1136/jnnp-2021-327462
18. Gibbon S, Hamid C, Threlfall A, et al. Multi-modal retinal imaging for investigating neurovascular health. *Eye*. 2023:1-2. doi:10.1038/s41433-023-02830-3
19. Potter GM, Chappell FM, Morris Z, Wardlaw JM. Cerebral perivascular spaces visible on magnetic resonance imaging: development of a qualitative rating scale and its observer reliability. *Cerebrovasc Dis*. 2015;39(3-4):224-231. doi:10.1159/000375153
20. Gregoire SM, Chaudhary UJ, Brown MM, et al. The microbleed anatomical rating scale (MARS): reliability of a tool to map brain microbleeds. *Neurology*. 2009;73(21):1759-1766. doi:10.1212/WNL.0b013e3181c34a7d
21. Oliveira C, Harizman N, Girkin CA, et al. Axial length and optic disc size in normal eyes. *Br J Ophthalmol*. 2007;91(1):37-39. doi:10.1136/bjo.2006.102061
22. Brown R, Benveniste H, Black SE, et al. Understanding the role of the perivascular space in cerebral small vessel disease. *Cardiovasc Res*. 2018;114(11):1462-1473. doi:10.1093/cvr/cvy113
23. Wardlaw JM, Benveniste H, Nedergaard M, et al. Perivascular spaces in the brain: anatomy, physiology and pathology. *Nat Rev Neurol*. 2020;16(3):137-153. doi:10.1038/s41582-020-0312-z
24. Francis F, Ballerini L, Wardlaw JM. Perivascular spaces and their associations with risk factors, clinical disorders and neuroimaging features: a systematic review and meta-analysis. *Int J Stroke*. 2019;14(4):359-371. doi:10.1177/1747493019830321
25. Low A, Mak E, Rowe JB, Markus HS, O'Brien JT. Inflammation and cerebral small vessel disease: a systematic review. *Ageing Res Rev*. 2019;53(February):100916. doi:10.1016/j.arr.2019.100916
26. Wardlaw JM, Doubal F, Armitage P, et al. Lacunar stroke is associated with diffuse blood–brain barrier dysfunction. *Ann Neurol*. 2009;65(2):194-202. doi:10.1002/ana.21549
27. Ding J, Sigurðsson S, Jónsson PV, et al. Large perivascular spaces visible on magnetic resonance imaging, cerebral small vessel disease progression, and risk of dementia: the age, gene/environment susceptibility–Reykjavik study. *JAMA Neurol*. 2017;74(9):1105-1112. doi:10.1001/jamaneurol.2017.1397
28. Paradise M, Crawford JD, Lam BCP, et al. Association of dilated perivascular spaces with cognitive decline and incident dementia. *Neurology*. 2021;96(11):e1501-e1511. doi:10.1212/WNL.0000000000011537
29. Cheung N, Mosley T, Islam A, et al. Retinal microvascular abnormalities and subclinical magnetic resonance imaging brain infarct: a prospective study. *Brain*. 2010;133(Pt 7):1987-1993. doi:10.1093/brain/awq127
30. Ikram MK, De Jong FJ, Van Dijk EJ, et al. Retinal vessel diameters and cerebral small vessel disease: the Rotterdam Scan Study. *Brain J Neurol*. 2006;129(Pt 1):182-188. doi:10.1093/brain/awh688
31. Ballerini L, Fetit AE, Wunderlich S, et al. Retinal biomarkers discovery for cerebral small vessel disease in an older population. *Commun Comput Inf Sci*. 2020;1248 CCIS(July):400-409. doi:10.1007/978-3-030-52791-4_31
32. Mutlu U, Adams HHH, Hofman A, et al. Retinal microvascular calibers are associated with enlarged perivascular spaces in the brain. *Stroke*. 2016;47(5):1374-1376. doi:10.1161/STROKEAHA.115.012438
33. Ballerini L, McGrory S, Valdés Hernández MDC, et al. Quantitative measurements of enlarged perivascular spaces in the brain are associated with retinal microvascular parameters in older community-dwelling subjects. *Cereb Circ Cogn Behav*. 2020;1(August):100002. doi:10.1016/j.cccb.2020.100002
34. Alten F, Motte J, Ewering C, et al. Multimodal retinal vessel analysis in CADASIL patients. *PLoS One*. 2014;9(11):e112311. doi:10.1371/journal.pone.0112311
35. Iliff JJ, Wang M, Liao Y, et al. A paravascular pathway facilitates CSF flow through the brain parenchyma and the clearance of interstitial solutes, including amyloid $\beta$. *Sci Transl Med*. 2012;4(147):147ra111. doi:10.1126/scitranslmed.3003748
36. Jessen NA, Munk ASF, Lundgaard I, Nedergaard M. The glymphatic system—a beginner's guide. *Neurochem Res*. 2015;40(12):2583-2599. doi:10.1007/s11064-015-1581-6
37. Carlstrom LP, Eltanahy A, Perry A, et al. A clinical primer for the glymphatic system. *Brain*. 2022;145(3):843-857. doi:10.1093/brain/awab428
38. Hu P, Arfuso F, Madigan MC, et al. Evidence for a glymphatic system in human, primate, rat and mouse retina. *Invest Ophthalmol Vis Sci*. 2016;57(12). https://iovs.arvojournals.org/article.aspx?articleid=2559756
39. Rasmussen MK, Mestre H, Nedergaard M. The glymphatic pathway in neurological disorders. *Lancet Neurol*. 2018;17(11):1016-1024. doi:10.1016/S1474-4422(18)30318-1
40. Tian Y, Cai X, Zhou Y, et al. Impaired glymphatic system as evidenced by low diffusivity along perivascular spaces is associated with cerebral small vessel disease: a population-based study. *Stroke Vasc Neurol*. 2023;8:413-423. doi:10.1136/svn-2022-002191
41. Mestre H, Kostrikov S, Mehta RI, Nedergaard M. Perivascular spaces, glymphatic dysfunction, and small vessel disease. *Clin Sci*. 2017;131(17):2257-2274. doi:10.1042/CS20160381
42. Zhang W, Zhou Y, Wang J, et al. Glymphatic clearance function in patients with cerebral small vessel disease. *NeuroImage*. 2021;238:118257. doi:10.1016/j.neuroimage.2021.118257
43. Wang X, Lou N, Eberhardt A, et al. An ocular glymphatic clearance system removes $\beta$-amyloid from the rodent eye. *Sci Transl Med*. 2020;12(536):eaaw3210. doi:10.1126/scitranslmed.aaw3210
44. Jacobsen HH, Ringstad G, Jørstad ØK, Moe MC, Sandell T, Eide PK. The human visual pathway communicates directly with the subarachnoid space. *Invest Ophthalmol Vis Sci*. 2019;60(7):2773-2780. doi:10.1167/iovs.19-26997
45. Denniston AK, Keane PA. Paravascular pathways in the eye: is there an "ocular glymphatic system"? *Invest Ophthalmol Vis Sci*. 2015;56(6):3955-3956. doi:10.1167/iovs.15-17243

46. Wostyn P, De Groot V, Van Dam D, Audenaert K, De Deyn PP, Killer HE. The glymphatic system: a new player in ocular diseases? *Invest Ophthalmol Vis Sci*. 2016;57(13):5426-5427. doi:10.1167/iovs.16-20262
47. Chan-Ling T, Uddin MN, Koina ME, Behar-Cohen FF, Hu P. Compelling structural and functional evidence for glymphatics and lymphatics in human posterior eye: enhanced immune response and glymphatic/lymphatic changes in glaucoma pathogenesis. *Invest Ophthalmol Vis Sci*. 2019;60(9):4274.
48. Kasi A, Liu C, Faiq MA, Chan KC. Glymphatic imaging and modulation of the optic nerve. *Neural Regen Res*. 2021;17(5):937-947. doi:10.4103/1673-5374.324829
49. Wostyn P, De Deyn PP. The retinal nerve fiber layer as a window to the glymphatic system. *Clin Neurol Neurosurg*. 2020;188:105593. doi:10.1016/j.clineuro.2019.10559
50. Osaguona VB. Differential diagnoses of the pale/white/atrophic disc. *Community Eye Health*. 2016;29(96):71-74.

## SUPPORTING INFORMATION

Additional supporting information can be found online in the Supporting Information section at the end of this article.

**How to cite this article:** Gibbon S, Low A, Hamid C, et al. Association of optic disc pallor and RNFL thickness with cerebral small vessel disease in the PREVENT-Dementia study. *Alzheimer's Dement*. 2024;16:e12633. https://doi.org/10.1002/dad2.12633

## 5.5. Conclusion

In this study, we explored the relationship between optic disc pallor, pRNFL thickness, and four MRI markers of cSVD. Our findings revealed a significant association between optic disc pallor and enlarged perivascular spaces, independent of covariates. This is a novel finding. While no other associations were identified and effect sizes were modest, this result suggests that optic disc pallor may be a marker for cerebrovascular damage.

This study makes several important contributions to the field. It is the first to explore the relationship between fundus image-derived optic disc pallor measurements and MRI markers of cSVD. Notably, the novel association between optic disc pallor and perivascular spaces provides new insights into both screening and potential mechanisms. For instance, with further refinement and validation, optic disc pallor could be developed as a screening tool to identify individuals who might benefit from MRI scans. Moreover, our findings suggest for the first time that optic disc pallor could serve as a marker of glymphatic dysfunction, shedding light on a possible underlying mechanism.

# Chapter 6

# Optic disc pallor and lacunar stroke

## 6.1. Introduction

In the previous chapter, we uncovered an association between optic disc pallor and MRI-visible enlarged perivascular spaces, a core feature of cSVD. In this chapter, I extend the analysis to a cohort of patients (Mild Stroke Study (MSS))[116–118] who experienced a mild ischaemic stroke, subcategorised as either cortical or lacunar.

While cortical strokes are usually caused by cardio embolism or large artery disease, the underlying cause of lacunar strokes is typically cSVD.[2,5,39] Therefore, this chapter continues to address the second objective – exploring optic disc pallor in a cerebrovascular disease. Previous retinal imaging work in the same cohort observed differences in vessel-based metrics in lacunar compared to cortical stroke,[117,118] however the role of optic disc pallor remains unexplored. I hypothesised that lacunar stroke patients would have paler optic discs than cortical stroke patients, and that pallor would positively correlate with MRI-based cSVD ratings.

## 6.2. Acknowledgement of contribution

MSS was led by Dr Fergus Doubal and Prof. Joanna Wardlaw. Dr. Doubal coordinated the study and oversaw retinal photography, while Prof. Wardlaw coded the MRI brain scans and provided oversight. I extend my gratitude to all those involved in creating and maintaining the MSS, including the patients.

Regarding the current study, Dr Doubal provided clinical guidance – helping decide which covariates to include and how to interpret the results. Dr Francesca Chappell provided guidance on which statistical tests to apply. All authors commented on the manuscript.

## 6.3. My contribution to this work

I led:

- Generating the research question, and study design.
- Reviewing the literature.
- Preparing the images for processing.
- Processing of retinal images including quality control.
- Combining datasets (MRI, *PallorMetrics*, clinical data).
- Performing the analysis.
- Creating the tables and figures.
- Drafting the manuscript.
- Incorporating co-authors' comments and finalising the manuscript.
- Writing this chapter.

## 6.4. Published article

BMJ Neurology Open

# Association between optic disc pallor and lacunar stroke

Samuel Gibbon ,[1,2] Fergus Doubal,[1] Francesca Chappell ,[1,3] Joanna M Wardlaw,[1,3] Baljean Dhillon,[2,3] Thomas MacGillivray[2,3]

**To cite:** Gibbon S, Doubal F, Chappell F, *et al*. Association between optic disc pallor and lacunar stroke. *BMJ Neurology Open* 2024;**6**:e000789. doi:10.1136/bmjno-2024-000789

Received 07 June 2024
Accepted 19 August 2024

## ABSTRACT

**Objective** To test for associations between optic disc pallor and two clinical variables: ischaemic stroke subtype (cortical and lacunar) and cerebral small vessel disease (SVD) scores in a cohort of hospital patients admitted with mild stroke (Mild Stroke Study 1).

**Methods** We used previously validated software, *PallorMetrics*, to quantify optic disc pallor in colour fundus photographs of patients diagnosed as having either cortical (n=92) or lacunar (n=92) stroke. We used logistic regression to assess the relationship between stroke type and disc pallor in several zones and ordinal logistic regression to assess the relationship between disc pallor and total SVD score. The left and right eyes were analysed separately.

**Results** In the right eye, independent of age, sex, disc area, hypertension and diabetes, increased optic disc pallor was significantly associated with lacunar stroke in all zones (for global pallor: OR per SD increase=1.55, 95% CI 1.11 to 2.17, p=0.011) and total SVD score in the temporal superior (standardised β=0.36, SE=0.15, p=0.020) and nasal-inferior zones (standardised β=0.44, SE=0.15, p=0.004) in the right eye. Weaker trends were observed in the left eye; however, these did not reach statistical significance.

**Conclusion** Optic disc pallor may be associated with SVD severity and lacunar stroke, which may reflect vascular damage to the optic nerve or its pathways. Our findings underscore the utility of colour fundus photography to learn more about SVD pathology.

### WHAT IS ALREADY KNOWN ON THIS TOPIC

⇒ Cerebral small vessel disease (SVD) causes lacunar stroke, which accounts for around 25% of all ischaemic strokes and differs from other ischaemic strokes in terms of prognosis, therapy and prevention strategies. The retina, particularly the optic disc, due to its vascular similarity to the brain, has been identified as a potential site for biomarkers that could help in understanding and diagnosing SVD and stroke.

### WHAT THIS STUDY ADDS

⇒ This study found that optic disc pallor is significantly associated with the lacunar stroke subtype (compared with atheromatous large artery cortical strokes) and higher SVD scores. This finding suggests that optic disc pallor could be a marker of chronic small vessel vascular impairment affecting the optic nerve and may serve as a non-invasive indicator of SVD severity.

### HOW THIS STUDY MIGHT AFFECT RESEARCH, PRACTICE OR POLICY

⇒ The association between optic disc pallor and SVD highlights another feature of retinal fundus imaging that can act as a convenient and non-invasive method for assessing brain health and SVD severity. This could potentially lead to improved diagnostic tools and more targeted therapeutic strategies to prevent SVD-related stroke and cognitive decline, influencing clinical practice and policy in stroke management and prevention.



[1]Centre for Clinical Brain Sciences, The University of Edinburgh, Edinburgh, UK
[2]Robert O Curle Ophthalmology Suite, Institute for Regeneration and Repair, The University of Edinburgh, Edinburgh, UK
[3]UK Dementia Research Institute Centre, The University of Edinburgh, Edinburgh, UK

**Correspondence to**
Samuel Gibbon;
samuel.gibbon@ed.ac.uk

## INTRODUCTION

Cerebral small vessel disease (SVD) is an age-associated condition impacting the perforating small blood vessels of the central nervous system and constitutes a significant factor in the development of stroke, dementia and cognitive decline.[1–3] In particular, SVD is a major cause of lacunar stroke,[4 5] which accounts for around 25% of all ischaemic strokes[6 7] and differs from other ischaemic strokes with regard to prognosis, therapy and prevention strategies.[6 8–10] SVD can be detected in the brain with MRI. Key visible indicators of SVD include lacunes, microbleeds, white matter hyperintensities (WMHs) and enlarged perivascular spaces.[1–4] However, MRI is expensive, with limited availability. Instead, the retina, owing to its homology with the brain,[11] particularly with regard to the microvasculature, has become a target for biomarker discovery and mechanistic insight into SVD and stroke.[12]

Previous work using colour fundus photographs investigating the eye–brain connection in SVD and lacunar stroke has shown increased microvasculature signs in lacunar compared with cortical stroke, including wider retinal venules,[13 14] decreased fractal dimension,[15] narrower arterioles and greater arteriovenous nipping,[14] highlighting the importance of vascular changes in lacunar stroke. Most other work looking at retinal

features and stroke has also focused on the retinal vasculature.[13–18] However, an under-researched feature of the retina that could provide further insight into SVD is the optic disc.

A pale disc, for instance, indicates optic atrophy and represents loss or damage to retinal ganglion cell (RGC) axons along the anterior visual pathway, and to some extent, a loss of vasculature.[19] The quantity of RGC axons is captured by the retinal nerve fibre layer (RNFL), which can be measured with three-dimensional scanning technology, optical coherence tomography (OCT). Thinning of the peripapillary RNFL (pRNFL; circular OCT scan around the optic disc) has been associated with SVD,[12] Alzheimer's disease, mild cognitive impairment,[20] increased risk of dementia,[21] future cognitive decline[22] and increased cardiovascular risk.[23] One study looked directly at pRNFL defects and stroke,[24] finding increased defects (and hence thinner pRNFL) in acute stroke compared with controls. However, research investigating optic disc pallor/atrophy and stroke is scant; we found just one study,[25] with the authors reporting a high prevalence of optic atrophy in patients who had ischaemic stroke; stroke subtypes were not assessed.

One potential reason for the scarcity of research in this area could be the need for specialist ophthalmological assessment to diagnose optic atrophy/pallor, which can vary among observers.[26] Recently, we developed an automatic method of obtaining continuous measurements of optic disc pallor from colour fundus photographs,[27] which may act as a proxy for pRNFL thickness and the detection of defects. In the current study, we explore associations between optic disc pallor and two clinical features: ischaemic stroke subtype (cortical and lacunar) and total SVD scores in a prospective study of minor stroke and SVD.

## METHODS

### Participants and image capture

The Mild Stroke Study 1 population has been described in detail elsewhere.[13 15 28] Briefly, 220 patients who had experienced a clinical ischaemic or minor cortical stroke were recruited from a hospital stroke service in Edinburgh, UK. Due to legacy problems with data linkage, retinal fundus photographs were available for 186 patients. All patients underwent MRI (1.5 T; Signa LX; General Electric) at presentation and had retinal fundus images (Canon CR-DGi; Canon USA) taken within 4 weeks of stroke onset. The MRI sequence included axial diffusion-weighted, T2-weighted, fluid-attenuated inversion recovery (FLAIR) and gradient echo, while the retinal photography was six-field (including optic disc centred) of both eyes. Retinal imaging was carried out according to the Early Treatment Diabetic Retinopathy Study protocol,[29] which always captured the right eye first, and administered 1% tropicamide as necessary (two drops per eye) to dilate the pupil. Prior to dilation, patients were screened for glaucoma and a history of glaucoma.

### Stroke classification

#### Clinical

A stroke physician (author FD) examined all patients and assessed stroke severity using the NIH Stroke Scale.[30] The stroke clinical syndrome was classified as either lacunar or cortical based on the Oxfordshire Community Stroke Project classification.[31] Briefly, cortical stroke was defined as a partial anterior circulation stroke syndrome or, if in the posterior circulation, visual field loss. Lacunar stroke was defined by pure motor weakness and/or sensory loss in the face and arm, arm and leg, or all three, as well as ataxic hemiparesis or clumsy hand dysarthria syndrome.[13 32]

#### Radiological

A consultant neuroradiologist (author JW) identified and located acute ischaemic stroke lesions (low signal on apparent diffusion coefficient (ADC) map, high signal on diffusion imaging), old ischaemic stroke lesions (high/low FLAIR signal, high T2 signal, no signal on diffusion imaging/ADC map) and old haemorrhages (low gradient-echo signal). Lacunar infarcts were defined as acute ischaemic lesions, round and under 2 cm in the centrum semiovale, internal capsule, brainstem or basal ganglia. Cortical lesions were defined as acute ischaemic lesions affecting cortical and adjacent subcortical tissue in a known cortical arterial branch territory, including striatocapsular infarcts (>2 cm diameter in the basal ganglia).[32] Clinical ratings were combined with MRI-based measures (whether the recent infarct was cortical or lacunar) to produce a final stroke subtype classification. Where the two differed, the radiological classification was preferred.

### Total SVD score

Total SVD score (ordinal score of 0–4) was calculated according to Staal's (2014) method,[33] whereby one point was allocated for each of four MRI features of SVD: presence of lacunes, presence of microbleeds, moderate to severe enlarged perivascular spaces (grades 2–4) and WMHs (Fazekas score 2 or 3 for deep WMH and Fazekas score 3 for WMH extending into deep white matter).

### Optic disc pallor quantification

We generated continuous measures of optic disc pallor from colour fundus photographs using previously validated software, *PallorMetrics*.[27] Briefly, a set of deep learning-based convolutional neural networks segmented the optic disc to the inner edge of the border tissue and calculated pallor based on the reflectance of red and green light in the neuroretinal rim relative to a control region. Visible retinal vasculature was segmented and subtracted from measurement and control regions. Measurements of pallor were then obtained for seven zones, in concordance with zones used for peripapillary OCT scans and aligned with the fovea, which was automatically detected by the software. Key stages in *PallorMetrics* for a single image are presented in figure 1.

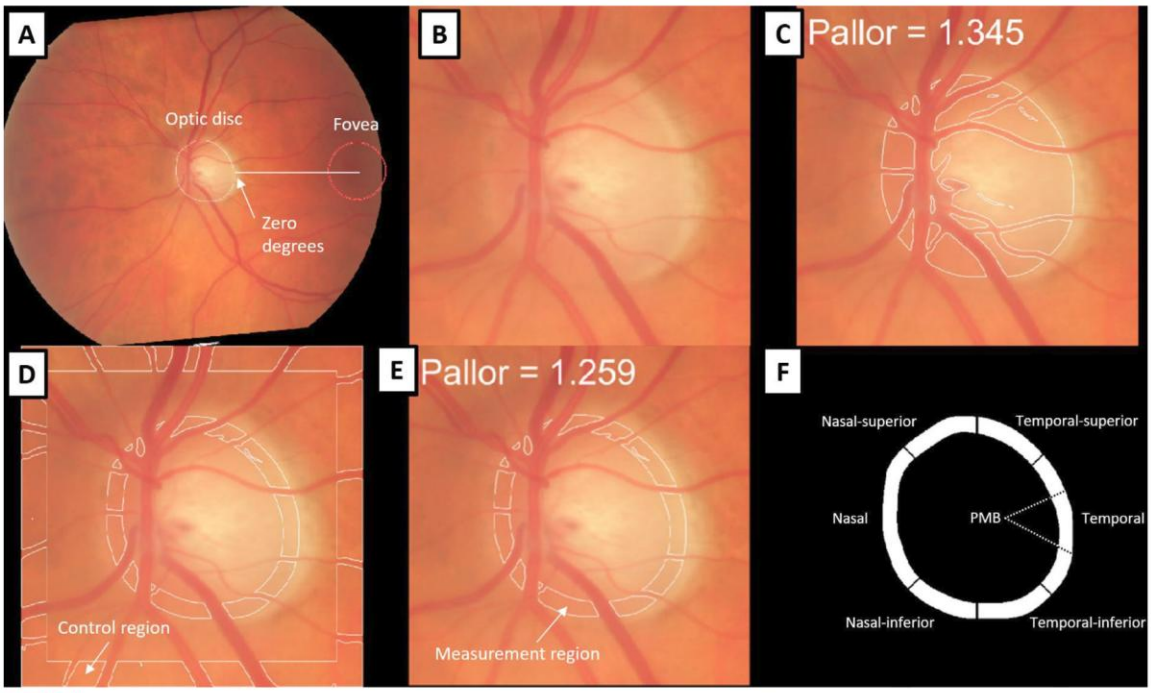


**Figure 1** Analysing optic disc pallor in a fundus image. (A) Full image rotated along the optic disc-fovea line (fovea location is predicted to lie within the red circle). (B) Image cropped to the optic disc. (C) Segmented whole disc with measured pallor value. (D) Segmented measurement and control region. (E) Measurement region with global pallor value. (F) Diagram of zones. Note: Retinal vessels are excluded in (C, D and E). PMB, papillomacular bundle.

When *PallorMetrics* failed at segmentation, we manually annotated features by fitting a deformable ellipse to the inner edge of the optic disc border tissue and marking the fovea with a single mouse click; if the fovea was not visible, we estimated its location based on its position relative to the optic disc and the vessel arc of the central arcades (procedure detailed in Gibbon *et al*[27]). Annotations were performed by the author, SG, who was masked to stroke type.

### Sample derivation

Of the 186 patients recruited, 354 fundus photographs were available. Of the 354 images presented to the software, 73 had segmentation errors and were subsequently annotated manually. Via visual inspection of all processed images, eight were rejected for one or more rotation errors (two images), overexposure (two images) and high myope (five images). The final sample contained 346 images from 184 patients. For comparison, the final sample in our previous work using the same dataset was 166.[15]

### Statistical analysis

We used logistic regression to assess the relationship between disc pallor and stroke type and ordinal logistic regression to assess the relationship between pallor and total SVD score. In accordance with previous work,[13 15] we controlled for age, sex, hypertension and diabetes; however, we included information on hyperlipidaemia, history of transient ischaemic attack, history of stroke and smoking status to table 1 for completeness. We also controlled for disc area. Correcting for multiple comparisons was not applied in this study because the primary aim was exploratory, intended to identify potential associations that could guide future research. The right eye was consistently paler than the left (table 1); therefore, the left and right eyes were assessed separately. Pallor, age and disc area were standardised before analysis. Differences in demographics and risk factors between the groups were assessed using t-tests (where one variable was continuous) or $\chi^2$ (where both variables were dichotomous). Missing data points were removed at the time of analysis. All statistical analysis was carried out in R (V.4.2.1; www. R-project. org). We used the 'polyr' package for ordinal logistic regression.

## RESULTS

Optic disc pallor was measured in 184 patients (346 images). The mean age was 68.6 years (SD=11.5) and the majority sex was male (66.8%). There were 92 patients with cortical stroke and 92 with lacunar stroke. Individuals who experienced lacunar stroke were younger than

Table 1 Demographics and study variables by stroke subtype and eye

| Variable | Stroke type | | | | P value |
|---|---|---|---|---|---|
| | Cortical | | Lacunar | | |
| N (participants) | 92 | | 92 | | |
| N (eyes) | 174 | | 172 | | |
| Age | 70.0 (11.2) | | 66.1 (11.5) | | 0.017 |
| Sex (female) | 48 (27.6%) | | 68 (39.5%) | | 0.117 |
| Small vessel disease score | | | | | |
| 0 | 46 (50%) | | 35 (38.0%) | | |
| 1 | 20 (21.7%) | | 16 (17.4%) | | |
| 2 | 16 (17.4%) | | 20 (21.7%) | | |
| 3 | 8 (8.7%) | | 13 (14.1%) | | |
| 4 | 2 (2.2%) | | 5 (5.4%) | | |
| Missing | 0 (0.0%) | | 3 (3.3%) | | |
| Risk factors | | | | | |
| Hypertension (years) | 112 (64.4%) | | 100 (58.1%) | | 0.543 |
| Hyperlipidaemia (years) | 65 (37.4%) | | 61 (35.5%) | | 1.000 |
| Missing | 0 (0.0%) | | 4 (2.3%) | | |
| Diabetes (years) | 20 (11.5%) | | 34 (19.8%) | | 0.225 |
| Smoking (ever) | 101 (58.0%) | | 97 (56.4%) | | 1.000 |
| Missing | 1 (0.6%) | | 1 (0.6%) | | |
| Transient ischaemic attacj history (years) | 17 (9.8%) | | 25 (14.5%) | | 0.273 |
| Stroke history (years) | 17 (9.8%) | | 17 (9.8%) | | |
| Optic disc pallor | | | | | |
| Eye | Left | Right | Left | Right | |
| N (eyes) | 86 | 88 | 88 | 84 | |
| Global | 1.16 (0.12) | 1.16 (0.11) | 1.16 (0.09) | 1.21 (0.12) | |
| Temporal | 1.21 (0.14) | 1.23 (0.14) | 1.22 (0.13) | 1.28 (0.15) | |
| Temporal-inferior | 1.15 (0.13) | 1.16 (0.12) | 1.15 (0.11) | 1.21 (0.12) | |
| Nasal-inferior | 1.07 (0.12) | 1.06 (0.10) | 1.08 (0.09) | 1.10 (0.11) | |
| Nasal | 1.14 (0.13) | 1.14 (0.10) | 1.15 (0.09) | 1.17 (0.13) | |
| Nasal-superior | 1.12 (0.12) | 1.12 (0.10) | 1.13 (0.09) | 1.17 (0.11) | |
| Temporal-superior | 1.12 (0.13) | 1.12 (0.11) | 1.13 (0.10) | 1.17 (0.13) | |
| Papillomacular bundle | 1.23 (0.15) | 1.25 (0.14) | 1.23 (0.13) | 1.30 (0.15) | |
| Nasal-temporal ratio | 0.947 (0.07) | 0.931 (0.06) | 0.951 (0.09) | 0.915 (0.07) | |
| Retinal covariates | | | | | |
| Disc area | 106 000 (29 000) | 103 000 (26 700) | 103 000 (23 900) | 105 000 (21 600) | |

Notes: Values are N (%) or mean (SD).

those with cortical stroke (mean age 66.1 compared with 70, p=0.017). There was no evidence of significant differences in male/female split, hypertension, cholesterol, diabetes, history of stroke, history of transient ischaemic attack or smoking status between stroke types. Demographic and study variables are summarised in table 1.

### Associations between disc pallor and stroke type

In the right eye, independent of covariates, increased optic disc pallor was significantly associated with lacunar stroke globally (OR per SD increase=1.54, CI: 1.12 to 2.19, p=0.011) and across all zones (figure 2). The left eye did not reach statistical significance; however, the direction was mostly the same, potentially indicating a small effect.

### Associations between disc pallor and total SVD score

Ordinal logistic models of the entire sample (lacunar and cortical) revealed significant associations between pallor and total SVD score in the temporal superior (standardised β=0.36, SE=0.15, p=0.020) and nasal-inferior

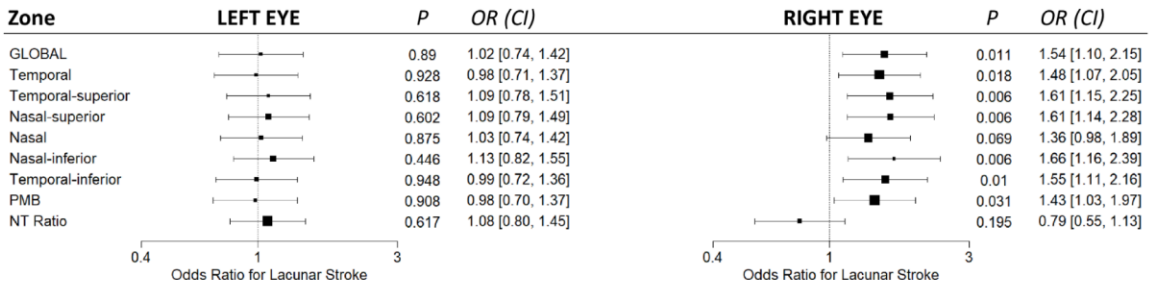


**Figure 2** Forest plot showing the associations between disc pallor and stroke type. Each eye is modelled separately. All models are adjusted for age, sex, disc area, hypertension diagnosis and diabetes. Continuous variables were standardised prior to analysis. PMB, papillomacular bundle; NT, nasal-temporal.

zones (standardised β=0.44, SE=0.15, p=0.004) in the right eye. The direction of β was the same in both eyes (except for the NT ratio in the right eye and nasal superior zone in the left eye), indicating that a statistical effect may have emerged given more data. Results are summarised in table 2.

## DISCUSSION

We show here that the optic disc is slightly paler in patients with lacunar stroke compared with cortical stroke. This effect was independent of covariates and held despite the patients with lacunar stroke being around 4 years younger than patients with cortical stroke. Furthermore, we show that increasing paleness of the disc may be weakly associated with total SVD score. Both findings were stronger for the right eye; however, this may be due to the imaging protocol and known differences between the eyes. Taken together, our findings suggest that SVD may be associated with damage to the optic nerve.

A pale optic disc is symptomatic of optic atrophy, which refers to the permanent loss or damage to retinal ganglion cell axons along the anterior visual pathway, with pallor usually beginning to show around 4–6 weeks after axonal damage.[19] The retinal imaging in the current study was carried out within 4 weeks of stroke occurrence; therefore, it is unlikely that the stroke itself caused the observed increase in paleness. More likely is that the observed increase in pallor is a long-term result of SVD, which has been associated with pRNFL thinning,[12] and by association—disc pallor. This hypothesis is consistent with the current demonstration of associations between disc pallor and both lacunar stroke and SVD severity.

One possible mechanism by which SVD and resulting lacunar stroke could cause optic disc pallor/atrophy is through effects on the blood supply to the optic nerve or its pathways. For example, if a lacunar infarct occurred in any part of an optic pathway, it could lead to retrograde demyelination along the optic nerve, manifesting as pallor in the optic disc. However, this scenario is rare, as lacunar strokes do not usually affect the visual system directly.[34] Optic disc pallor can reflect not only the loss of nerve fibres but also gliosis,[35] axonal degeneration and

**Table 2** Ordinal logistic regression results for SVD score and optic disc pallor, by zone and eye

| | Coefficients | | | |
|---|---|---|---|---|
| | Left eye | | Right eye | |
| Zone | β (SE) | P value | β (SE) | P value |
| Global | 0.07 (0.15) | 0.646 | 0.26 (0.16) | 0.101 |
| Temporal | 0.05 (0.16) | 0.756 | 0.24 (0.16) | 0.124 |
| Temporal-superior | 0.14 (0.15) | 0.350 | 0.36 (0.15) | 0.020* |
| Nasal-superior | −0.03 (0.15) | 0.844 | 0.09 (0.16) | 0.583 |
| Nasal | 0.06 (0.15) | 0.700 | 0.21 (0.16) | 0.188 |
| Nasal-inferior | 0.19 (0.15) | 0.210 | 0.44 (0.15) | 0.004** |
| Temporal-inferior | 0.02 (0.15) | 0.878 | 0.13 (0.16) | 0.422 |
| Papillomacular bundle | 0.04 (0.16) | 0.822 | 0.22 (0.16) | 0.164 |
| Nasal-temporal ratio | 0.04 (0.15) | 0.804 | −0.12 (0.15) | 0.412 |

All models were adjusted for age, sex, disc area, hypertension diagnosis and diabetes. Age, pallor and disc area were standardised prior to analysis.
*p<0.05 and **p<0.01.

other changes within the optic nerve head. It indicates chronic, longstanding optic nerve damage, which may be more aligned with the cumulative effects of chronic SVD.

Strengths of this study include the accuracy of stroke subtyping, which used both clinical and radiological features, the relatively large sample and the use of novel, validated software to quantify optic disc pallor in several zones.

This study has several limitations. First, associations were only statistically significant in the right eye and not the left. However, it is worth noting that the right eye was always captured first, using six flashes of light. This procedure may have had a subtle impact on image quality in the fellow eye, potentially due to patient fatigue or challenges in visualising the left optic disc. This claim remains to be tested and is beyond the scope of this study; empirically assessing image quality in fundus photographs is an area of much research and controversy.[36] Notwithstanding, associations in the left eye showed a trend, which may have borne out in a larger sample. Furthermore, there are known differences in RNFL thickness between the eyes,[37] which may have subtly affected the pallor measurement. Ocular dominance may also play a role; if patients are right-eye dominant, this could potentially lead to a thicker RNFL,[38] which may result in greater variation in pallor measurements. This increased variation could potentially enhance the ability to detect differences or trends through statistical testing. Unfortunately, neither ocular dominance nor handedness (a proxy) was available for the current cohort.

Second, although patients were screened for glaucoma, they were not screened for other optic neuropathies, such as non-arteritic anterior ischaemic optic neuropathy (NAAION), which could affect disc pallor. However, NAAION is rare, affecting between 2.3 and 10.3 people per 100 000,[39] making it unlikely that any patients in the study were affected. Even if one or two patients were affected, it is improbable that this would have significantly impacted the model estimates. Additionally, markers of optic disc dysfunction, such as colour vision deficiency and reduced visual acuity, which likely correlate with optic disc pallor, could have been useful covariates. Unfortunately, these variables were not collected.

Third, the study was cross-sectional in design, which precluded us from inferring a temporal association. In addition, most patients in the current study were white in ethnicity; therefore, further research is needed to determine if the results apply to other ethnicities. Finally, although we used MRI in deciding each stroke type and all patients had a definite stroke diagnosed by an expert panel, there may be some misclassification in stroke type. The classification used was a pragmatic system based on the most likely mechanism to explain the different stroke subtypes. We acknowledge that there will be a small group of people whose lacunar stroke may not have been caused by intrinsic SVD and also that there will be patients with coexistent small and large artery disease given the high prevalence of shared risk factors.

## CONCLUSION

We show here that the optic disc is slightly paler in lacunar compared with cortical stroke and that increasing disc pallor is weakly associated with increasing SVD severity. This may reflect RNFL loss or degeneration caused by vascular damage to the optic pathway. Our results strengthen the case for retinal fundus imaging as a convenient and promising method for exploring alterations in brain health linked to SVD.

**Contributors** SG led the project by contributing to the conceptualisation and methodology, developed the software used in the study, performed the formal analysis and investigation, was responsible for data curation and drafting the original manuscript and also created visualisations of the data. FD secured funding for the project, was involved in data curation and resource provision, supervised the study, participated in the investigation and contributed to the manuscript by reviewing and editing it. FC handled data curation and formal analysis, managed the project administration and contributed to the manuscript by reviewing and editing it. JMW was instrumental in acquiring funding and providing resources for the project and contributed to the manuscript through review and editing. BD contributed to the manuscript by reviewing and editing it. TMG supervised the project, provided the necessary resources and contributed to the manuscript by reviewing and editing it. SG is designated as the guarantor for this study, taking responsibility for the overall content and integrity of the manuscript.

**Funding** The authors declare that there is no conflict of interest. Funding includes the Chief Scientist Office CZB/4/281; Row Fogo Charitable Trust; Wellcome Trust RTF 075611; SG was supported by EASTBIO, a consortium of Scottish Universities, which is funded by the BBSRC (Biotechnology and Biological Sciences Research Council). JMW is supported by the UK Dementia Research Institute (award no. UKDRI-Edin002, DRIEdi17/18 and MRC MC_PC_17113), which receives its funding from DRI, funded by the UK Medical Research Council, Alzheimer's Society and Alzheimer's Research UK. FC was supported by the UK Dementia Research Institute, which receives its funding from DRI; the Fondation Leducq Network for the Study of Perivascular Spaces in Small Vessel Disease (16 CVD 05) and the Row Fogo Charitable Trust Centre for Research into Ageing and the Brain.

**Competing interests** None declared.

**Patient consent for publication** Not applicable.

**Ethics approval** This study involves human participants and was approved by Lothian Research Ethics Committee (reference number LREC/2002/8/64). Participants gave informed consent to participate in the study before taking part.

**Provenance and peer review** Not commissioned; internally peer reviewed.

**Data availability statement** Data are available upon reasonable request.



**ORCID iDs**
Samuel Gibbon http://orcid.org/0000-0002-5485-7523
Francesca Chappell http://orcid.org/0000-0002-7742-1757

## REFERENCES

1 Cannistraro RJ, Badi M, Eidelman BH, *et al*. CNS small vessel disease: A clinical review. *Neurology (ECronicon)* 2019;92:1146–56.
2 Wardlaw JM, Smith C, Dichgans M. Small vessel disease: mechanisms and clinical implications. *Lancet Neurol* 2019;18:684–96.
3 Li Q, Yang Y, Reis C, *et al*. Cerebral Small Vessel Disease. *Cell Transplant* 2018;27:1711–22.

4 Wardlaw JM, Smith EE, Biessels GJ, *et al*. Neuroimaging standards for research into small vessel disease and its contribution to ageing and neurodegeneration. *Lancet Neurol* 2013;12:822–38.
5 Wardlaw JM. What causes lacunar stroke? *J Neurol Neurosurg Psychiatry* 2005;76:617–9.
6 Norrving B. Long-term prognosis after lacunar infarction. *Lancet Neurol* 2003;2:238–45.
7 Regenhardt RW, Das AS, Lo EH, *et al*. Advances in Understanding the Pathophysiology of Lacunar Stroke: A Review. *JAMA Neurol* 2018;75:1273–81.
8 Das AS, Regenhardt RW, Feske SK, *et al*. Treatment Approaches to Lacunar Stroke. *J Stroke Cerebrovasc Dis* 2019;28:2055–78.
9 Grysiewicz RA, Ruland SD. Lacunar infarcts. In: Aminoff MJ, Daroff RB, eds. *Encyclopedia of the Neurological Sciences (Second Edition*). Academic Press, 2014: 815–8.
10 Ganesh A, Gutnikov SA, Rothwell PM, *et al*. Late functional improvement after lacunar stroke: a population-based study. *J Neurol Neurosurg Psychiatry* 2018;89:1301–7.
11 Patton N, Aslam T, Macgillivray T, *et al*. Retinal vascular image analysis as a potential screening tool for cerebrovascular disease: a rationale based on homology between cerebral and retinal microvasculatures. *J Anat* 2005;206:319–48.
12 Biffi E, Turple Z, Chung J, *et al*. Retinal biomarkers of Cerebral Small Vessel Disease: A systematic review. *PLoS One* 2022;17:e0266974.
13 Doubal FN, MacGillivray TJ, Hokke PE, *et al*. Differences in retinal vessels support a distinct vasculopathy causing lacunar stroke. *Neurology (ECronicon)* 2009;72:1773–8.
14 Lindley RI, Wang JJ, Wong M-C, *et al*. Retinal microvasculature in acute lacunar stroke: a cross-sectional study. *Lancet Neurol* 2009;8:628–34.
15 Doubal FN, MacGillivray TJ, Patton N, *et al*. Fractal analysis of retinal vessels suggests that a distinct vasculopathy causes lacunar stroke. *Neurology (ECronicon)* 2010;74:1102–7.
16 Cheung N, Liew G, Lindley RI, *et al*. Retinal fractals and acute lacunar stroke. *Ann Neurol* 2010;68:107–11.
17 Cheung CYL, Ikram MK, Chen C, *et al*. Imaging retina to study dementia and stroke. *Prog Retin Eye Res* 2017;57:89–107.
18 Doubal FN, Hokke PE, Wardlaw JM. Retinal microvascular abnormalities and stroke: a systematic review. *J Neurol Neurosurg Psychiatry* 2009;80:158–65.
19 Ahmad SS, Kanukollu VM. Optic atrophy. In: *StatPearls*. StatPearls Publishing, 2022. Available: http://www.ncbi.nlm.nih.gov/books/NBK559130/
20 Thomson KL, Yeo JM, Waddell B, *et al*. A systematic review and meta-analysis of retinal nerve fiber layer change in dementia, using optical coherence tomography. *Alzheimers Dement Diagn Assess Dis Monit* 2015;1:136–43.
21 Mutlu U, Colijn JM, Ikram MA, *et al*. Association of Retinal Neurodegeneration on Optical Coherence Tomography With Dementia: A Population-Based Study. *JAMA Neurol* 2018;75:1256–63.
22 Ko F, Muthy ZA, Gallacher J, *et al*. Association of Retinal Nerve Fiber Layer Thinning With Current and Future Cognitive Decline: A Study Using Optical Coherence Tomography. *JAMA Neurol* 2018;75:1198–205.
23 Chen Y, Yuan Y, Zhang S, *et al*. Retinal nerve fiber layer thinning as a novel fingerprint for cardiovascular events: results from the prospective cohorts in UK and China. *BMC Med* 2023;21:24.
24 Wang D, Li Y, Wang C, *et al*. Localized retinal nerve fiber layer defects and stroke. *Stroke* 2014;45:1651–6.
25 Wolz J, Audebert H, Laumeier I, *et al*. Telemedical assessment of optic nerve head and retina in patients after recent minor stroke or TIA. *Int Ophthalmol* 2017;37:39–46.
26 O'Neill EC, Danesh-Meyer HV, Kong GXY, *et al*. Optic disc evaluation in optic neuropathies: the optic disc assessment project. *Ophthalmology* 2011;118:964–70.
27 Gibbon S, Muniz-Terrera G, Yii FSL, *et al*. PallorMetrics: Software for Automatically Quantifying Optic Disc Pallor in Fundus Photographs, and Associations With Peripapillary RNFL Thickness. *Transl Vis Sci Technol* 2024;13:20.
28 Doubal FN, Dhillon B, Dennis MS, *et al*. Retinopathy in Ischaemic Stroke Subtypes. *Stroke J Cereb Circ* 2009;40:389–93.
29 Early Treatment Diabetic Retinopathy Study Design and Baseline Patient Characteristics: ETDRS Report Number 7. *Ophthalmology* 1991;98:741–56.
30 Brott T, Adams HP Jr, Olinger CP, *et al*. Measurements of acute cerebral infarction: a clinical examination scale. *Stroke* 1989;20:864–70.
31 Bamford J, Sandercock P, Dennis M, *et al*. Classification and natural history of clinically identifiable subtypes of cerebral infarction. *Lancet Lond Engl* 1991;337:1521–6.
32 Wardlaw JM, Doubal F, Armitage P, *et al*. Lacunar stroke is associated with diffuse blood-brain barrier dysfunction. *Ann Neurol* 2009;65:194–202.
33 Staals J, Makin SDJ, Doubal FN, *et al*. Stroke subtype, vascular risk factors, and total MRI brain small-vessel disease burden. *Neurology (ECronicon)* 2014;83:1228–34.
34 Gore M, Bansal K, Khan Suheb MZ, *et al*. Lacunar stroke. In: *StatPearls*. StatPearls Publishing, 2024. Available: http://www.ncbi.nlm.nih.gov/books/NBK563216/
35 Osaguona VB. Differential diagnoses of the pale/white/atrophic disc. *Community Eye Health* 2016;29:71–4.
36 Gonçalves MB, Nakayama LF, Ferraz D, *et al*. Image quality assessment of retinal fundus photographs for diabetic retinopathy in the machine learning era: a review. *Eye (Lond)* 2024;38:426–33.
37 Dalgliesh JD, Tariq YM, Burlutsky G, *et al*. Symmetry of retinal parameters measured by spectral-domain OCT in normal young adults. *J Glaucoma* 2015;24:20–4.
38 Choi JA, Kim JS, Park HYL, *et al*. Retinal nerve fiber layer thickness profiles associated with ocular laterality and dominance. *Neurosci Lett* 2014;558:197–202.
39 Hattenhauer MG, Leavitt JA, Hodge DO, *et al*. Incidence of nonarteritic anterior ischemic optic neuropathy. *Am J Ophthalmol* 1997;123:103–7.

## 6.5. Conclusion

In this study, we investigated the relationship between optic disc pallor and two key clinical variables: ischemic stroke subtype (cortical and lacunar) and MRI-based cSVD ratings. We found that optic disc pallor was significantly associated with lacunar stroke subtype and cSVD severity in the right eye, independent of covariates. We observed a trend in the left eye, but this did not reach statistical significance. These findings suggest that cSVD and resulting lacunar stroke may cause damage to the optic nerve and its pathways. In the next chapter, I will present our work investigating optic disc pallor in a neurological disease.

# Chapter 7

# Optic disc pallor and Parkinson's disease

## 7.1. Introduction

In Chapters 5 and 6, I examined optic disc pallor in cSVD, a cerebrovascular disease. However, as discussed in Chapter 2, optic disc pallor is arguably more neuronal than vascular in nature, as it primarily reflects the loss of RGC axons. In this chapter, I shift focus to investigate optic disc pallor in PD, thereby addressing the third objective: to explore optic disc pallor in a neurodegenerative disease.

As discussed in Chapter 2, the characteristic depletion of dopaminergic neurons in PD may extend to the cells in the retina, causing retinal layer thinning.[81] Indeed, many studies have observed a thinner RNFL and the GCIPL in both the macula and around the optic disc in PD patients compared to controls.[119–121] Based on these observations, I formed three hypotheses:

1. Optic discs would appear paler in individuals with PD compared to controls.
2. Pallor would be detectable even before a PD diagnosis.
3. Pallor would become more pronounced as the disease progressed.

To test these hypotheses, I used data from the UK Biobank, which contained 103 individuals with diagnosed PD at the time of ophthalmic assessment (prevalent PD), and 412 individuals who were diagnosed with PD at a later date (incident PD), as well as a sample of individuals within whom an age- and sex-matched control group could be formed.

## 7.2. Acknowledgement of contribution

Dr Thomas MacGillivray and Dr David Breen contributed to the published article by reviewing and editing it.

## 7.3. My contribution to this work

I led:

- Generating the research question, and study design featured in the paper.
- Applying for access to the UK Biobank.
- Conducting a literature review.
- Manual annotation of retinal images including quality control.
- Deciding which statistical tests to conduct.
- Deciding which covariates to use.
- Performing the data and statistical analysis.
- Creating the tables and figures.
- Drafting the manuscript.
- Incorporating co-authors' comments and finalising the manuscript.
- Writing this chapter.

## 7.4. Published article

RESEARCH ARTICLE

# Optic Disc Pallor in Parkinson's Disease: A UK Biobank Study

Samuel Gibbon, MSc,[1,2] David P. Breen, MBChB, PhD,[1,3,4] Thomas J. MacGillivray, PhD,[1,2*] and UK Biobank Eye & Vision Consortium

**ABSTRACT:** **Background:** Recent studies have suggested that retinal changes measured with optical coherence tomography are detectable in early Parkinson's disease (PD), highlighting the potential of ophthalmic biomarkers for diagnosis and monitoring.
**Objective:** We set out to investigate the relationship between optic disc pallor measured in fundoscopy images and both prevalent and incident PD.
**Methods:** We analyzed color fundus photographs from 787 UK Biobank participants: 89 with prevalent PD, 317 with incident PD, and 381 age- and sex-matched controls. Optic disc pallor in several zones was quantified using semi-automated software. We used logistic and linear regression, adjusted for relevant covariates, to test for associations between disc pallor and PD status and duration.
**Results:** Participants with prevalent PD had significantly paler optic discs globally (OR per standard deviation [SD] increase = 1.39 [CI: 1.08–1.81], $P = 0.012$) and across several zones compared to controls. Each year since PD diagnosis was associated with a 1.37 SD increase in global pallor (standardized $\beta = 1.37$ [SE = 0.61], $P = 0.029$), and a similar increase across several zones, however, this finding was sensitive to outliers with long disease duration. No significant associations were observed for the incident PD group.
**Conclusions:** Optic disc pallor is significantly associated with PD and may become more pronounced with disease duration. This suggests that optic disc pallor, measured in routinely taken color fundus photographs, may serve as a biomarker for PD-related neurodegeneration. 

**Key Words:** Parkinson's disease; optic disc pallor; retina; color fundus photographs; PallorMetrics

Optical coherence tomography (OCT) enables the imaging of retinal layers and is increasingly used to assess structural changes within the eye in neurodegenerative disorders, including Parkinson's disease (PD).[1-5] OCT is typically focused on one of two key landmarks in the retina: the macula or the optic disc. In the macula, the ganglion cell layer and the inner plexiform layer (GCIPL) have shown significant alterations in PD, with a recent meta-analysis indicating a notable decrease in GCIPL thickness compared to controls.[6] By comparison, around the optic disc, the retinal nerve fiber layer (RNFL) appears to be more affected in PD than GCIPL thickness, with a recent meta-analysis revealing thinner peripapillary RNFL (pRNFL) in PD patients compared to controls, with the greatest thinning observed in temporal regions.[7] The mechanisms of nerve cell loss in the eye are thought to reflect similar neurodegenerative processes occurring in the brain.[8] In PD, the degeneration of dopaminergic neurons in the brain may extend to the retinal ganglion cells, leading to thinning of the retinal layers.[9]

Despite the imaging capabilities of OCT, there can be technical challenges for movement disorder patients

[1]Centre for Clinical Brain Sciences, University of Edinburgh, Edinburgh, UK; [2]Robert O Curle Ophthalmology Suite, Institute for Regeneration and Repair, University of Edinburgh, Edinburgh, UK; [3]Anne Rowling Regenerative Neurology Clinic, University of Edinburgh, Edinburgh, UK; [4]Usher Institute of Population Health Sciences and Informatics, University of Edinburgh, Edinburgh, UK



*__Correspondence to:__ Dr. Thomas J MacGillivray, Centre for Clinical Brain Sciences, Chancellor's Building, University of Edinburgh, 49 Little France Crescent, Edinburgh, EH16 4SB, UK; E-mail: t.j.macgillivray@ed.ac.uk

**Financial disclosure/conflict of interest**: The authors report no financial disclosures or conflict of interest.

**Funding agency**: Samuel Gibbon was supported by the Biotechnology and Biological Sciences Research Council (grant number: BB/M010996/1). The funders had no role in the design or conduct of this work.

**Received:** 18 September 2024; **Revised:** 6 January 2025; **Accepted:** 7 January 2025

**Published online in Wiley Online Library (wileyonlinelibrary.com). DOI: 10.1002/mds.30127**

due to the requirement to maintain a stable position and gaze during scan acquisition, which may take anywhere from 15 seconds to 2 minutes (depending on the machine, imaging protocol, and patient). A quicker and simpler alternative is color fundus photography, which takes only a few seconds to acquire. Furthermore, color fundus photographs are more commonly collected in the population (ie, during routine high-street eye examinations).

Recently, we developed a new approach to examine pRNFL thickness by measuring the paleness of the neuro-retinal rim (hereafter referred to as *optic disc pallor*) in color fundus photographs (*PallorMetrics*),[10] under the assumption that a pale disc primarily indicates the loss or degeneration of the pRNFL.[10-13] One previous study has observed optic disc pallor in PD,[14] most notably in the temporal region; however, this study was based on subjective clinical observation. By comparison, the *PallorMetrics* software generates quantitative measurements of optic disc pallor both globally and in specific zones akin to those used by modern OCT devices. *PallorMetrics* has previously been used to investigate disc pallor in relation to MRI features of cerebral small vessel disease,[15] lacunar stroke,[16] and myopia (manuscript under review).

In the current study, we aimed to investigate the relationship between optic disc pallor and prevalent and incident PD using data from the UK Biobank. We hypothesized that (1) optic discs would be paler in prevalent PD compared to controls, (2) pallor would become more pronounced with advancing disease duration, and (3) pallor would be detectable even prior to PD diagnosis.

## Patients and Methods

### Participants and Image Capture

The UK Biobank recruited approximately 500,000 UK-based participants aged 40–69 between 2006 and 2010 (https://www.ukbiobank.ac.uk/). Alongside questionnaires and physical measurements, a subset of just under 70,000 participants received detailed ophthalmic assessment between 2009 and 2010, including single-field color fundus photography (45° field-of-view) and OCT of each eye, both centered on the macula. Photographs and scans were captured using a digital Topcon-1000 integrated camera (Topcon 3D OCT1000 Mark II, Topcon Corp., Tokyo, Japan). The same model device was used for all participants. The right eye was imaged first. The UK Biobank has Research Tissue Bank approval from the North-West Research Ethics Committee (ref: 06/MRE08/75).

### Case Definition

PD diagnosis was defined as the first occurrence of PD according to ICD-10 G20 code (any position) within NHS linked health records. In the UK Biobank, ICD-10 codes were derived from primary care, hospital inpatient admissions, death records, and self-reported medical conditions. Participants with a G20 code before ophthalmic assessment were defined as prevalent PD, whereas those with a G20 code after ophthalmic assessment were defined as incident PD.

### Sample Derivation and Exclusions

A total of 68,508 participants underwent color fundus photography. We selected one eye per participant for our analyses. The right eye was always chosen if available because it was captured first and therefore likely to be of better quality. In cases where the right eye photograph was not available (400 participants), the left eye was used. In cases where multiple photographs were captured for a single eye, we selected the second instance for analysis, which was usually better quality.

Based on previous findings of reduced RNFL in dementia,[3] and in accordance with similar research,[5] we removed participants with a diagnosis of all-cause dementia at the time of imaging (UK Biobank Algorithmically Defined Outcome; Field ID = 42,018). Based on ICD-10 codes, we removed participants with ocular disorders that may affect optic disc appearance, encompassing glaucoma (H40), multiple sclerosis (G35), optic neuritis (H46), visual pathway disorder (H47), blindness (H54), and retinal detachment/breaks (H33). Cataracts (H26), previous ocular surgery (self-reported), and diabetes (E10 and E11) can also affect optic disc appearance, but their prevalence is high. Rather than excluding these participants, we opted to account for these variables statistically and perform sensitivity analyses. Disc pallor varied substantially by ethnicity (Fig. S1; Table 1). Therefore, we excluded participants with missing ethnicity data (n = 8). After exclusions, fundus photographs were available for 66,390 participants, of whom 103 individuals had a confirmed diagnosis of PD (prevalent PD), and 412 individuals later developed PD (incident PD).

We then created an age- and sex-matched control group using the "matchit" package in R with a ratio of 1:1, combining incident and prevalent PD, generating 515 controls. After quality control (detailed below), the final sample contained 89 individuals with prevalent PD, 317 with incident PD, and 381 controls. In effect, this meant that the ratio of prevalent PD to controls was over 4:1, and the ratio of incident PD to controls was 1.2:1.

### Optic Disc Pallor Quantification

Optic disc pallor was measured using previously validated software, *PallorMetrics*.[10] Briefly, a deep learning-based approach segmented the optic disc to the inner edge of the border tissue and localized the fovea (Fig. 1A). For the current study, we used a semi-automated version, in which we hand-corrected the optic disc segmentation for each image by dragging the edges of a deformable ellipse (procedure detailed in Ref. 10).

**TABLE 1** *Participant demographics and study variables*

| | Controls (N = 381) | Prevalent (N = 89) | *P*-value | Incident (N = 317) | *P*-value |
|---|---|---|---|---|---|
| Age | 62.7 (5.25) | 61.1 (6.29) | 0.033* | 62.9 (5.05) | 0.610 |
| Sex (female) | 148 (38.8%) | 36 (40.4%) | 0.874 | 123 (38.8%) | 1.000 |
| Ethnic category | | | | | |
| White | 368 (95.8%) | 83 (93.3%) | - | 292 (92.1%) | - |
| Black | 3 (0.8%) | 1 (1.1%) | - | 9 (2.8%) | - |
| Other/Mixed | 4 (1.0%) | 2 (2.2%) | - | 5 (1.6%) | - |
| South Asian | 6 (1.6%) | 3 (3.4%) | - | 11 (3.5%) | - |
| Non-White ethnicity | 13 (3.4%) | 6 (6.7%) | - | 25 (7.9%) | 0.015* |
| Hypertension | 130 (34.1%) | 26 (29.2%) | 0.447 | 128 (40.4%) | 0.104 |
| Diabetes | 19 (5.0%) | 2 (2.2%) | - | 16 (5.0%) | 1.000 |
| Cataract | 19 (5.0%) | 5 (5.6%) | - | 22 (6.9%) | 0.352 |
| Eye surgery | 21 (5.5%) | 5 (5.6%) | -- | 27 (8.5%) | 0.158 |
| Pallor | | | | | |
| Global | 1.27 (0.23) | 1.33 (0.25) | 0.026* | 1.27 (0.22) | 0.869 |
| Temporal | 1.41 (0.30) | 1.49 (0.31) | 0.013* | 1.40 (0.28) | 0.935 |
| Temporal-inferior | 1.26 (0.23) | 1.32 (0.25) | 0.033* | 1.25 (0.22) | 0.929 |
| Nasal-inferior | 1.12 (0.19) | 1.16 (0.21) | 0.071 | 1.13 (0.18) | 0.553 |
| Nasal | 1.17 (0.20) | 1.22 (0.22) | 0.054 | 1.18 (0.19) | 0.416 |
| Nasal-superior | 1.17 (0.19) | 1.21 (0.22) | 0.067 | 1.17 (0.19) | 0.655 |
| Temporal-superior | 1.25 (0.26) | 1.32 (0.27) | 0.029* | 1.25 (0.24) | 0.916 |
| PMB | 1.44 (0.31) | 1.53 (0.32) | 0.012* | 1.43 (0.29) | 0.949 |
| NT ratio | 0.84 (0.09) | 0.82 (0.08) | 0.042* | 0.85 (0.09) | 0.184 |
| Retinal covariates | | | | | |
| Disc area (pixels) | 25,200 (5370) | 25,000 (5110) | 0.636 | 25,400 (5870) | 0.765 |

*Note*: All values are N (%) or mean (standard deviation). *P*-values are for comparisons between controls vs. prevalent PD, and controls vs. incident PD. * *P*-value <0.05; ** *P*-value <0.01, - statistical test failed to converge due to low sample size in one group.
Abbreviations: PMB, papillomacular bundle; NT ratio, nasal temporal ratio; PD, Parkinson's disease.

Although this process took longer than the fully automatic version, it minimized segmentation error. The optic disc was cropped from the image (Fig. 1B). A measurement region was then designated starting from the disc border of the cropped image, extending 30 pixels inwards (Fig. 1D). Zones were then overlaid onto this area following the standard OCT peripapillary scan pattern (Fig. 1C). The intersection of the disc-fovea axis with the measurement region was assigned a zero-degree value (Fig. 1A). The temporal zone extends from −45° to 45°, the temporal superior zone from −45° to −90°, and so on (Fig. 1C). The papillomacular bundle (PMB), a thick bundle of axons originating in the macula that allows for sharp central vision, is a special case of the temporal zone, extending from −15° to 15°. A control region was automatically defined by the software as starting at the outer border of the cropped optic disc image and extending 50 pixels inwards (Fig. 1E). Vessels were excluded from the measurement and control regions. Lastly, pallor was quantified by the software based on the ratio of red/green light reflectance within each zone relative to the control region. The result is a dimensionless measure of pallor (global pallor), pallor in six zones (sectoral pallor) (Fig. 1F), pallor in the PMB, and the nasal-temporal ratio. Optic disc analyses were performed in MATLAB (version R2022b, Natick, Massachusetts: The MathWorks Inc.) within the UK Biobank's Research Analysis Platform. Key stages in the pipeline are presented in Figure 1.

## Quality Control

All images (controls, incident PD, prevalent PD) were put into a single directory, shuffled, and presented for annotation randomly with their filenames occluded.

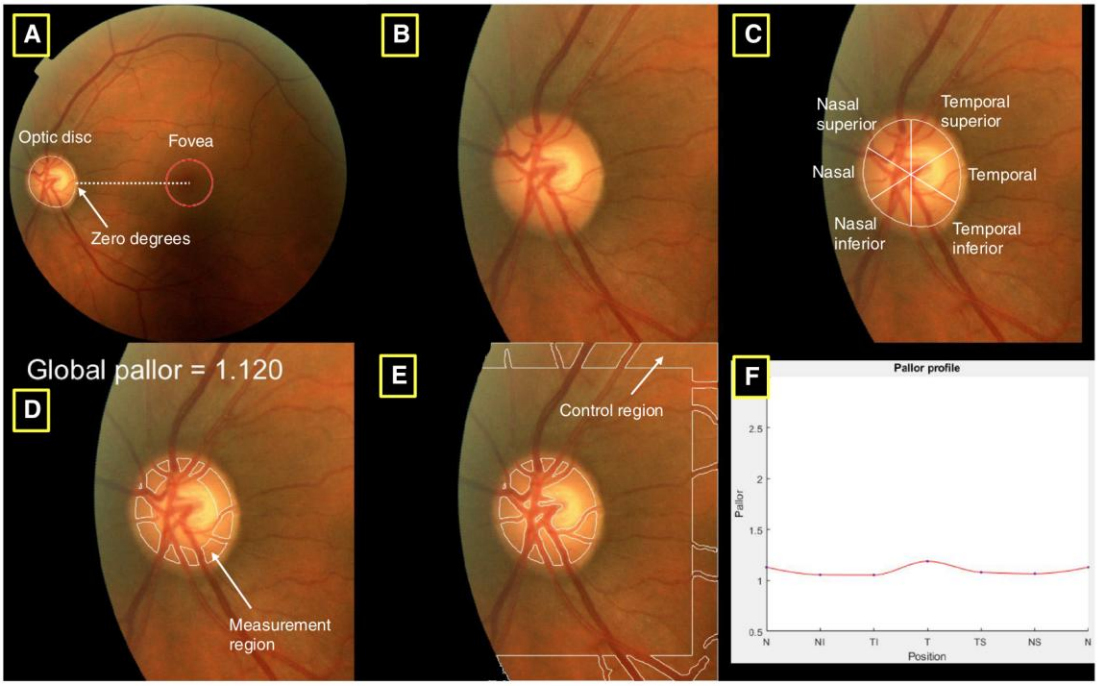


**FIG. 1.** Key visualizations of *PallorMetrics* for a single image. (**A**) Image is rotated along the optic disc-fovea axis, (**B**) cropped optic disc, (**C**) zones, (**D**) measurement region, (**E**) control region, and (**F**) optic disc pallor profile. [Color figure can be viewed at wileyonlinelibrary.com]

Images were rejected for one or more of the following reasons: under- or over-exposure of the optic disc or control region, uneven illumination over the optic disc or control region, disc border unclear, abnormal presentation of the disc or retina, and failure to locate fovea. Example images from each rejection category are presented in Figure S2. One hundred and thirty-one images (25.4%) were rejected from the control group, 14 images (13.6%) were rejected from the prevalent PD group, and 90 images (21.8%) were rejected from the incident PD group. Manual disc segmentation and quality control were carried out using a single annotator (author S.G.).

## Statistical Analysis and Covariates

Differences in demographics and retinal measures between the groups (control vs. prevalent PD, control vs. incident PD) were assessed using $t$ tests where one variable was continuous, or $\chi^2$ where both variables were dichotomous. We used logistic regression to estimate the odds of prevalent PD versus controls, and incident PD versus controls, with disc pallor as a predictor. The small sample size precluded the use of survival analysis (eg, Cox regression). In accordance with similar work,[5] all models were adjusted for age, sex, ethnic category, hypertension, cataract, diabetes, previous eye surgery, and disc area. These covariates were chosen prior to analysis, and no subsequent adaptations were made. Optic disc pallor, age, and disc area were standardized prior to analysis to have a zero mean and unit variance. Self-reported ethnicity was categorized into four groups defined by the UK Census (White, Black, Other/Mixed, South Asian); however, there were too few samples in each group, which precluded us from including ethnic category as a covariate. Instead, we used a binary ethnicity variable (White/non-White). Only two participants with prevalent PD had diabetes; therefore, we excluded diabetes as a covariate for prevalent cases (as opposed to adjusting for this covariate or removing cases). To determine whether the duration of disease affected disc pallor, we fitted linear regression models between pallor and "years since- and years to diagnosis." As before, models were adjusted for the covariates listed above. We carried out sensitivity analyses in all models by removing participants with cataracts, previous eye surgery, diabetes, and non-White ethnicity. In the PD duration models, we also conducted a sensitivity analysis by removing "outliers" (defined as individuals with a PD duration of more than 15 years). These outliers were identified based on a visual inspection of Figure S3. Analyses were conducted in R (version 4.2.1; www. R-project.org). Statistical significance was set at $P < 0.05$.

## Results

Compared with controls, those with prevalent PD were around 1.6 years younger ($P = 0.033$), and those with incident PD had a higher proportion of non-White ethnicity (7.9% compared with 3.4%). These differences were expected given the nature of how we derived the control group (see Methods—Sample derivation and exclusions). There were no other significant differences between the groups. Optic disc pallor steadily decreased with age (Fig. S4) and varied by ethnicity (Fig. S1). Demographics and study variables are summarized in Table 1. The sample derivation flowchart is presented in Figure 2.

### Associations between Optic Disc Pallor and PD

After adjusting for covariates, and compared to the control group, participants with prevalent PD had paler optic discs globally (OR per standard deviation [SD] increase = 1.39 [CI: 1.08–1.81], $P = 0.012$) and across several zones. The point estimate was slightly higher in the temporal zone (OR per SD increase = 1.40 [CI: 1.08–1.81], $P = 0.010$) compared to the nasal zones (OR per SD increase = 1.37 for nasal zone, 1.33 for nasal-inferior, 1.35 for nasal-superior). The direction of association was consistent across all zones. No statistically significant associations were observed for the incident PD group; however, a trend was observed with the direction consistent across all zones, suggesting a slight increase in pallor compared with controls. In sensitivity analyses, removing participants with cataracts (N = 24) caused a slight reduction in estimates, removing participants with previous eye surgery (N = 26) slightly increased the estimates, removing participants with diabetes (N = 21) increased the estimates, and removing participants with non-White ethnicity (N = 19) slightly reduced the estimates; all associations bar one (nasal-superior pallor in the sensitivity to cataract analysis) remained statistically significant. Results are summarized in Table 2 and plotted in Fig. S5.

### Associations between Optic Disc Pallor and PD Duration

In the prevalent PD group, and independent of covariates, each year since PD diagnosis was associated with a 1.37 SD increase in global pallor (standardized $\beta = 1.37$ [SE = 0.61], $P = 0.029$). The effect was strongest in the PMB zone (standardized $\beta = 1.57$ [SE = 0.62], $P = 0.012$), and present in the temporal (standardized $\beta = 1.52$ [SE = 0.62], $P = 0.016$) and nasal-superior zones (standardized $\beta = 1.46$ [SE = 0.57], $P = 0.013$). In sensitivity analyses, removing participants with cataracts (n = 5) and then eye surgery (n = 5) reduced the strength of estimates and rendered the associations with global

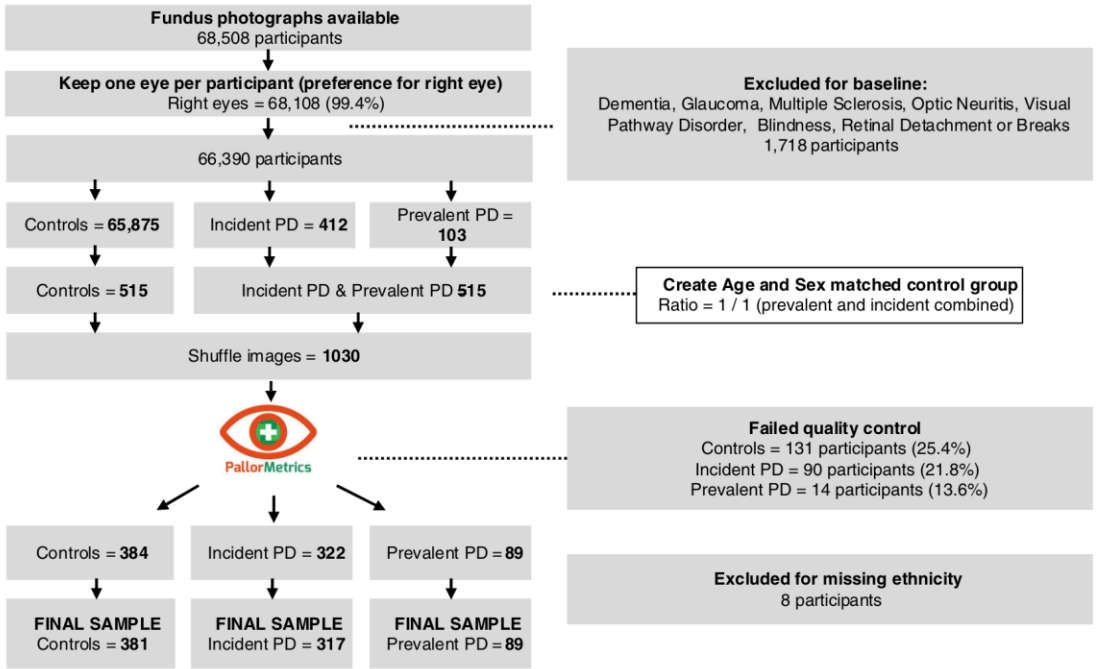


**FIG. 2.** Sample derivation flowchart. [Color figure can be viewed at wileyonlinelibrary.com]

**TABLE 2** *Logistic regression results comparing prevalent PD and incident PD to controls*

| | Prevalent PD | | | Incident PD | | |
|---|---|---|---|---|---|---|
| **Pallor** | **1 SD** | **Odds ratio per SD increase (CI)** | ***P* value** | **1 SD** | **Odds ratio per SD increase (CI)** | ***P* value** |
| Global | 0.24 | 1.39 (1.08–1.81) | 0.012* | 0.23 | 1.06 (0.90–1.25) | 0.490 |
| Temporal | 0.30 | 1.40 (1.08–1.81) | 0.010* | 0.29 | 1.04 (0.88–1.22) | 0.680 |
| Temporal-inferior | 0.23 | 1.38 (1.07–1.78) | 0.014* | 0.23 | 1.03 (0.87–1.22) | 0.717 |
| Nasal-inferior | 0.19 | 1.33 (1.04–1.71) | 0.025* | 0.18 | 1.10 (0.93–1.29) | 0.262 |
| Nasal | 0.20 | 1.37 (1.06–1.77) | 0.015* | 0.19 | 1.12 (0.95–1.32) | 0.169 |
| Nasal-superior | 0.20 | 1.35 (1.04–1.74) | 0.022* | 0.19 | 1.09 (0.92–1.28) | 0.322 |
| Temporal-superior | 0.25 | 1.38 (1.07–1.78) | 0.014* | 0.24 | 1.05 (0.89–1.23) | 0.582 |
| PMB | 0.31 | 1.40 (1.08–1.81) | 0.011* | 0.30 | 1.04 (0.88–1.22) | 0.664 |
| NT ratio | 0.09 | 0.83 (0.65–1.06) | 0.141 | 0.09 | 1.10 (0.94–1.28) | 0.231 |
| Sensitivity analysis | | | | | | |
| Without cataract (N = 24 removed) | | | | | | |
| Global | 0.24 | 1.36 (1.04–1.78) | 0.023* | | | |
| Temporal | 0.30 | 1.37 (1.05–1.78) | 0.019* | | | |
| Temporal-inferior | 0.24 | 1.36 (1.05–1.78) | 0.021* | | | |
| Nasal-inferior | 0.19 | 1.28 (0.99–1.65) | 0.060 | | | |
| Nasal | 0.20 | 1.33 (1.03–1.74) | 0.030* | | | |
| Nasal-superior | 0.20 | 1.32 (1.02–1.72) | 0.037* | | | |
| Temporal-superior | 0.26 | 1.34 (1.03–1.74) | 0.028* | | | |
| PMB | 0.31 | 1.37 (1.06–1.79) | 0.019* | | | |
| NT ratio | 0.09 | 0.83 (0.64–1.06) | 0.140 | | | |
| Without eye surgery (N = 26 removed) | | | | | | |
| Global | 0.24 | 1.41 (1.08–0.32) | 0.011* | | | |
| Temporal | 0.30 | 1.41 (1.09–1.84) | 0.009** | | | |
| Temporal-inferior | 0.23 | 1.40 (1.08–1.83) | 0.011* | | | |
| Nasal-inferior | 0.19 | 1.34 (1.04–1.74) | 0.024* | | | |
| Nasal | 0.20 | 1.38 (1.06–1.79) | 0.016* | | | |
| Nasal-superior | 0.20 | 1.36 (1.05–1.76) | 0.022* | | | |
| Temporal-superior | 0.25 | 1.39 (1.07–1.80) | 0.013* | | | |
| PMB | 0.31 | 1.41 (1.09–1.84) | 0.010* | | | |
| NT ratio | 0.09 | 0.82 (0.64–1.05) | 0.120 | | | |
| Without diabetes (N = 21 removed) | | | | | | |
| Global | 0.24 | 1.45 (1.12–1.90) | 0.005** | | | |
| Temporal | 0.30 | 1.44 (1.11–1.88) | 0.006** | | | |

*(Continues)*

**TABLE 2** *Continued*

| | Prevalent PD | | | Incident PD | | |
|---|---|---|---|---|---|---|
| **Pallor** | **1 SD** | **Odds ratio per SD increase (CI)** | ***P* value** | **1 SD** | **Odds ratio per SD increase (CI)** | ***P* value** |
| Temporal-inferior | 0.24 | 1.43 (1.10–1.86) | 0.008** | | | |
| Nasal-inferior | 0.19 | 1.40 (1.09–1.81) | 0.009** | | | |
| Nasal | 0.20 | 1.44 (1.12–1.87) | 0.005** | | | |
| Nasal-superior | 0.20 | 1.40 (1.08–1.82) | 0.010* | | | |
| Temporal-superior | 0.26 | 1.43 (1.11–1.86) | 0.007** | | | |
| PMB | 0.31 | 1.44 (1.11–1.87) | 0.006** | | | |
| NT ratio | 0.08 | 0.85 (0.67–1.09) | 0.208 | | | |
| White ethnicity only (N = 19 removed) | | | | | | |
| Global | 0.23 | 1.36 (1.05–1.76) | 0.020* | | | |
| Temporal | 0.30 | 1.36 (1.05–1.76) | 0.019* | | | |
| Temporal-inferior | 0.23 | 1.34 (1.03–1.73) | 0.027* | | | |
| Nasal-inferior | 0.19 | 1.30 (1.02–1.67) | 0.036* | | | |
| Nasal | 0.20 | 1.35 (1.05–1.73) | 0.021* | | | |
| Nasal-superior | 0.19 | 1.33 (1.03–1.71) | 0.027* | | | |
| Temporal-superior | 0.25 | 1.35 (1.04–1.74) | 0.023* | | | |
| PMB | 0.30 | 1.36 (1.06–1.77) | 0.018* | | | |
| NT ratio | 0.09 | 0.85 (0.66–1.09) | 0.212 | | | |

*Note*: All models were adjusted for age, sex, ethnicity, hypertension, cataract, diabetes, previous eye surgery, and disc area, with the exception of diabetes in the prevalent PD models (only 2 cases).
Abbreviations: PD, Parkinson's disease; SD, standard deviation of the mean; CI, confidence interval; PMB, papillomacular bundle; NT ratio, nasal-temporal ratio.
*$P$-value <0.05;
**$P$-value <0.01.

pallor non-significant (significant associations with other zones were upheld). Removing participants with diabetes (n = 2) and non-White ethnicity (n = 6) strengthened all the estimates. However, removing participants with PD duration >15 years (n = 5) rendered all associations non-significant, indicating that the previously observed associations were strongly influenced by these five data points. There was no association between disc pallor and time to diagnosis in the incident PD group. Results are summarized in Table 3, and a visual representation showing the relationship between disc pallor and PD duration for the prevalent PD group is presented in Figure S3.

## Discussion

We found that optic disc pallor was significantly higher in individuals with PD compared with controls, globally and across all zones. For each standard deviation increase in global optic disc pallor, the likelihood of being in the prevalent PD group compared to the age- and sex-matched control group increased by 39%. Odds ratios were strongest temporally and weakest nasally, which is consistent with existing OCT studies in PD.[7,17] We also found that optic disc pallor increased with PD *duration* globally and across three zones. However, this association was strongly influenced by five individuals with PD duration of >15 years, so it should be interpreted with caution. These findings represent a step forward because, in comparison to OCT, color fundus photography is less expensive, quicker to acquire, more likely to be collected routinely (ie, during routine high-street eye exams), and more directly correlates with clinical observation via slit-lamp. Furthermore, fundus photography is widely

**TABLE 3** *Linear regression results for the association between optic disc pallor and years since diagnosis and years to diagnosis*

| | Years living with PD (prevalent PD group) | | | Years to diagnosis (incident PD group) | | |
|---|---|---|---|---|---|---|
| **Pallor** | **1 SD** | **β per SD increase (SE)** | ***P*-value** | **1 SD** | **β per SD increase (SE)** | ***P*-value** |
| Global | 0.25 | 1.37 (0.61) | 0.029* | | −0.11 (0.19) | 0.565 |
| Temporal | 0.31 | 1.52 (0.62) | 0.016* | | −0.06 (0.19) | 0.733 |
| Temporal-inferior | 0.24 | 1.12 (0.62) | 0.077 | | −0.17 (0.19) | 0.366 |
| Nasal-inferior | 0.21 | 1.02 (0.59) | 0.088 | | −0.07 (0.18) | 0.708 |
| Nasal | 0.22 | 1.07 (0.58) | 0.071 | | −0.18 (0.18) | 0.330 |
| Nasal-superior | 0.22 | 1.46 (0.57) | 0.013* | | −0.20 (0.18) | 0.272 |
| Temporal-superior | 0.27 | 1.32 (0.61) | 0.035* | | −0.01 (0.19) | 0.949 |
| PMB | 0.32 | 1.57 (0.62) | 0.012* | | −0.06 (0.19) | 0.742 |
| NT ratio | 0.08 | −1.06 (0.62) | 0.089 | | −0.14 (0.17) | 0.401 |
| Sensitivity analysis | | | | | | |
| Without cataract (N = 5 removed) | | | | | | |
| Global | 0.25 | 1.23 (0.65) | 0.061 | | | |
| Temporal | 0.31 | 1.44 (0.65) | 0.029* | | | |
| Nasal-superior | 0.22 | 1.31 (0.61) | 0.035* | | | |
| PMB | 0.31 | 1.50 (0.65) | 0.024* | | | |
| Without eye surgery (N = 5 removed) | | | | | | |
| Global | 0.25 | 1.24 (0.65) | 0.061 | | | |
| Temporal | 0.30 | 1.46 (0.65) | 0.029* | | | |
| Nasal-superior | 0.22 | 1.31 (0.61) | 0.035* | | | |
| PMB | 0.31 | 1.51 (0.65) | 0.023* | | | |
| Without diabetes (N = 2 removed) | | | | | | |
| Global | 0.25 | 1.56 (0.65) | 0.018* | | | |
| Temporal | 0.31 | 1.66 (0.64) | 0.012* | | | |
| Nasal-superior | 0.22 | 1.64 (0.60) | 0.008** | | | |
| PMB | 0.32 | 1.71 (0.64) | 0.009** | | | |
| White ethnicity only (N = 6 removed) | | | | | | |
| Global | 0.25 | 1.44 (0.66) | 0.031* | | | |
| Temporal | 0.30 | 1.60 (0.65) | 0.016* | | | |
| Nasal-superior | 0.21 | 1.59 (0.64) | 0.015* | | | |
| PMB | 0.31 | 1.63 (0.64) | 0.013* | | | |
| Without outliers (N = 5 removed with PD duration > 15 years) | | | | | | |
| Global | 0.25 | 0.50 (0.44) | 0.260 | | | |
| Temporal | 0.31 | 0.60 (0.45) | 0.185 | | | |
| Nasal-superior | 0.21 | 0.57 (0.42) | 0.178 | | | |
| PMB | 0.32 | 0.64 (0.45) | 0.159 | | | |

*Note*: All models were adjusted for age, sex, ethnicity, hypertension, cataract, diabetes, previous eye surgery, and disc area, with the exception of diabetes in the prevalent PD models (only 2 cases). Significant *P*-values in bold. **P*-value <0.05; ***P*-value <0.01.
Abbreviations: PD, Parkinson's disease; SD, standard deviation of the mean; CI, confidence interval; PMB, papillomacular bundle; NT ratio, nasal-temporal ratio.

accessible in both community and clinical settings, making it a practical tool for the potential monitoring of neurodegenerative conditions like PD.

Although the link between pRNFL thinning and PD is well established,[7] research on the association between PD and optic disc pallor (which largely results from pRNFL thinning) is scant. One previous study reported an association[14]; however, its assessment of optic disc pallor was subjective and grouped under "optic nerve disorders" (including optic nerve head drusen, atrophy, and pallor) that were present in around two-thirds of the 85 patients studied. By contrast, the current study uses quantitative measures of disc pallor from a larger sample and provides numerical estimates from statistical models that account for relevant covariates.

Previous work has used deep learning to investigate color fundus photographs for signs of PD. In one study utilizing the UK Biobank, a deep learning classifier was reported to distinguish PD from age- and sex-matched controls with an accuracy of 68%, irrespective of incident and prevalent PD.[18] Also using UK Biobank images, another study found that an individual's retinal age gap (retinal age minus chronological age) was associated with future risk of developing PD.[19] A further study used color fundus photographs to predict the Hoehn and Yahr score, achieving an accuracy of between 65% and 75%.[20] Although interesting and valuable, these studies arguably suffer from the "black box" problem inherent in deep learning-based classifiers. Other than providing GradCAM images (heatmaps) that show "where" in an image the model is drawing inference from, they offer little clinically meaningful information. By contrast, optic disc pallor is a widely understood clinical sign in fundoscopic observation, indicating damage to the optic nerve and its pathways. Furthermore, our method uses segmentation and mathematical analysis, making the process transparent and understandable to clinicians and patients.

Although optic disc pallor is thought to be largely influenced by the number and health of the nerve fibers that course over the neuro-retinal rim (eg, the pRNFL), it is possible that disc pallor could also result from a reduction in other retinal layers, such as the inner nuclear layer (INL) and the GCIPL, which contain the dopaminergic cells that are characteristically depleted in PD.[9] In this respect, our results align with findings from a cross-sectional analysis of the AlzEye cohort and the UK Biobank, which demonstrated that individuals with PD had thinner GCIPL and INL compared with controls.[5] Optic disc pallor may also be influenced by perfusion. A recent meta-analysis of nine OCT angiography studies found reduced macula perfusion density in PD patients compared with controls.[21] Whereas OCT-based studies emphasize retinal layer thinning and OCT angiography studies emphasize perfusion of the retinal microvasculature, our quantitative analysis of optic disc pallor may provide an additional, easily interpretable biomarker for PD. This complementary approach enriches the spectrum of retinal biomarkers available for PD assessment and highlights the multifaceted impact of PD on the retina. Further work should assess the unique association between optic disc pallor and retinal layers in a normal population.

Similar to retinal layer thickness,[22] optic disc pallor has a wide distribution over the healthy population. In the current dataset of 787 participants, values of global pallor ranged from 0.63 to 2.0 (mean = 1.27, standard deviation = 0.23). As a result, establishing a universal cut-off value to identify patients with "high" optic disc pallor is challenging. This means that pallor values for a given individual may have limited prognostic value unless extreme. A better approach could be to measure the *rate-of-change* in pallor using consecutive images, thereby enabling the monitoring of PD progression and potentially facilitating the earlier detection of abnormal changes. Further work could assess if the rate-of-change in pallor correlates with other measures of symptoms.

In accordance with OCT findings, we observed that the effects of disc pallor in PD were slightly stronger in the temporal zones. This suggests that retinal changes in PD might reflect broader retinal neurodegeneration rather than isolated macular atrophy that leads to temporal pallor. Furthermore, current OCT studies indicate that macular changes in PD may be non-linear, with perifoveal changes strongest superiorly and weakest temporally.[6] Optic disc pallor may follow a similar pattern. Further work could test this hypothesis using concurrent OCT and fundus imaging data. However, the finding that temporal pallor has the strongest association with PD is probably not disease specific and instead likely reflects the underlying anatomy of the RNFL and its blood supply. The temporal aspect of the optic disc is generally more vulnerable to damage due to its thinner RNFL and less robust vascular network.[23]

In the current study, 22.8% of images were rejected for low quality, which is not unusual for color fundus photographs,[24] especially given the age of the participants. Recent work has found that demographic factors can influence the likelihood that an image will be rejected for "low quality." For example, images are more likely to be rejected if they are from certain demographic groups such as males, non-White individuals, older adults, those with higher body mass index (BMI) or blood pressure, or those from the population of interest.[25] In our study, we observed that more images were rejected from the control group (25%) compared to only 13.6% from the PD group, suggesting that our quality-based exclusions did not disproportionately affect the PD group.

The associations between pallor and PD duration did not fully survive sensitivity analysis to cataracts and previous eye surgery. This suggests that these two factors may influence optic disc pallor and should be carefully

controlled in future work. However, removing participants with diabetes *increased* model estimates, for both PD duration and logistic models assessing prevalent PD versus controls. This suggests that diabetes may act as a confounding factor, potentially masking the true relationship between optic disc pallor and PD. Individuals with diabetes have a higher risk of developing PD[26]; therefore, diabetes-related changes in the eye (eg, diabetic retinopathy or other vascular complications) might obscure the effects of PD on optic nerve health. Future studies should carefully account for diabetes to better isolate the impact of PD on optic disc pallor.

The trend toward decreasing pallor with age (Fig. S4) may seem counterintuitive, especially because the RNFL typically thins with age.[27] However, there are several potential explanations for this observation. As glial cells proliferate in response to chronic cellular stress, neurodegeneration, or vascular changes[28]—a process that intensifies with age—the optic nerve head's tissue density may increase.[29] This could alter the reflective properties of the neuro-retinal rim, making it appear darker and potentially reducing the observed pallor. Second, senile miosis, the age-related decrease in pupil size, might also play a role. Smaller pupils reduce the amount of light and contrast in fundus images, potentially diminishing the apparent pallor scores for older individuals. Finally, because the pallor measure relies on relative contrast between the measurement and control region, localized changes to either of these will affect the result. These could include changes to the retinal pigment epithelium,[30] lens opacity, refractive index, or the extracellular matrix and connective tissue composition of the optic nerve head. In short, although we believe pRNFL thickness remains the primary determinant of optic disc pallor, there is a complex interplay of various other age-related factors that may influence the optic disc's appearance over time.

The strengths of this study include the use of novel software to mathematically quantify optic disc pallor in several zones, the relatively large sample size with the use of an age- and sex- matched control group, and the robust inclusion/exclusion criteria.

This study has some limitations. First, the associations between disc pallor and PD duration did not survive sensitivity analysis to outliers (removing five participants with PD duration >15 years rendered the associations non-significant). This means that we must interpret this trend with caution. However, the five individuals with long PD duration are valid data points with images that passed all quality control checks; therefore, these data highlight the need for further investigation to better understand the potential effects of long-term PD on the retina. Second, pallor varied substantially across different ethnicities (Fig. S1), but due to the limited number of participants in each ethnic category, we were unable to fully account for this heterogeneity in our statistical models. Third, *PallorMetrics* can be either fully- or semi-automated. In the current study, we opted for the semi-automated version to minimize processing error and retain as many participants/images as possible. This is both a strength in the sense that more images were successfully processed, and measurement error was minimized, and a limitation in that the results may not be precisely replicable. However, we point to an inter-annotator agreement score of 94.2% in previous work[10] that demonstrates that the methodology is replicable in our hands. Fourth, we relied on ICD-10 codes for diagnostic definitions, which may not capture cases coded in outpatient clinics, thereby leading to case under-ascertainment. Fifth, the effect sizes are relatively small, and replication in a larger, more diverse cohort is required. Sixth, UK Biobank data does not currently allow us to explore PD phenotype or severity, limiting our ability to further stratify the groups.

## Conclusion

This study revealed significant associations between optic disc pallor in color fundus photographs and PD, with the temporal zones showing the strongest effect. Pallor severity also correlated with PD duration, although this effect was strongly influenced by five individuals with long PD duration, so it should be interpreted cautiously. Our findings highlight the potential of optic disc pallor as a biomarker complementary to OCT measures for assessing PD-related neurodegeneration. Future research should focus on longitudinal assessments (including in a prodromal PD population) and include a more ethnically diverse sample to enhance the generalizability of these findings.

**Author Roles:** 1) Research project: A. Conception, B. Organization, C. Execution; 2) Statistical Analysis: A. Design, B. Execution, C. Review and Critique; 3) Manuscript Preparation: A. Writing of the first draft, B. Review and Critique.
SG: 1A, 1B, 1C, 2A, 2B, 3A
DPB: 2C, 3C
TJM: 2C, 3C

**Acknowledgments:** We kindly thank the support of Amazon Web Services for providing free computing services through an "Enhanced Credits" grant, which allowed us to process images on the UK Biobank Research Analysis Platform.

**Full financial disclosures for the previous 12 months:** S.G. has no conflicts of interest to report. T.J.M, is a founder, non-executive director, and scientific advisor at Eye to the Future Limited. D.P.B has received project grants from the Reta Lila Weston Trust and the Mary Kinross Charitable Trust and honoraria from Bial Pharma UK Ltd and Springer Nature Limited. The authors report no conflicts of interest.

### Data Availability Statement

This research was conducted using data from the UK Biobank under project ID 95450. Data directly supporting the results of this work are available only to the immediate research team members due to UK

Biobank's access control policy. Bona fide researchers can, however, apply for access at ukbiobank.ac.uk/enable-your-research/apply-for-access. UK Biobank data are available for approved researchers via successful application (https://www.ukbiobank.ac.uk/enable-your-research/apply-for-access). Retinal variables and processed images generated for the current study will be made available to UK Biobank approved researchers upon completion of this project. The *PallorMetrics* software is available upon request from the lead author.

## References


1. Cunha LP, Pires LA, Cruzeiro MM, et al. Optical coherence tomography in neurodegenerative disorders. Arq Neuropsiquiatr 2021;80(2):180–191. https://doi.org/10.1590/0004-282X-ANP-2021-0134
2. Thomson KL, Yeo JM, Waddell B, Cameron JR, Pal S. A systematic review and meta-analysis of retinal nerve fiber layer change in dementia, using optical coherence tomography. Alzheimers Dement 2015;1(2):136–143. https://doi.org/10.1016/j.dadm.2015.03.001
3. Mutlu U, Colijn JM, Ikram MA, et al. Association of Retinal Neurodegeneration on optical coherence tomography with dementia: a population-based study. JAMA Neurol 2018;75(10):1256–1263. https://doi.org/10.1001/jamaneurol.2018.1563
4. Alber J, Goldfarb D, Thompson LI, et al. Developing retinal biomarkers for the earliest stages of Alzheimer's disease: what we know, what we don't, and how to move forward. Alzheimers Dement 2020;16(1):229–243. https://doi.org/10.1002/alz.12006
5. Wagner SK, Romero-Bascones D, Cortina-Borja M, et al. Retinal optical coherence tomography features associated with incident and prevalent Parkinson disease. Neurology 2023;101(16):e1581–e1593. https://doi.org/10.1212/WNL.0000000000207727
6. Huang L, Zhang D, Ji J, Wang Y, Zhang R. Central retina changes in Parkinson's disease: a systematic review and meta-analysis. J Neurol 2021;268(12):4646–4654. https://doi.org/10.1007/s00415-020-10304-9
7. Huang L, Wang C, Wang W, Wang Y, Zhang R. The specific pattern of retinal nerve fiber layer thinning in Parkinson's disease: a systematic review and meta-analysis. J Neurol 2021;268(11):4023–4032. https://doi.org/10.1007/s00415-020-10094-0
8. Carelli V, Morgia CL, Ross-Cisneros FN, Sadun AA. Optic neuropathies: the tip of the neurodegeneration iceberg. Hum Mol Genet 2017;26(R2):R139–R150. https://doi.org/10.1093/hmg/ddx273
9. Lee JY, Martin-Bastida A, Murueta-Goyena A, et al. Multimodal brain and retinal imaging of dopaminergic degeneration in Parkinson disease. Nat Rev Neurol 2022;18(4):203–220. https://doi.org/10.1038/s41582-022-00618-9
10. Gibbon S, Muniz-Terrera G, Yii FSL, et al. PallorMetrics: software for automatically quantifying optic disc pallor in fundus photographs, and associations with Peripapillary RNFL thickness. Transl Vis Sci Technol 2024;13(5):20. https://doi.org/10.1167/tvst.13.5.20
11. Ahmad SS, Kanukollu VM. Optic atrophy. Handb Pediatr Retin OCT Eye-Brain Connect 2022;5:292–295. https://doi.org/10.1016/B978-0-323-60984-5.00064-0
12. Aleman TS, Huang J, Garrity ST, et al. Relationship between optic nerve appearance and retinal nerve fiber layer thickness as explored with spectral domain optical coherence tomography. Transl Vis Sci Technol 2014;3(6):4. https://doi.org/10.1167/tvst.3.6.4
13. Yang HK, Oh JE, Han SB, Kim KG, Hwang JM. Automatic computer-aided analysis of optic disc pallor in fundus photographs. Acta Ophthalmol 2019;97(4):e519–e525. https://doi.org/10.1111/aos.13970
14. Borm CDJM, Werkmann M, de Graaf D, et al. Undetected ophthalmological disorders in Parkinson's disease. J Neurol 2022;269(7):3821–3832. https://doi.org/10.1007/s00415-022-11014-0
15. Gibbon S, Low A, Hamid C, et al. Association of optic disc pallor and RNFL thickness with cerebral small vessel disease in the PREVENT-dementia study. Alzheimers Dement 2024;16(3):e12633. https://doi.org/10.1002/dad2.12633
16. Gibbon S, Doubal F, Chappell F, Wardlaw JM, Dhillon B, MacGillivray T. Association between optic disc pallor and lacunar stroke. BMJ Neurology Open 2024;6:e000789. https://doi.org/10.1136/bmjno-2024-000789
17. Murueta-Goyena A, Romero-Bascones D, Teijeira-Portas S, et al. Association of retinal neurodegeneration with the progression of cognitive decline in Parkinson's disease. NPJ Park Dis 2024;10(1):1–10. https://doi.org/10.1038/s41531-024-00637-x
18. Tran C, Shen K, Liu K, et al. Deep learning predicts prevalent and incident Parkinson's disease from UK biobank fundus imaging. Sci Rep 2024;14(1):3637. https://doi.org/10.1038/s41598-024-54251-1
19. Hu W, Wang W, Wang Y, et al. Retinal age gap as a predictive biomarker of future risk of Parkinson's disease. Age Ageing 2022;51(3):afac062. https://doi.org/10.1093/ageing/afac062
20. Ahn S, Shin J, Song SJ, et al. Neurologic dysfunction assessment in Parkinson disease based on fundus photographs using deep learning. JAMA Ophthalmol 2023;141(3):234–240. https://doi.org/10.1001/jamaophthalmol.2022.5928
21. Katsimpris A, Papadopoulos I, Voulgari N, et al. Optical coherence tomography angiography in Parkinson's disease: a systematic review and meta-analysis. Eye 2023;37(14):2847. https://doi.org/10.1038/s41433-023-02438-7
22. Mehta N, Waheed NK. Diversity in optical coherence tomography normative databases: moving beyond race. Int J Retina Vitr 2020;6(1):5. https://doi.org/10.1186/s40942-020-0208-5
23. Anatomy of the Human Optic Nerve: Structure and Function; Accessed September 10, 2024. https://openresearchlibrary.org/viewer/d8f4fa31-ebfc-487c-b13f-e8af83844def.
24. MacGillivray TJ, Cameron JR, Zhang Q, et al. Suitability of UK biobank retinal images for automatic analysis of morphometric properties of the vasculature. PLoS One 2015;10(5):e0127914. https://doi.org/10.1371/JOURNAL.PONE.0127914
25. Engelmann J, Storkey A, Bernabeu L, Linares M. Exclusion of poor quality fundus images biases health research linking retinal traits and systemic health. Invest Ophthalmol Vis Sci 2023;64(8):2922.
26. Komici K, Femminella GD, Bencivenga L, Rengo G, Pagano G. Diabetes mellitus and Parkinson's disease: a systematic review and meta-analyses. J Parkinsons Dis 2021;11(4):1585–1596. https://doi.org/10.3233/JPD-212725
27. Feuer WJ, Budenz DL, Anderson DR, et al. Topographic differences in the age-related changes in the retinal nerve fiber layer of Normal eyes measured by stratus™ optical coherence tomography. J Glaucoma 2011;20(3):133–138. https://doi.org/10.1097/IJG.0b013e3181e079b2
28. Colonna M, Butovsky O. Microglia function in the central nervous system during health and neurodegeneration. Annu Rev Immunol 2017;35:441–468. https://doi.org/10.1146/annurev-immunol-051116-052358
29. Johnson EC, Morrison JC. Friend or foe? Resolving the impact of glial responses in glaucoma. J Glaucoma 2009;18(5):341–353. https://doi.org/10.1097/IJG.0b013e31818c6ef6
30. Bonilha VL. Age and disease-related structural changes in the retinal pigment epithelium. Clin Ophthalmol Auckl NZ 2008;2(2):413–424. https://doi.org/10.2147/opth.s2151


## Supporting Data

Additional Supporting Information may be found in the online version of this article at the publisher's web-site.

## 7.5. Conclusion

In this study, we showed that optic disc pallor is significantly higher in individuals with PD compared to age- and sex-matched controls. We also showed that pallor increases with PD duration. Put another way, the longer an individual had been living with PD, the paler their discs. However, this association was sensitive to outliers – removing 5 individuals with a PD duration of greater than 15 years nullified the effect. There were no associations between disc pallor and incident PD. These results are novel, suggesting that fundus images contain information that may help with PD diagnosis and monitoring progression. However, longitudinal imaging data are needed to explore how the disc changes in the prodromal stage of the disease.

# Chapter 8

# Discussion and conclusion

## 8.1 Aim and objectives

The overall aim of my PhD was to learn about brain health through images of the retina. After engaging with the literature, I identified optic disc pallor as a potential marker of neurological dysfunction. Based on this, I established three core objectives:

**Objective 1:** To develop a method of quantifying optic disc pallor in fundus images.

**Objective 2:** To investigate optic disc pallor in a cerebrovascular disease.

**Objective 3:** To investigate optic disc pallor in a neurodegenerative disease.

Based on these objectives, I carried out several investigations which resulted in four publications. In this chapter, I will summarise the main findings from these investigations, discuss how they contribute to my overall aim, and outline future areas of research.

## 8.2 Main findings and areas for future research

### 8.2.1 Objective 1: To develop a method of quantifying optic disc pallor in fundus images.

#### 8.2.1.1 *Summary of findings*

For the first objective – developing a tool to quantify optic disc pallor – I made significant progress. *PallorMetrics* fills a critical gap in optic disc assessment by offering a quantitative and user-friendly alternative to subjective clinical descriptions. The software automatically measures optic disc pallor globally and within specific zones, drawing on segmentation principles akin to those used in modern OCT scans of the pRNFL. The measurements were validated by demonstrating associations with pRNFL thickness and effectively distinguishing clinically defined pallor in an external dataset. Its performance across various imaging systems, formats, and resolutions further highlights its robustness and versatility.

To enhance its usability for large datasets, I developed two methods for automated quality control: a manual threshold method and a machine learning classifier. The manual method showed good sensitivity, a higher negative predictive value, and a lower false negative rate, making it conservative and suitable for ensuring data reliability in statistical analyses. In contrast, the decision tree classifier achieved a higher AUC (0.88 compared to 0.81 for the manual method), but left some outliers remaining. These automated quality control methods are now integrated into *PallorMetrics*, enabling its application to large datasets without the need for labour-intensive manual inspection.

Externally, *PallorMetrics* has been run on a set of approximately 3,500 fundus images from the Northern Ireland Cohort for the Longitudinal Study of Ageing (NICOLA).[122] Feedback from the NICOLA team has been positive, with the software and quality control running as expected.

#### *8.2.1.2 Areas for future research*

A key next step for *PallorMetrics* is to evaluate its repeatability using a dataset with multiple images of the same eye. Incorporating repeat imaging would allow us to determine how factors such as image quality, brightness, and minor variations in imaging conditions affect

the results. This evaluation would strengthen confidence in *PallorMetrics'* performance and support its further application in research and clinical settings.

The selection of the control region is another potential area for improvement in *PallorMetrics*. In the current implementation, the control region is defined as a square around the optic disc. While this approach is robust in most cases, it may be less suitable when peripapillary atrophy extends into the control region – a scenario more common in older individuals. Future iterations of the software could adopt an adaptive approach, dynamically adjusting the shape, size, and position of the control region based on image-specific characteristics. For example, multiple smaller control regions could be defined across the retina, with algorithms selecting the most appropriate regions or calculating a weighted average of measurements. Incorporating automated quality assessments to exclude regions affected by artifacts, shadows, or anomalies, such as peripapillary atrophy, could further enhance accuracy. These refinements might improve measurement consistency and adaptability across diverse imaging scenarios.

Further refinement of the quality control methods could be another area of focus. While the manual threshold and decision tree methods perform well, exploring hybrid or more advanced machine learning approaches could improve the balance between sensitivity and specificity. Incorporating these enhancements might strengthen *PallorMetrics'* reliability and adaptability.

*PallorMetrics* currently does not support fundus images with a 30° field of view, as these images are rare in clinical practice and were not included in the training set. Future versions may be adapted to accommodate image with this resolution.

I have an ongoing collaboration with the team at Moorfields Eye Hospital, who are planning to implement the *PallorMetrics* software on the AlzEye dataset.[123] This dataset

includes approximately 1.8 million fundus images, making it one of the world's largest resources for retinal imaging studies. The primary aim of this collaboration is to investigate the utility of optic disc pallor as a potential biomarker in the emerging field of oculomics, which explores how ocular features can reveal insights into systemic and neurological health.[124,125]

**8.2.2 Objective 2:** To investigate optic disc pallor in a cerebrovascular disease.

#### *8.2.2.1 Summary of findings*

For the second objective – investigating optic disc pallor in a cerebrovascular disease – significant progress was made, with two published studies (chapters 5 & 6) providing complementary insights.

In the PREVENT Dementia cohort, we identified a novel association between optic disc pallor and enlarged perivascular spaces, a key MRI marker of cSVD. This finding is promising, as it suggests that optic disc pallor may act as a non-invasive alternative to MRI. Further, this work benefited from *PallorMetrics'* fully automated approach to fundus image analysis, which enhances scalability and positions the software as a viable tool for application to larger datasets.

In the Mild Stroke Study, we extended the analysis to examine the relationship between optic disc pallor and both ischemic stroke subtype and cSVD severity. Optic disc pallor was significantly associated with the lacunar stroke subtype, a clinical hallmark of cSVD, and correlated with overall cSVD burden, reinforcing its relevance in assessing disease characteristics. These results provide further evidence that cSVD may affect the optic nerve and its pathways.

#### *8.2.2.2 Areas for future research*

Future research should incorporate longitudinal data to investigate whether changes in optic disc pallor correspond to the progression of cSVD. Both analyses relied on cross-sectional data. Now that wave two of data collection for the PREVENT Dementia study is complete, there is an opportunity to explore correlations between changes in optic disc pallor, brain imaging findings, clinical features, and possibly even functional outcomes. Such studies would offer valuable insights into the temporal dynamics and potential clinical utility of optic disc pallor in tracking disease progression.

In the PREVENT study, optic disc pallor may serve as a marker of glymphatic dysfunction affecting both the brain and the visual pathway. Further research could investigate the relationship between glymphatic function and optic disc appearance. This could include longitudinal studies to examine whether changes in optic disc pallor correlate with glymphatic impairment over time, as well as experimental models to explore the mechanisms linking glymphatic dysfunction to RNFL loss. One promising measure of glymphatic function is diffusion tensor imaging along the perivascular space (DTI-ALPS).[126] DTI-ALPS is used to quantify the directional diffusion of water molecules along perivascular spaces, providing insights into the efficiency of waste clearance in the brain. This technique has shown potential in identifying impairments in glymphatic function, which may be linked to neurodegenerative diseases and other conditions affecting brain health.[127,128] Using DTI-ALPS alongside retinal imaging could offer a powerful approach to studying the relationship between glymphatic dysfunction and optic disc changes, furthering our understanding of how the brain and visual pathways are interconnected. Such research could provide valuable insights into how impaired glymphatic function may affect both brain health and retinal changes.

Another area for future research could focus on leveraging the unique characteristics of the PREVENT Dementia cohort, which includes individuals with subtle markers of cSVD while being otherwise healthy. This cohort presents an opportunity to study early signs of cerebrovascular deterioration and how these early markers relate to subsequent cognitive decline or other vascular brain pathologies.

**8.2.3 Objective 3:** To investigate optic disc pallor in a neurodegenerative disease.

#### *8.2.3.1 Summary of findings*

For the third objective – investigating optic disc pallor in a neurodegenerative disease – significant progress was made, culminating in a publication using data from the UK Biobank. This work provided several key insights into the potential role of optic disc pallor in Parkinson's disease.

First, it was demonstrated that optic disc pallor is significantly increased in individuals with prevalent PD compared to age- and sex-matched controls. This finding supports the hypothesis that pallor reflects RGC axon loss, a characteristic feature of PD-related neurodegeneration. Furthermore, pallor was significantly associated with disease duration, with longer-standing PD linked to greater pallor, underscoring its potential as a marker of disease progression.

Regarding incident PD, however, there was limited support for the hypothesis that optic disc pallor is associated with PD – a trend was observed that did not reach statistical significance. This suggests that while pallor may reflect existing neurodegenerative changes, further studies are needed to investigate whether it may be a preclinical marker of PD.

#### *8.2.3.2 Areas for future research*

Further work should move beyond statistical associations and look toward predictive modelling. For example, it would be of great value to assess whether adding optic disc pallor to a predictive model that already includes readily available information like age, sex, BMI, and smoking status leads to a significant improvement in the model's performance. Such a model may have clinical utility.

In the current study, I investigated the association between optic disc pallor at a single time point and future PD, compared to an age- and sex-matched control group. However, a more effective approach would be to use repeat imaging data from the same individuals, allowing for the measurement of the rate of change within each person over time. Longitudinal studies of this nature would provide valuable insights. An ideal resource for such research is the Scottish Collaborative Optometry-Ophthalmology Network e-research project (SCONe), which is collecting fundus images linked to healthcare data from optician practices across Scotland. As of December 2024, the SCONe dataset contained 429 individuals with a probable PD diagnosis (ICD-10 code G20), contributing a total of 1,635 images, of which 1,300 were captured before diagnosis. This presents a unique opportunity to examine retinal imaging data from several years prior to a PD diagnosis. Exploring optic disc pallor and other retinal biomarkers in this cohort is a research priority.

An important point not touched upon in the published article regards the ethical and practical questions about the potential use of optic disc pallor to identify individuals at risk for PD. Unlike cSVD, where early detection could inform vascular risk management, PD currently lacks curative treatments, complicating the clinical utility of early biomarkers. Future efforts must carefully consider how such findings would be communicated to patients, the psychological implications of risk prediction, and the pathways for follow-up care and

support. Notwithstanding, identifying PD in its earliest stages allows for better management of symptoms to improve quality of life for patients for longer.

## 8.3 Additional remarks

### 8.3.1 The link between cerebral small vessel disease and Parkinson's disease

There is growing evidence that cSVD plays a significant role in several neurological disorders, including PD and Alzheimer's disease (both neurodegenerative diseases), and multiple sclerosis (a neuroinflammatory disease).[129] Regarding PD, neuroimaging of patients often reveals radiological features of cSVD, such as lacunar infarcts and white matter lesions, which may be identified during the initial evaluation of newly diagnosed PD patients but are more commonly observed in the later stages of the disease.[129,130] Both cSVD progression and severity have been linked to incident parkinsonism, which suggests a causal role of cSVD in PD.[131] cSVD also correlates with the Hoehn and Yahr score of functional disability in PD.[132] When cSVD coexists with PD, it exacerbates clinical symptoms, including impairments in gait, cognition, and mood.[133] This overlap may also contribute to a faster progression of PD.[129] Such evidence suggests that PD progression may be slowed by treating vascular risk factors – this hypothesis remains to be tested.[134]

In this thesis, I observed increased optic disc pallor in PD and cSVD in three independent datasets (two for cSVD and one for PD). For cSVD, associations were observed in the basal ganglia (Chapter 5). This raises the possibility that damage to the optic nerve might represent the end result of a shared pathogenic pathway between cerebrovascular dysfunction and neurodegeneration. For example, it is possible that cSVD lesions in the basal ganglia could disrupt the dopaminergic pathway.[135] Given the basal ganglia's critical role in motor control and its reliance on dopaminergic signalling,[135] damage to this region could

impair the transmission of dopamine, thereby exacerbating motor symptoms in PD. However, this is speculative and remains to be tested.

### 8.3.2 A cautionary note on communicating results to the public

Retinal measures are not intended to replace clinical diagnosis or serve as standalone diagnostic tools for neurological disorders. Instead, they are supplemental, providing additional information that may in the future aid and refine diagnoses. While this distinction may seem obvious to researchers and clinicians, it is less so for early-stage researchers and may be entirely misunderstood by the public. Headlines of the type "The eye can diagnose dementia" are common.

A striking example is the media coverage of the recent Wagner et al. (2023) study on OCT in Parkinson's disease, published *Neurology*, a high-profile journal.[121] *The Independent,* a UK newspaper, ran the headline, "AI eye scans can detect Parkinson's up to seven years before symptoms appear, scientists say."[136] While this may be technically true, the actual study reported a group mean difference of less than 2 microns in retinal layer thickness – an amount within the measurement error of most OCT devices and associated software. This means that while a statistical difference exists at the group level, an individual scan would offer no meaningful prognostic value.

Such reporting can mislead the public into believing they can simply have their eyes tested for signs of Parkinson's disease, which is most certainly not the case. Clear communication is essential to ensure that the potential of retinal imaging as a research tool is understood without overstating its current clinical applicability. In my own work, I have tried to express this sentiment through careful use of language.

## 8.4 Conclusion

The aim of this thesis was to learn about brain health through images of the retina. I identified optic disc pallor as a potential biomarker of brain health, given its underlying association with RNFL thinning, which is present in many neurological disorders. I developed a method of quantifying optic disc pallor based in fundus images and applied the method to three datasets investigating cSVD and PD. Regarding cSVD, I found that optic disc pallor was associated with an MRI based marker of cSVD – enlarged perivascular spaces. Regarding PD, I found that optic disc pallor was higher in PD compared to age- and sex-matched controls, and that pallor increased with disease duration. Together, these results suggest that optic disc pallor might reflect a shared pathological mechanism between cSVD and PD. Areas for future research include assessing the repeatability of *PallorMetrics*, carrying out longitudinal assessment of both cSVD and PD, and incorporating the pallor measures into a predictive model of PD.

# References


1. GBD 2016 Neurology Collaborators. Global, regional, and national burden of neurological disorders, 1990-2016: a systematic analysis for the Global Burden of Disease Study 2016. *Lancet Neurol*. 2019;18(5):459-480. doi:10.1016/S1474-4422(18)30499-X

2. Wardlaw JM, Smith EE, Biessels GJ, et al. Neuroimaging standards for research into small vessel disease and its contribution to ageing and neurodegeneration. *Lancet Neurol*. 2013;12(8):822-838. doi:10.1016/S1474-4422(13)70124-8

3. Bloem BR, Okun MS, Klein C. Parkinson's disease. *The Lancet*. 2021;397(10291):2284-2303. doi:10.1016/S0140-6736(21)00218-X

4. Lee JY, Martin-Bastida A, Murueta-Goyena A, et al. Multimodal brain and retinal imaging of dopaminergic degeneration in Parkinson disease. *Nat Rev Neurol*. 2022;18(4):203-220. doi:10.1038/s41582-022-00618-9

5. Cannistraro RJ, Badi M, Eidelman BH, Dickson DW, Middlebrooks EH, Meschia JF. CNS small vessel disease. *Neurology*. 2019;92(24):1146-1156. doi:10.1212/WNL.0000000000007654

6. London A, Benhar I, Schwartz M. The retina as a window to the brain—from eye research to CNS disorders. *Nat Rev Neurol*. 2013;9(1):44-53. doi:10.1038/nrneurol.2012.227

7. Chalkias IN, Tegos T, Topouzis F, Tsolaki M. Ocular biomarkers and their role in the early diagnosis of neurocognitive disorders. *Eur J Ophthalmol*. 2021;31(6):2808-2817. doi:10.1177/11206721211016311

8. Cheung CY, Mok V, Foster PJ, Trucco E, Chen C, Wong TY. Retinal imaging in Alzheimer's disease. *J Neurol Neurosurg Psychiatry*. 2021;92(9):983-994. doi:10.1136/jnnp-2020-325347

9. Silverstein SM, Demmin DL, Schallek JB, Fradkin SI. Measures of Retinal Structure and Function as Biomarkers in Neurology and Psychiatry. *Biomark Neuropsychiatry*. 2020;2:100018. doi:10.1016/j.bionps.2020.100018

10. McClard CK, Shah V. Pediatric Optic Disc Pallor. *Int Ophthalmol Clin*. 2018;58(4):125. doi:10.1097/IIO.0000000000000244

11. Osaguona VB. Differential diagnoses of the pale/white/atrophic disc. *Community Eye Health*. 2016;29(96):71-74.

12. Ahmad SS, Kanukollu VM. Optic Atrophy. In: *StatPearls*. StatPearls Publishing; 2022. Accessed August 29, 2022. http://www.ncbi.nlm.nih.gov/books/NBK559130/

13. Yii F, Gibbon S, MacGillivray T. Sectoral changes in neuroretinal rim pallor across refractive error. *Ophthalmol Sci*. Published online January 7, 2025:100705. doi:10.1016/j.xops.2025.100705

14. Cameron JR, Megaw RD, Tatham AJ, et al. Lateral thinking – Interocular symmetry and asymmetry in neurovascular patterning, in health and disease. *Prog Retin Eye Res*. 2017;59:131-157. doi:10.1016/j.preteyeres.2017.04.003

15. Simple Anatomy of the Retina by Helga Kolb – Webvision. Accessed September 18, 2024. https://webvision.med.utah.edu/book/part-i-foundations/simple-anatomy-of-the-retina/

16. Erskine L, Herrera E. Connecting the Retina to the Brain. *ASN Neuro*. 2014;6(6):1759091414562107. doi:10.1177/1759091414562107

17. Anatomy of the Human Optic Nerve: Structure and Function. Accessed September 10, 2024. https://openresearchlibrary.org/viewer/d8f4fa31-ebfc-487c-b13f-e8af83844def

18. Sharif NA. Degeneration of retina-brain components and connections in glaucoma: Disease causation and treatment options for eyesight preservation. *Curr Res Neurobiol*. 2022;3:100037. doi:10.1016/j.crneur.2022.100037

19. Fonnum F. Glutamate: A Neurotransmitter in Mammalian Brain. *J Neurochem*. 1984;42(1):1-11. doi:10.1111/j.1471-4159.1984.tb09689.x

20. Patton N, Aslam T, MacGillivray T, Pattie A, Deary IJ, Dhillon B. Retinal vascular image analysis as a potential screening tool for cerebrovascular disease: A rationale based on homology between cerebral and retinal microvasculatures. *J Anat*. 2005;206(4):319-348. doi:10.1111/j.1469-7580.2005.00395.x

21. O'Leary F, Campbell M. The blood–retina barrier in health and disease. *FEBS J*. 2023;290(4):878-891. doi:10.1111/febs.16330

22. Kadry H, Noorani B, Cucullo L. A blood–brain barrier overview on structure, function, impairment, and biomarkers of integrity. *Fluids Barriers CNS*. 2020;17(1):69. doi:10.1186/s12987-020-00230-3

23. Goel M, Picciani RG, Lee RK, Bhattacharya SK. Aqueous Humor Dynamics: A Review. *Open Ophthalmol J*. 2010;4:52. doi:10.2174/1874364101004010052

24. Li HJ, Sun ZL, Yang XT, Zhu L, Feng DF. Exploring Optic Nerve Axon Regeneration. *Curr Neuropharmacol*. 2017;15(6):861-873. doi:10.2174/1570159X14666161227150250

25. Kashani AH, Asanad S, Chan JW, et al. Past, present and future role of retinal imaging in neurodegenerative disease. *Prog Retin Eye Res*. 2021;83:100938. doi:10.1016/j.preteyeres.2020.100938

26. Cheung CY lui, Ikram MK, Chen C, Wong TY. Imaging retina to study dementia and stroke. *Prog Retin Eye Res*. 2017;57:89-107. doi:10.1016/j.preteyeres.2017.01.001

27. Panwar N, Huang P, Lee J, et al. Fundus Photography in the 21st Century—A Review of Recent Technological Advances and Their Implications for Worldwide Healthcare. *Telemed J E Health*. 2016;22(3):198-208. doi:10.1089/tmj.2015.0068

28. MacGillivray T, McGrory S, Pearson T, Cameron J. Retinal imaging in early Alzheimer's disease. *Neuromethods*. 2018;137:199-212. doi:10.1007/978-1-4939-7674-4_14

29. Ritchie CW, Wells K, Gregory S, et al. The PREVENT Dementia programme: Baseline demographic, lifestyle, imaging and cognitive data from a midlife cohort study investigating risk factors for dementia. Published online July 16, 2023:2023.07.14.23292648. doi:10.1101/2023.07.14.23292648

30. Oberwahrenbrock T, Traber GL, Lukas S, et al. Multicenter reliability of semiautomatic retinal layer segmentation using OCT. *Neurol Neuroimmunol Neuroinflammation*. 2018;5(3):e449. doi:10.1212/NXI.0000000000000449

31. Cannistraro RJ, Badi M, Eidelman BH, Dickson DW, Middlebrooks EH, Meschia JF. CNS small vessel disease: A clinical review. *Neurology*. 2019;92(24):1146-1156. doi:10.1212/WNL.0000000000007654

32. Wardlaw JM, Smith C, Dichgans M. Small vessel disease: mechanisms and clinical implications. *Lancet Neurol*. 2019;18(7):684-696. doi:10.1016/S1474-4422(19)30079-1

33. Li Q, Yang Y, Reis C, et al. Cerebral Small Vessel Disease. *Cell Transplant*. 2018;27(12):1711-1722. doi:10.1177/0963689718795148

34. van Veluw SJ, Shih AY, Smith EE, et al. Detection, risk factors, and functional consequences of cerebral microinfarcts. *Lancet Neurol*. 2017;16(9):730-740. doi:10.1016/S1474-4422(17)30196-5

35. Georgakis MK, Duering M, Wardlaw JM, Dichgans M. WMH and long-term outcomes in ischemic stroke: A systematic review and meta-analysis. *Neurology*. 2019;92(12):e1298-e1308. doi:10.1212/WNL.0000000000007142

36. Cuadrado-Godia E, Dwivedi P, Sharma S, et al. Cerebral Small Vessel Disease: A Review Focusing on Pathophysiology, Biomarkers, and Machine Learning Strategies. *J Stroke*. 2018;20(3):302-320. doi:10.5853/jos.2017.02922

37. Federico A, Di Donato I, Bianchi S, Di Palma C, Taglia I, Dotti MT. Hereditary cerebral small vessel diseases: a review. *J Neurol Sci*. 2012;322(1-2):25-30. doi:10.1016/j.jns.2012.07.041

38. Gore M, Bansal K, Khan Suheb MZ, Asuncion RMD. Lacunar Stroke. In: *StatPearls*. StatPearls Publishing; 2024. Accessed February 21, 2024. http://www.ncbi.nlm.nih.gov/books/NBK563216/

39. Regenhardt RW, Das AS, Lo EH, Caplan LR. Advances in Understanding the Pathophysiology of Lacunar Stroke: A Review. *JAMA Neurol*. 2018;75(10):1273-1281. doi:10.1001/jamaneurol.2018.1073

40. Norrving B. Long-term prognosis after lacunar infarction. *Lancet Neurol*. 2003;2(4):238-245. doi:10.1016/S1474-4422(03)00352-1

41. Das AS, Regenhardt RW, Feske SK, Gurol ME. Treatment Approaches to Lacunar Stroke. *J Stroke Cerebrovasc Dis Off J Natl Stroke Assoc*. 2019;28(8):2055-2078. doi:10.1016/j.jstrokecerebrovasdis.2019.05.004

42. Grysiewicz RA, Ruland SD. Lacunar Infarcts. In: Aminoff MJ, Daroff RB, eds. *Encyclopedia of the Neurological Sciences (Second Edition)*. Academic Press; 2014:815-818. doi:10.1016/B978-0-12-385157-4.00417-6

43. Ganesh A, Gutnikov SA, Rothwell PM, Study for the OV. Late functional improvement after lacunar stroke: a population-based study. *J Neurol Neurosurg Psychiatry*. 2018;89(12):1301-1307. doi:10.1136/jnnp-2018-318434

44. Hilal S, Mok V, Youn YC, Wong A, Ikram MK, Chen CLH. Prevalence, risk factors and consequences of cerebral small vessel diseases: data from three Asian countries. *J Neurol Neurosurg Psychiatry*. 2017;88(8):669-674. doi:10.1136/jnnp-2016-315324

45. Khan U, Porteous L, Hassan A, Markus HS. Risk factor profile of cerebral small vessel disease and its subtypes. *J Neurol Neurosurg Psychiatry*. 2007;78(7):702-706. doi:10.1136/jnnp.2006.103549

46. Lau KK, Tsang ACO, Teo KC, et al. Age-Specific Associations of Renal Impairment and Cerebral Small Vessel Disease Burden in Chinese with Ischaemic Stroke. *J Stroke Cerebrovasc Dis*. 2019;28(5):1274-1280. doi:10.1016/j.jstrokecerebrovasdis.2019.01.018

47. Kim H, Yun CH, Thomas RJ, et al. Obstructive sleep apnea as a risk factor for cerebral white matter change in a middle-aged and older general population. *Sleep*. 2013;36(5):709-715B. doi:10.5665/sleep.2632

48. Su C, Wu H, Yang X, Zhao B, Zhao R. The relation between antihypertensive treatment and progression of cerebral small vessel disease. *Medicine (Baltimore)*. 2021;100(30):e26749. doi:10.1097/MD.0000000000026749

49. Wardlaw J, Bath PMW, Doubal F, et al. Protocol: The Lacunar Intervention Trial 2 (LACI-2). A trial of two repurposed licenced drugs to prevent progression of cerebral small vessel disease. *Eur Stroke J*. 2020;5(3):297-308. doi:10.1177/2396987320920110

50. Low A, Prats-Sedano MA, McKiernan E, et al. Modifiable and non-modifiable risk factors of dementia on midlife cerebral small vessel disease in cognitively healthy middle-aged adults: the PREVENT-Dementia study. *Alzheimers Res Ther*. 2022;14(1):154. doi:10.1186/s13195-022-01095-4

51. Biffi E, Turple Z, Chung J, Biffi A. Retinal biomarkers of Cerebral Small Vessel Disease: A systematic review. *PloS One*. 2022;17(4):e0266974. doi:10.1371/journal.pone.0266974

52. Strimbu K, Tavel JA. What are Biomarkers? *Curr Opin HIV AIDS*. 2010;5(6):463-466. doi:10.1097/COH.0b013e32833ed177

53. Wardlaw JM, Valdés Hernández MC, Muñoz-Maniega S. What are White Matter Hyperintensities Made of? *J Am Heart Assoc Cardiovasc Cerebrovasc Dis*. 2015;4(6):e001140. doi:10.1161/JAHA.114.001140

54. Nowogrodzki J. The world's strongest MRI machines are pushing human imaging to new limits. *Nature*. 2018;563(7729):24-26. doi:10.1038/d41586-018-07182-7

55. Ls C, Ty W, R K, et al. Retinal microvascular abnormalities and MRI-defined subclinical cerebral infarction: the Atherosclerosis Risk in Communities Study. *Stroke*. 2006;37(1). doi:10.1161/01.STR.0000195134.04355.e5

56. W L, Ek L, R K, et al. Associations between findings on cranial magnetic resonance imaging and retinal photography in the elderly: the Cardiovascular Health Study. *Am J Epidemiol*. 2007;165(1). doi:10.1093/aje/kwj350

57. Cheung N, Mosley T, Islam A, et al. Retinal microvascular abnormalities and subclinical magnetic resonance imaging brain infarct: a prospective study. *Brain J Neurol*. 2010;133(Pt 7):1987-1993. doi:10.1093/brain/awq127

58. Fn D, R de H, Tj M, et al. Retinal arteriolar geometry is associated with cerebral white matter hyperintensities on magnetic resonance imaging. *Int J Stroke Off J Int Stroke Soc*. 2010;5(6). doi:10.1111/j.1747-4949.2010.00483.x

59. McGrory S, Ballerini L, Doubal FN, et al. Retinal microvasculature and cerebral small vessel disease in the Lothian Birth Cohort 1936 and Mild Stroke Study. *Sci Rep*. 2019;9(1):6320. doi:10.1038/s41598-019-42534-x

60. Langner SM, Terheyden JH, Geerling CF, et al. Structural retinal changes in cerebral small vessel disease. *Sci Rep*. 2022;12(1):9315. doi:10.1038/s41598-022-13312-z

61. Wang R, Wu X, Zhang Z, et al. Retinal ganglion cell-inner plexiform layer, white matter hyperintensities, and their interaction with cognition in older adults. *Front Aging Neurosci*. 2023;15. doi:10.3389/fnagi.2023.1240815

62. Qu M, Kwapong WR, Peng C, et al. Retinal sublayer defect is independently associated with the severity of hypertensive white matter hyperintensity. *Brain Behav*. 2020;10(2):e01521. doi:10.1002/brb3.1521

63. Hilal S, Cheung CY, Wong TY, Schmetterer L, Chen C. Retinal parameters, cortical cerebral microinfarcts, and their interaction with cognitive impairment. *Int J Stroke*. 2023;18(1):70-77. doi:10.1177/17474930221097737

64. Morris HR, Spillantini MG, Sue CM, Williams-Gray CH. The pathogenesis of Parkinson's disease. *The Lancet*. 2024;403(10423):293-304. doi:10.1016/S0140-6736(23)01478-2

65. Picillo M, Palladino R, Moccia M, et al. Gender and non motor fluctuations in Parkinson's disease: A prospective study. *Parkinsonism Relat Disord*. 2016;27:89-92. doi:10.1016/j.parkreldis.2016.04.001

66. Gaenslen A, Swid I, Liepelt-Scarfone I, Godau J, Berg D. The patients' perception of prodromal symptoms before the initial diagnosis of Parkinson's disease. *Mov Disord*. 2011;26(4):653-658. doi:10.1002/mds.23499

67. Belvisi D, Pellicciari R, Fabbrini A, et al. Risk factors of Parkinson disease. *Neurology*. 2020;95(18):e2500-e2508. doi:10.1212/WNL.0000000000010813

68. Df M, Er R, K S, Ja M, Jp P, W S. Neurodegenerative Disease Mortality among Former Professional Soccer Players. *N Engl J Med*. 2019;381(19). doi:10.1056/NEJMoa1908483

69. Helmich RC, Bloem BR. The Impact of the COVID-19 Pandemic on Parkinson's Disease: Hidden Sorrows and Emerging Opportunities. *J Park Dis*. 10(2):351-354. doi:10.3233/JPD-202038

70. Fang X, Han D, Cheng Q, et al. Association of Levels of Physical Activity With Risk of Parkinson Disease: A Systematic Review and Meta-analysis. *JAMA Netw Open*. 2018;1(5):e182421. doi:10.1001/jamanetworkopen.2018.2421

71. Quik M, Perez XA, Bordia T. Nicotine as a potential neuroprotective agent for Parkinson's disease. *Mov Disord Off J Mov Disord Soc*. 2012;27(8):947-957. doi:10.1002/mds.25028

72. Bagga P, Chugani AN, Patel AB. Neuroprotective effects of caffeine in MPTP model of Parkinson's disease: A (13)C NMR study. *Neurochem Int*. 2016;92:25-34. doi:10.1016/j.neuint.2015.11.006

73. Je A. Does vigorous exercise have a neuroprotective effect in Parkinson disease? *Neurology*. 2011;77(3). doi:10.1212/WNL.0b013e318225ab66

74. Ritz B, Lee PC, Lassen CF, Arah OA. Parkinson disease and smoking revisited. *Neurology*. 2014;83(16):1396-1402. doi:10.1212/WNL.0000000000000879

75. El-Agnaf OMA, Salem SA, Paleologou KE, et al. Detection of oligomeric forms of α-synuclein protein in human plasma as a potential biomarker for Parkinson's disease. *FASEB J*. 2006;20(3):419-425. doi:10.1096/fj.03-1449com

76. Emamzadeh FN, Surguchov A. Parkinson's Disease: Biomarkers, Treatment, and Risk Factors. *Front Neurosci*. 2018;12:612. doi:10.3389/fnins.2018.00612

77. Murman D. Early treatment of Parkinson's disease: opportunities for managed care. *Am J Manag Care*. Published online September 22, 2012. Accessed October 14, 2024. https://www.semanticscholar.org/paper/Early-treatment-of-Parkinson's-disease%3A-for-managed-Murman/d5872b15116f84f9bb6fbd8e482a3be9d9a0f4f9

78. Chahine LM, Beach TG, Brumm MC, et al. In vivo distribution of α-synuclein in multiple tissues and biofluids in Parkinson disease. *Neurology*. 2020;95(9):e1267-e1284. doi:10.1212/WNL.0000000000010404

79. Siderowf A, Concha-Marambio L, Lafontant DE, et al. Assessment of heterogeneity among participants in the Parkinson's Progression Markers Initiative cohort using α-synuclein seed amplification: a cross-sectional study. *Lancet Neurol*. 2023;22(5):407-417. doi:10.1016/S1474-4422(23)00109-6

80. Kim KT. Lumbar puncture: considerations, procedure, and complications. *Encephalitis*. 2022;2(4):93-97. doi:10.47936/encephalitis.2022.00045

81. Lee JY, Martin-Bastida A, Murueta-Goyena A, et al. Multimodal brain and retinal imaging of dopaminergic degeneration in Parkinson disease. *Nat Rev Neurol*. 2022;18(4):203-220. doi:10.1038/s41582-022-00618-9

82. I OL, Tg B, Ge S, Dg W, Ch A, N C. Phosphorylated α-synuclein in the retina is a biomarker of Parkinson's disease pathology severity. *Mov Disord Off J Mov Disord Soc*. 2018;33(8). doi:10.1002/mds.27392

83. Witkovsky P. Dopamine and retinal function. *Doc Ophthalmol Adv Ophthalmol*. 2004;108(1):17-40. doi:10.1023/b:doop.0000019487.88486.0a

84. Chrysou A, Jansonius NM, van Laar T. Retinal layers in Parkinson's disease: A meta-analysis of spectral-domain optical coherence tomography studies. *Parkinsonism Relat Disord*. 2019;64:40-49. doi:10.1016/j.parkreldis.2019.04.023

85. Ma JP, Robbins CB, Pead E, et al. Ultra-Widefield Imaging of the Retinal Macrovasculature in Parkinson Disease Versus Controls With Normal Cognition Using Alpha-Shapes Analysis. *Transl Vis Sci Technol*. 2024;13(1):15. doi:10.1167/tvst.13.1.15

86. Ma JP, Robbins C, Pead E, et al. Retinal vascular changes in Parkinson's disease on ultra-widefield retinal imaging. *Invest Ophthalmol Vis Sci*. 2021;62(8):1779.

87. Harizman N, Oliveira C, Chiang A, et al. The ISNT rule and differentiation of normal from glaucomatous eyes. *Arch Ophthalmol*. 2006;124(11):1579-1583. doi:10.1001/archopht.124.11.1579

88. eOphtha. Understanding Optic Disc Pallor- Shades of White. Accessed April 17, 2023. https://www.eophtha.com/posts/understanding-optic-disc-pallor-shades-of-white

89. O.D BJWS. Shedding Light on a Pale Optic Nerve. Accessed April 21, 2023. https://www.reviewofoptometry.com/article/shedding-light-on-a-pale-optic-nerve

90. Kline's_Neuro-Ophthalmology_Review_Manual_---- _(Chapter_10_The_Pale_Optic_Disc_Optic_Atrophy).

91. Ahmad SS, Kanukollu VM. Optic Atrophy. *Handb Pediatr Retin OCT Eye-Brain Connect*. Published online May 5, 2022:292-295. doi:10.1016/B978-0-323-60984-5.00064-0

92. Kang S, Kim US amuel. Using ImageJ to evaluate optic disc pallor in traumatic optic neuropathy. *Korean J Ophthalmol KJO*. 2014;28(2):164-169. doi:10.3341/kjo.2014.28.2.164

93. Yang HK, Oh JE, Han SB, Kim KG, Hwang JM. Automatic computer-aided analysis of optic disc pallor in fundus photographs. *Acta Ophthalmol (Copenh)*. 2019;97(4):e519-e525. doi:10.1111/aos.13970

94. Gibbon S, Muniz-Terrera G, Yii FS, et al. A method for quantifying sectoral optic disc pallor in fundus photographs and its association with peripapillary RNFL thickness. Published online November 13, 2023. doi:10.48550/arXiv.2311.07213

95. Zhou Y, Wagner SK, Chia MA, et al. AutoMorph: Automated Retinal Vascular Morphology Quantification Via a Deep Learning Pipeline. *Transl Vis Sci Technol*. 2022;11(7):12. doi:10.1167/tvst.11.7.12

96. Fu H, Wang B, Shen J, et al. Evaluation of Retinal Image Quality Assessment Networks in Different Color-spaces. Published online January 9, 2020. doi:10.48550/arXiv.1907.05345

97. Engelmann J, Storkey A, Bernabeu MO. QuickQual: Lightweight, convenient retinal image quality scoring with off-the-shelf pretrained models. Published online July 25, 2023. doi:10.48550/arXiv.2307.13646

98. Taylor AM, Pattie A, Deary IJ. Cohort profile update: The Lothian birth cohorts of 1921 and 1936. *Int J Epidemiol*. 2018;47(4):1042-1060. doi:10.1093/ije/dyy022

99. Zhang Z, Yin FS, Liu J, et al. ORIGA(-light): an online retinal fundus image database for glaucoma analysis and research. *Annu Int Conf IEEE Eng Med Biol Soc IEEE Eng Med Biol Soc Annu Int Conf*. 2010;2010:3065-3068. doi:10.1109/IEMBS.2010.5626137

100. Decencière E, Zhang X, Cazuguel G, et al. FEEDBACK ON A PUBLICLY DISTRIBUTED IMAGE DATABASE: THE MESSIDOR DATABASE. *Image Anal Stereol*. 2014;33(3):231-234. doi:10.5566/ias.1155

101. UK Biobank - UK Biobank. February 9, 2024. Accessed February 21, 2024. https://www.ukbiobank.ac.uk

102. Ritchie CW, Ritchie K. The PREVENT study: a prospective cohort study to identify mid-life biomarkers of late-onset Alzheimer's disease. *BMJ Open*. 2012;2(6):e001893. doi:10.1136/bmjopen-2012-001893

103. cataract dataset. Accessed February 21, 2024. https://www.kaggle.com/datasets/jr2ngb/cataractdataset

104. Porwal P, Pachade S, Kamble R, et al. Indian Diabetic Retinopathy Image Dataset (IDRiD): A Database for Diabetic Retinopathy Screening Research. *Data*. 2018;3(3):25. doi:10.3390/data3030025

105. Kovalyk O, Morales-Sánchez J, Verdú-Monedero R, Sellés-Navarro I, Palazón-Cabanes A, Sancho-Gómez JL. PAPILA: Dataset with fundus images and clinical data of both eyes of the same patient for glaucoma assessment. *Sci Data*. 2022;9(1):291. doi:10.1038/s41597-022-01388-1

106. Bajwa MN, Singh GAP, Neumeier W, Malik MI, Dengel A, Ahmed S. G1020: A Benchmark Retinal Fundus Image Dataset for Computer-Aided Glaucoma Detection. Published online May 28, 2020. doi:10.48550/arXiv.2006.09158

107. Jin K, Huang X, Zhou J, et al. FIVES: A Fundus Image Dataset for Artificial Intelligence based Vessel Segmentation. *Sci Data*. 2022;9(1):475. doi:10.1038/s41597-022-01564-3

108. Ocular Disease Recognition. Accessed February 21, 2024. https://www.kaggle.com/datasets/andrewmvd/ocular-disease-recognition-odir5k

109. Pachade S, Porwal P, Thulkar D, et al. Retinal fundus multi-disease image dataset (Rfmid): A dataset for multi-disease detection research. *Data*. 2021;6(2):1-14. doi:10.3390/data6020014

110. Rainio O, Teuho J, Klén R. Evaluation metrics and statistical tests for machine learning. *Sci Rep*. 2024;14(1):6086. doi:10.1038/s41598-024-56706-x

111. Aguinis H, Gottfredson RK, Joo H. Best-Practice Recommendations for Defining, Identifying, and Handling Outliers. *Organ Res Methods*. 2013;16(2):270-301. doi:10.1177/1094428112470848

112. van Etten ES, de Boer I, Steenmeijer S r., et al. Optical coherence tomography detects retinal changes in hereditary cerebral amyloid angiopathy. *Eur J Neurol*. 2020;27(12):2635-2640. doi:10.1111/ene.14507

113. Parisi V, Pierelli F, Coppola G, et al. Reduction of optic nerve fiber layer thickness in CADASIL. *Eur J Neurol*. 2007;14(6):627-631. doi:10.1111/j.1468-1331.2007.01795.x

114. Rufa A, Pretegiani E, Frezzotti P, et al. Retinal nerve fiber layer thinning in CADASIL: an optical coherence tomography and MRI study. *Cerebrovasc Dis Basel Switz*. 2011;31(1):77-82. doi:10.1159/000321339

115. Mutlu U, Colijn JM, Ikram MA, et al. Association of Retinal Neurodegeneration on Optical Coherence Tomography With Dementia: A Population-Based Study. *JAMA Neurol*. 2018;75(10):1256-1263. doi:10.1001/jamaneurol.2018.1563

116. Doubal FN, Dhillon B, Dennis MS, Wardlaw JM. Retinopathy in Ischaemic Stroke Subtypes. *Stroke J Cereb Circ*. 2009;40(2):389-393. doi:10.1161/STROKEAHA.108.529388

117. Doubal FN, MacGillivray TJ, Hokke PE, Dhillon B, Dennis MS, Wardlaw JM. Differences in retinal vessels support a distinct vasculopathy causing lacunar stroke. *Neurology*. 2009;72(20):1773-1778. doi:10.1212/WNL.0b013e3181a60a71

118. Doubal FN, MacGillivray TJ, Patton N, Dhillon B, Dennis MS, Wardlaw JM. Fractal analysis of retinal vessels suggests that a distinct vasculopathy causes lacunar stroke. *Neurology*. 2010;74(14):1102-1107. doi:10.1212/WNL.0b013e3181d7d8b4

119. Huang L, Wang C, Wang W, Wang Y, Zhang R. The specific pattern of retinal nerve fiber layer thinning in Parkinson's disease: a systematic review and meta-analysis. *J Neurol*. 2021;268(11):4023-4032. doi:10.1007/s00415-020-10094-0

120. Huang L, Zhang D, Ji J, Wang Y, Zhang R. Central retina changes in Parkinson's disease: a systematic review and meta-analysis. *J Neurol*. 2021;268(12):4646-4654. doi:10.1007/s00415-020-10304-9

121. Wagner SK, Romero-Bascones D, Cortina-Borja M, et al. Retinal Optical Coherence Tomography Features Associated With Incident and Prevalent Parkinson Disease. *Neurology*. 2023;101(16):e1581-e1593. doi:10.1212/WNL.0000000000207727

122. Neville CE, Young IS, Kee F, et al. Northern Ireland Cohort for the Longitudinal Study of Ageing (NICOLA): health assessment protocol, participant profile and patterns of participation. *BMC Public Health*. 2023;23(1):466. doi:10.1186/s12889-023-15355-x

123. Wagner SK, Hughes F, Cortina-Borja M, et al. AlzEye: longitudinal record-level linkage of ophthalmic imaging and hospital admissions of 353 157 patients in London, UK. *BMJ Open*. 2022;12(3):e058552. doi:10.1136/bmjopen-2021-058552

124. Suh A, Ong J, Kamran SA, et al. Retina Oculomics in Neurodegenerative Disease. *Ann Biomed Eng*. 2023;51(12):2708-2721. doi:10.1007/s10439-023-03365-0

125. Wagner SK, Fu DJ, Faes L, et al. Insights into Systemic Disease through Retinal Imaging-Based Oculomics. *Transl Vis Sci Technol*. 2020;9(2):6. doi:10.1167/tvst.9.2.6

126. Taoka T, Masutani Y, Kawai H, et al. Evaluation of glymphatic system activity with the diffusion MR technique: diffusion tensor image analysis along the perivascular space (DTI-ALPS) in Alzheimer's disease cases. *Jpn J Radiol*. 2017;35(4):172-178. doi:10.1007/s11604-017-0617-z

127. Park CJ, Kim SY, Kim JH, et al. Evaluation of glymphatic system activity using diffusion tensor image analysis along the perivascular space and amyloid PET in older adults with objectively normal cognition: a preliminary study. *Front Aging Neurosci*. 2023;15. doi:10.3389/fnagi.2023.1221667

128. Clark O, Delgado-Sanchez A, Cullell N, Correa SAL, Krupinski J, Ray N. Diffusion tensor imaging analysis along the perivascular space in the UK biobank. *Sleep Med*. 2024;119:399-405. doi:10.1016/j.sleep.2024.05.007

129. Paolini Paoletti F, Simoni S, Parnetti L, Gaetani L. The Contribution of Small Vessel Disease to Neurodegeneration: Focus on Alzheimer's Disease, Parkinson's Disease and Multiple Sclerosis. *Int J Mol Sci*. 2021;22(9):4958. doi:10.3390/ijms22094958

130. Bohnen NI, Albin RL. White matter lesions in Parkinson disease. *Nat Rev Neurol*. 2011;7(4):229-236. doi:10.1038/nrneurol.2011.21

131. Jacob MA, Cai M, Bergkamp M, et al. Cerebral Small Vessel Disease Progression Increases Risk of Incident Parkinsonism. *Ann Neurol*. 2023;93(6):1130-1141. doi:10.1002/ana.26615

132. Ma X, Li S, Li C, et al. Total Cerebral Small Vessel Score Association With Hoehn and Yahr Stage in Parkinson's Disease. *Front Aging Neurosci*. 2021;13:682776. doi:10.3389/fnagi.2021.682776

133. Chen H, Wan H, Zhang M, et al. Cerebral small vessel disease may worsen motor function, cognition, and mood in Parkinson's disease. *Parkinsonism Relat Disord*. 2021;83:86-92. doi:10.1016/j.parkreldis.2020.12.025

134. Visser AE, de Vries NM, Richard E, Bloem BR. Tackling vascular risk factors as a possible disease modifying intervention in Parkinson's disease. *Npj Park Dis*. 2024;10(1):1-4. doi:10.1038/s41531-024-00666-6

135. The role of brain vasculature in neurodegenerative disorders | Nature Neuroscience. Accessed December 11, 2024. https://www.nature.com/articles/s41593-018-0234-x

136. AI can detect Parkinson's up to seven years before symptoms appear, study finds. The Independent. August 23, 2023. Accessed December 11, 2024.

https://www.independent.co.uk/tech/ai-eye-scan-parkinsons-diagnosis-b2397774.html